THE MECHANICS OF BONDS BETWEEN CONCRETE AND FRP PLATE USING THREE PARAMETER ELASTIC FOUNDATION MODELS

A Thesis
Submitted to the Graduate Faculty
of the
North Dakota State University
of Agriculture and Applied Science

By

Linjing Che

In Partial Fulfillment of the Requirements
for the Degree of
MASTER OF SCIENCE

Major Department:
Construction Management and Engineering

July 2011

Fargo, North Dakota

North Dakota State University
Graduate School

Title
THE MECHANICS OF BONDS BETWEEN CONCRETE AND FRP PLATE USING THREE PARAMETER ELASTIC FOUNDATION MODELS

By

LINJING CHE

The Supervisory Committee certifies that this ***disquisition*** complies with North Dakota State University's regulations and meets the accepted standards for the degree of

MASTER OF SCIENCE

SUPERVISORY COMMITTEE:

ZHILI (JERRY) GAO
Chair

CHARLES MCINTYRE

JONGCHUL SONG

SIVAPALAN GAJAN

Approved:

03-01-2013	YONG BAI
Date	Department Chair

ABSTRACT

Traditional metallic materials lead steel-reinforced concrete structures to a durability problem due to its low value of resistance to corrosion. The superior performances of FRP, including the high resistance to corrosion, the flexible and complex shapes… give it a big advantage. However, premature failure due to debonding of adhesives between concrete and reinforcing materials is the major concern for all types of reinforcement containing FRP plate reinforcement. This thesis gradually develops three elastic foundation models, which are mainly derived from the solution of superficial stress in the foundations-soil system. The one-parameter Winkler's elastic foundation model is simple and easy. The two-parameter elastic foundation model thinks over the interfacial shear force of the joint bond. And the three-parameter foundation model additionally considers the adhesive layer's transverse displacement to meet the boundary condition of zero shear stress. Finite element analysis (FEA) is used to compare with the proposed three foundation methods.

ACKNOWLEDGEMENTS

There are many people who helped me greatly in the finish of this thesis. Great thanks to my adviser, Dr. Jerry Gao, for his guidance, understanding and encouragement throughout my graduate study. He was not only my good advisor, but also a best friend. His direction and advice have been helpful in many respects, showing her dedication to my academic and professional growth. I also extend my thanks to Drs. Sivaplan Gajan, Charles McIntyre, Jongchul Song for their support to my work and making time in their busy schedules, to serve on my committee.

The members of Center for Writer at NDSU, past and present, deserve my thanks. They help me a lot in revise my thesis' grammar and structure, in addition to other study related work, such as thesis revise, oral English practice and speech organization.

Last and most importantly, I am desirous to thank my parents, my brother, my friends, and co-workers. I was grateful for their support and patient understanding for my thesis far exceeded that which could reasonably be asked or expected.

TABLE OF CONTENTS

LIST OF TABLES

Table Page

LIST OF FIGURES

Figure Page

LIST OF SYMBOLS

σ …… Direct stress (Pa)

E …… Modulus of elasticity (MPa)

ε …….. Strain

h ……..…. Height

h_a …… Height of beam

h_b …… Height of beam

h_f …… Height of FRP plate

b ……..…. Thickness

k_a …… Shear stiffness of adhesive

I ……..... Moment of inertia of section

q ……..…. Distributed load

$w(x)$ ……..... Transverse displacements

$M(x)$ …….. Bending moment about the x-x axis

$N(x)$ ……..….. Axial force about the x-x axis

$Q(x)$ ……..….. Shear force about the x-x axis

CHAPTER 1. INTRODUCTION

1.1. Background

Reinforced concrete as a traditional and qualified construction material is widely used due to its durability and fire resistance. However, combined with the great financial losses, corrosion of the steel is still a serious problem that needs to be solved, especially at the harbor, wharf, road, bridge, and some other soil-related aggressive environments. Then anticipated service life of a structure is hopeless to fulfill when faced with the sharply reduced overall strength.

It is known that a new, properly constructed, alkaline (pH 13) concrete cover of 2 inches will inhibit corrosion of the rebar. This alkalinity and its protection will decrease over time due to carbon dioxide (CO_2) and other acidic materials in the environment penetrating into the concrete and dropping the pH below 11, at which point the natural corrosion inhibition is lost. Also, if air and water (moisture) are in contact with the rebar, corrosion will take place, because CO_2 absorbed from the atmosphere decreases the pH (carbonation). Another main source of corrosion is from salt (chloride ions). This process can originate from salt water and deicing materials penetrating the concrete and migrating to the rebar level where they accelerate corrosion. These corrosion products expand, and cause the concrete to degrade and spoil [1].

Early in 1990, Dr. Metha, in his book Concrete in the Marine Environment [2], points out that corrosion has exceeded the freezing and erosion, and is becoming the most severe damage for concrete. Especially for highway bridges, Bezad Bavarian gives us Figure 1Figure 1 to show the distribution of annual corrosion costs. According to the report of the United States in 2002, the cost

of corrosion accounts for approximately 3% of the Gross Domestic Product (GNP), or $276 billion dollars [3], $20 billion annually of which were attributed to the oversight of the Department of Defense (DoD). For appropriateness and to estimate cost effectively, several proposed technologies were further analyzed during 2003. A variety of commercial and emerging corrosion prevention and control (CPC) technologies were also established at that time. One selected area of great pith and moment was that of maintaining and improving steel-reinforced concrete infrastructure and infrastructure components.

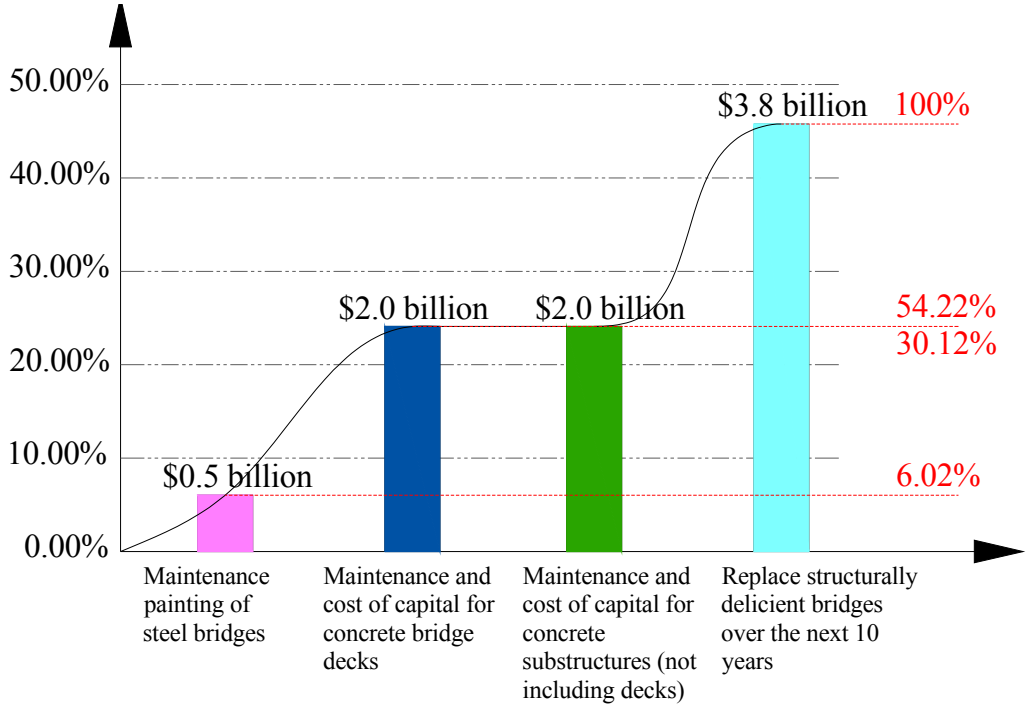

Figure 1. Annual direct cost of corrosion for highway bridges

Several statistics over the last 25 years indicate that the corrosion of steel in concrete has become a costly problem in the United States. Approximately half of the nearly 600,000 bridges in the U.S. Federal Aid Highway system have structural deficiencies or are functionally outmoded. A

quarter of U.S. bridge decks are badly deteriorated according to US Federal Highway Administration (FHWA) estimates. Even severely, with the existing of road-salt application, expensive repairs are often required within 5 to 10 years. This harsh situation is spreading to the entire world. Research indicates that the service life of buildings in the Arabian Gulf may be 5 to 15 years. Reinforced concrete bridges near the seashore in Japan show rapid deterioration within 10 years of construction.

1.2. Related Durability-Increasing Methods

To overcome the durability problem that steel-reinforced concrete brings to us, researchers tried lots of measures: epoxy-coated rebar [4], cathodic protection [5], and increasing the thickness of the concrete cover. Each method has its advantage and disadvantage due to its original properties. For instance, cathodic protection method is outstanding in protecting a great deal of metallic structures in various environments, from storage tanks, fuel pipelines, and offshore oil-well platforms to metal bars in concrete structures. However, three significant problems ---- cathodic shield, cathodic disbond, and the generation of hydrogen ions, are adversely manifest. Similarly, the protective method of increasing the thickness also has its corresponding pros and cons. Obviously, this method is a very simple and practical way, because it perfectly meets the durability quality and subjects to the requirements of the effective reinforced anchorage; up to optimum, leads to a reduction in the out-of-plane deflection rate of the steel plate; and effectively avoids the exposure of steel to the outside world, thus relieving the steel corrosion. Also, the two layers of concrete covering both sides of the steel plate are a great help in decreasing

the secondary moment. In contrast, the oversized protective layer will inevitably lead to economic waste by neglecting the concrete tensile effect. The cracks intensified by the oversized protective layer under the action of forces will finally affect the performance of concrete components (such as damaging the decoration surface and bringing people panic anxiety). An overview of these methods is given in Table 1.

Table 1. A brief comparison of various durability-increasing methods

Method	Pros	Cons
Epoxy-coated FRP sheet [4]	The most popular choice	Bond degradation between the sheet and the concrete. The bond strength of a coated FRP sheet will have a decrease when compare to a steel sheet without coat.
Cathodic protection [5]	Protecting a great deal of metallic structures in various environments	Athodic shield, cathodic disbond, and the generation of hydrogen ions
Increasing thickness of concrete cover	Simple and practical	Economic waste intensified cracks

1.3. Previous Work

As an innovative and effective substitution, Fiber Reinforced Polymer (FPR), made of a fibers-reinforced polymer matrix, is produced because of its outstanding corrosion resistance; flexible, complex shapes; electromagnetic transparency and high strength-density ratio. In this FRP-reinforced method, the efficient force transfer is crucially depending on the quality of FRP-concrete interface. What needs to be stated is that the terminology “interface” is defined as the adhesive, adherents, bonded joint, and even the relative slip between two parts in contact. Actually, a lot of premature failure caused by the debonding of adhesives between concrete and reinforcing materials is the major concern for FRP reinforcement. Therefore, it is need to soundly

understand the behavior of the FRP-reinforced concrete interface in relation to structural safety for a wide variety of applications [6][7][8][9][10].

As far back as the 1970's, the interfacial stress between concrete and the plate has received great attention. Numerous experiments and research were conducted to assess the mechanism of FRP-reinforced concrete structures. At early stage, the experiments mostly attributed the stress to the maximum axial force and the minimum bonded length [11][12] without considering the strains. Lately, experiments measured the axial strains along the interface, including Axial compression test, pull-out test, single-lap test, and double-shear test [13][14][15][16].

In addition, practical-use structural applications were also put into action and established both design guidelines and code provisions for further FPR design and construction. However, real experiences told us that premature failure due to delamination of adhesives between the FRP plate and concrete is the major concern. Quantitatively characterizing the kinetics of debond growth along the concrete-to-FRP interface is becoming the most pressing matter of the moment [17][18]. In order to obtain a high level of insight into the mechanical stress analysis of such new materials and to guarantee their structural function under service conditions, several methods and models were proposed to evaluate the accurate bond strength. J. Yang et al. present Fourier series and the minimization of complementary energy to solve the interfacial stresses in FRP-strengthened beams undergoing thermal and mechanical loads placed at the mid-span symmetrically [19]. Boucif Guenaneche et al. use linear elastic theory to consider the interfacial slip generated by the time-dependent slow deformations (ex. creep and shrinkage) and the adherent shear deformations

[20]. With the help of higher-order beam theory, Rabinovitch and Frostig apply a 2D linear elastic continuum to simulate the adhesive part with negligible longitudinal stiffness [41].

1.4. Problem Statement

However, above methods, combined with other relative methods, such as high-order beam theory and the fracture mechanics model, take both bending deformations and shear deformation into account, but are relatively complex due to integration with high-order variables. Not to mention the encountered, tired endless integrals in the way to problem solving, the higher equilibrium equations are also not a small challenge.

Then, an investigation on how to effectively calculate the bending deformations and shear deformation with a much simpler method is desired.

1.5. Purpose and Objectives

Based on the problem stated in the above paragraph, the purpose of the study in this thesis is to simply the solution method. In general, the objectives to reach can be summarized:

1) Clarify the parameters affecting the bond strength.
2) Exactly capture the interfacial normal stress and shear stress.
3) Properly model the interfacial stress.
4) Generate a usefully solution method for the given model.

1.6. Organization of Thesis

This thesis is organized by a logical sequence – the sequence that the author study and unfold the interfacial stress-related problem. Chapter 1 introduces background and defines the

problem statement as well as the study objectives. The detailed study methodology is described in Chapter 2. Chapter 3 reviews the mechanical properties of interface, by analyzing the existing test of bonded structures, and distinguishing the most appropriate one for current problem. From the chosen test, the data of impacting parameters is obtained and how these parameters influence the interfacial stress is discussed. Chapter 4 builds a bond-slip constitutive relation based on the chosen test for further mechanical study, completely considers the possible failure types and the affecting factors of bending reinforcement, and analyzes current existing interfacial stress analysis model. Chapter 5 uses the created parameter foundation models to solve the interfacial stress problem following a logic sequence from one-parameter model to three-parameter model. Chapter 6 verifies the accuracy of the created models by comparing with other existing methods and data. Chapter 7 concludes the study findings and discusses the potential future study areas.

CHAPTER 2. METHODOLOGY

This study gradually develops three elastic-foundation models, which is mainly derived from the solution of superficial stress in the foundations-soil system. The one-parameter Winkler's elastic foundation model is simple and easy to use by representing the stiffness of the vertical springs with a parameter, *k*. The two-parameter elastic foundation model calculates the interfacial shear force of the joint bond on the basis of the one-parameter one. The three-parameter model additionally considers the adhesive layer's transverse displacement to meet the boundary condition of zero shear stress. Finite element analysis (FEA) as a reference group is adopted to validate the three proposed foundation methods. The structure performance and durability under service conditions need to be taken into account [21]. The details of study methodology (The sequence of this methodology are illustrated in Figure 2) are:

1) Collecting the existing experimental and theoretical research results, and discussing their rationality and the further problems.
2) Based on the in-plane shear test, proposing reliable numerical model, discussing the spin-off failure mechanism, and obtaining the bond - slip constitutive relations for FRP-plated concrete interface.
3) According to the numerical model and constructive relations gained from in-plane shear research, comprehensively studying the interfacial flexural peeling and shear peeling problem.
4) Studying the possible failure types and the affecting factors of bending reinforcement.

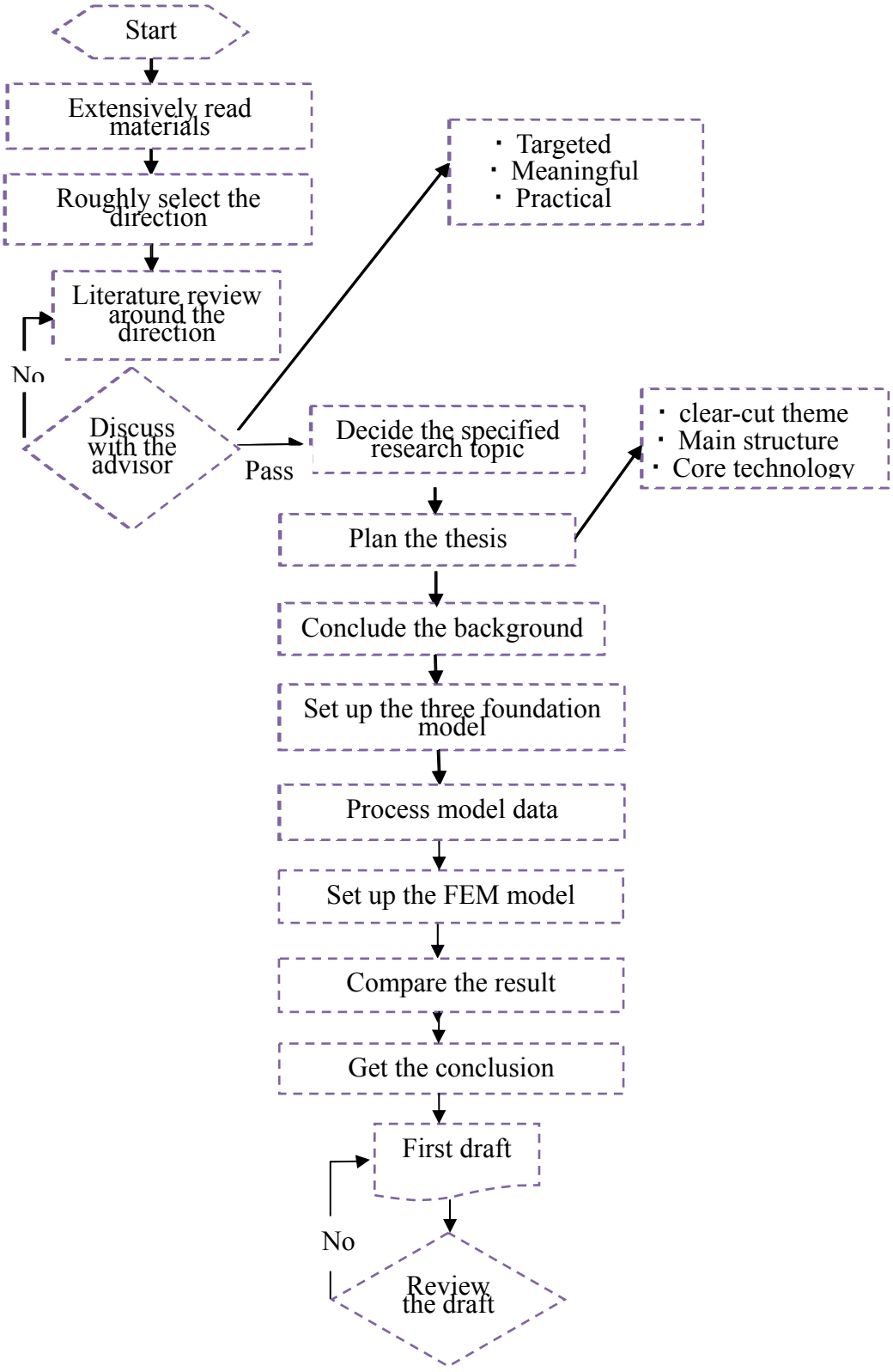

Figure 2. A flowchart of methodology

5) Proposing own numerical models to discuss the bond's failure mechanism according to the characters of shear and peeling stress, by following the logic developing sequence from one-parameter to three-parameter model.
6) Comparing the results from this thesis with existing methods to approve the reasonableness and accuracy.

CHAPTER 3. MECHANICAL PROPERTIES OF INTERFACE

3.1. Introduction

With the general growth of construction requirements quality, safety, and durability in many civil fields, it is hardly surprising that the FPR-bonded concrete has attracted considerable attention in recent years. In an attempt to ensure “safety-guard” assumptions about how FPR plates improve the properties of the structure (the assumption that FPR plates limit the cracks along the concrete surface, for example), studies have focused on anything from different mechanical, structural, or aesthetic uses of FRP plates to strength of the concrete. While some researchers have looked at why it performs outstanding on the basis of a mechanical advantage, other workers are focused on the properties of multifarious FRP. Accordingly, H.R. Meyer-Piening and Koganti M. Rao suggest that research on FRP-faced beams can be studied by the following five parameters: boundary conditions, ratio of FRP thicknesses, FRP’s fiber orientation, thickness to width ratio, and length to width ratio [22]. Experiments show that large number damages of FRP-reinforced concrete structures occur because of the interfacial peeling, so the accurate interfacial peeling strength model and the exact bond-slip model are of paramount essence in establishment of the FRP-reinforced concrete structure calculation theory. To this end, scholars from various countries have conducted a lot of the research in this area.

3.2. Test of Bonded Structures

To better evaluate the resistance of the bonded structures, and monitor the interfacial stress along the bond interface, several tests can be adopted. Various testing devises are devised

according to the types of the test. This thesis shortly reviews some of the most popular test as following sections [23].

3.2.1. Peel tests

This type of test is outstanding in testing the interfacial fracture resistance while a thin layer placed on a thick adherent or between two adherents. As in Figure 3, by executing forces to tear two adherents apart from each other or tear an adhesive layer from its substrate, it is widely suitable in all kinds of structure, especially for some non-symmetrical ones.

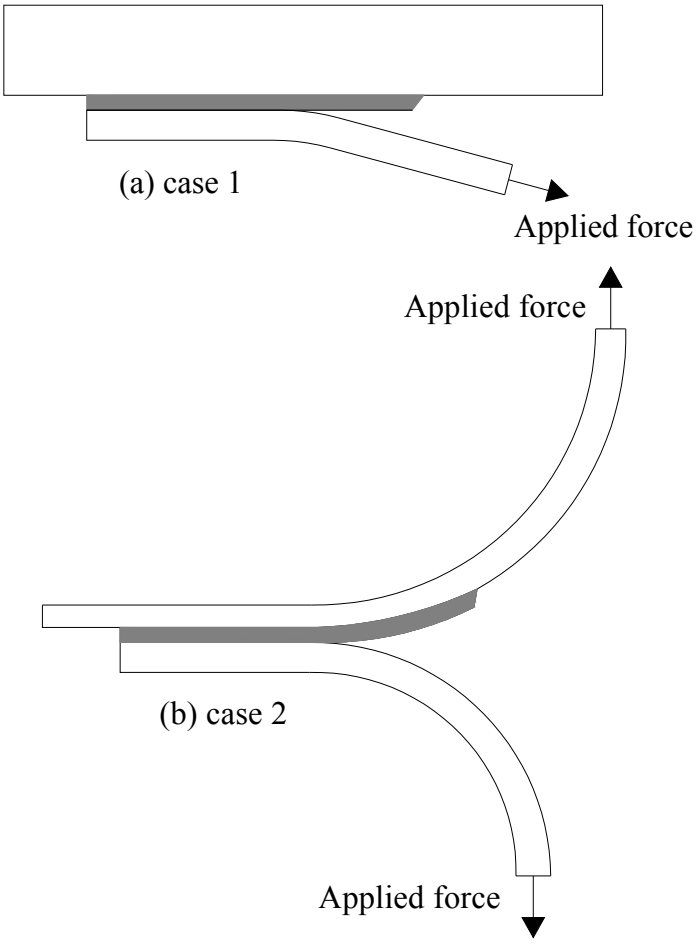

Figure 3. Peel test

3.2.2. Wedge tests

As in Figure 4, in this test, an opening or tensile load, normal to the crack, are directly executed on the bond by inserting a wedge in between the two parts of bonded structures. During the process of testing, a critical energy release rate can be derived by monitoring the crack length. However, with the different thickness of the two bonded adherents and the adhesive, especially when adhesive exhibits a high stiffness, a sliding or in-plane shear mode can be introduced that one adherents slide over another in the longitudinal direction.

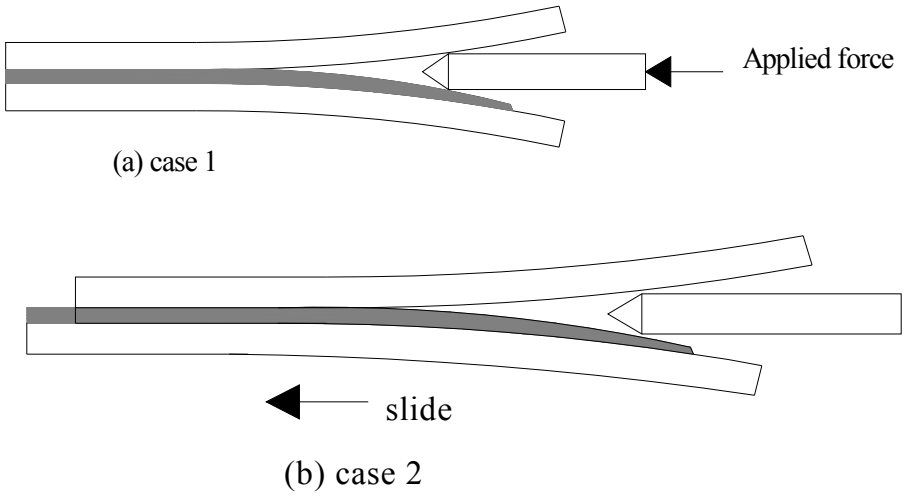

Figure 4. Wedge test

3.2.3. Double cantilever beam tests

As in Figure 5, by applying opposite opening or tensile forces, normal to the crack, on the two adherents at the end, this test value resistance of bond in a fracture mechanics framework.

However, in most cases, the crack in this test is fragile and easy to propagate along the entire interface of the composites, so this type of crack must be limited to avoid totally separation

from two adjacent adherents. The collapse velocity of the composites depends on the different thickness of the two bonded adherents and the adhesive, and the bonding stresses between them. In the industry, the type of composite is not recommended to put into practice.

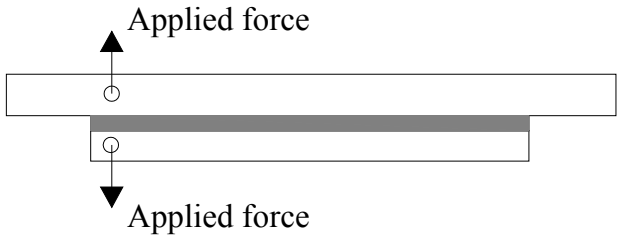

Figure 5. Double cantilever beam tests

3.2.4. End notch flexure tests

As in Figure 6, the two adjacent adherents in this test are fixed at one end and loaded on the other side. Open cracks of the bond are not permitted in this type of test, and only force perpendicular to the interface is accepted rather than axial force.

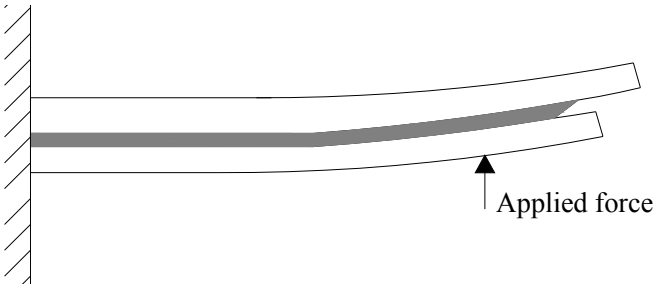

Figure 6. End notch flexure tests

3.2.5. Mixed-mode delaminating beam tests

As in Figure 7, two starting cracks subjected to four point loads are consisted this test. This test is kind of complexity with crack due to the peeling force normal to the bonded interface and

the slide of two adherents due to the shear force executing on the adhesive. The thicknesses of adherents have a great influence on the failure types.

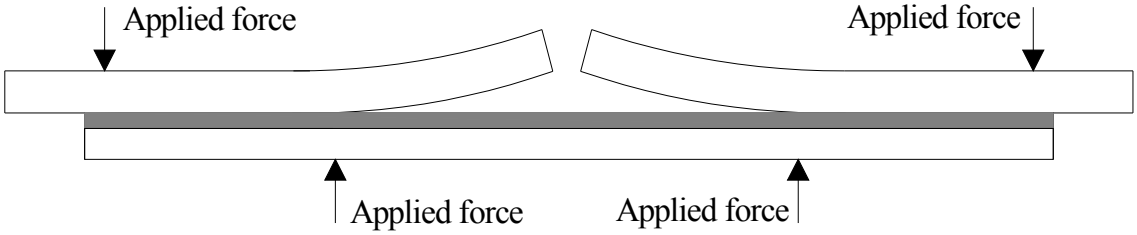

Figure 7. Mixed-mode delaminating beam tests

3.2.6. In-plane shear test

This type of test is the most widely used method in practical engineering applications, especially for concrete beam related area. All of following analysis in this thesis about the constitutive relations is also based on this test, as in Figure 8.

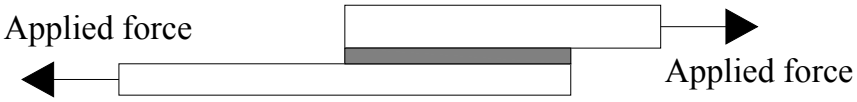

Figure 8. In-plane shear test

3.3. Types of In-Plane Shear Test

Interfacial shear properties can be generally studied by the in-plane shear test. Although different researchers use a variety of in-plane shear test methods, all of the tests can be integrated into the basic mechanical model (Table 2) as classified by Chen et al. (2001) in his paper [12].

Table 2. Types of in-plane shear test [12]

Single lap	Near-end	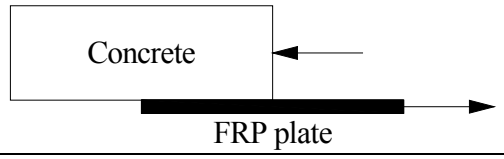
	Far-end	
Double lap	Near-end	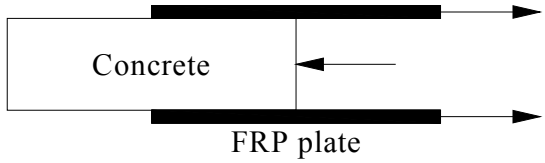
	Far-end	

Comparing the result from those in-plane shear tests, the reasons for shear peeling damage can be demonstrated in the following five points [24]:

1) Laminated peeling debonding within the FRP plate;

2) Interfacial peeling debonding between the FRP and the adhesive;

3) Laminated peeling debonding within the adhesive layer;

4) Interfacial peeling debonding between the concrete beam and the adhesive;

5) Laminated peeling debonding within the concrete beam.

For the current most commonly used organic layer, since adhesive layer and fibers can infiltrate well with each other, and the tensile strength of the adhesive layer is much higher than

that of concrete, the first four failure modes are not acceptable in the case of reliable layer construction and not allowed in FRP-reinforced concrete, otherwise will be treated as inferior quality in materials and construction. Thus the "ideal reliable" interface debonding is ripping off at the concrete bottom.

3.4. Impacting Parameters

3.4.1. Concrete strength

As the peeling failure happens at the concrete bottom, the strength of concrete takes a significant impact the interfacial bonding performance and the peeling capacity. Many researchers have pointed out that the interfacial failure is mainly associated with the concrete strength. [25][26].

3.4.2. Bonding length

The bonding length of FRP plate is an important influence factor. If the bonding length is smaller than the effective anchorage length Le, the bonding length has a positive impact on the peeling capacity.

3.4.3. Stiffness of FRP sheet

Studies from experiments have shown that the greater the stiffness of FRP plate is, the more uniform the interfacial bonding stress can be.

3.4.4. Width ratio

One phenomenon observed from the tests is that the width of peeled concrete is bigger than that of the FRP part.

Therefore, the width of affected concrete under shear force is bigger than the FRP plate, and the peeling stress is positively influenced by the width ratio b_b / b_f (b_b is the width of concrete adherend, b_f is the width of FRP plate), however, the increase is not infinite; there is a highest peeling capacity limitation.

3.4.5. Adhesive

In the in-plane shear test, the tension force directly instruct on the FRP plate, so the adhesive layer between the FRP and concrete is close to pure shear stress state. The tensile strength of common organic layer is greatly higher than that of concrete, so the adhesive has little effect on the bonding properties of the interface. Although studies have shown [27] that a very soft layer (shear stiffness is 1 / 20 ~ 1 / 5 than a common layer) can improve the interfacial peeling capacity, but this theory is not approved by most of the academic researchers.

3.4.6. Position and the end constraints

If the non-bonding length of the loaded component is not surplus enough, the concentration of the shear force at the end is obvious, and the corner of the concrete block will be stripped off. That means, in the in-plane shear test, the minimum value of the non-bonding length of the loaded component is required to avoid concrete collapse in the corner area.

3.5. Bond-Slip Constitutive Relation

The in-plane shear test is not only used to determine the FRP-concrete interfacial peeling capacity, but also suitable for local bond - slip constitutive relations. The following equation

illustrates one of the widely recognized theories. By arranging serious strain gauges on the surfaces of FRP plate, axial strain distribution ε_f (ε_f is the axial strain distribution of the FRP plate) can be easily measured. Next, the local bonding stress τ is obtained by conducting differential.

$$\tau_f = \frac{E_f d\varepsilon_f}{dx} \tag{1}$$

The local strain S_f can also be achieved by integration from the free end of the FRP plate.

$$S_f = \int \varepsilon_f dx \tag{2}$$

Although this method is very simple in theory, many difficulties have encountered in the tests. First, the interfacial bonding stress gained from the differential equation $\frac{d\varepsilon_f}{dx}$ is not precise as expected, since the gauges cannot be arranged closely enough. More importantly, the interfacial cracks at the middle bottom of concrete component and the random distribution of material composition have a great influence on the measured FRP strain. For example，if concrete cracks just under the strain gauge, the measured strain will be much greater than that of adjacent the strain gauge; If the strain gauge just attached a piece of aggregate, the measured strain will be much smaller than that of adjacent the strain gauge.

Therefore, many researchers have found that even for different specimens with same parameters, the measured local bond - slip relationships result in different outcomes. That means, the local bond-slip relationships are hard to be obtained by putting gauges of the strain distribution. Then, it is obvious that the results get from the in-plane shear test is not reliable relatively.

3.6. Summary

This chapter focuses on of a comprehensive review of the mechanical properties of concrete - FRP interface, collects and collates the knowledge of the existing test results, analysis, and bond - slip constitutive models. This information provides a reliable experimental basis for the in-depth analysis on the FRP-concrete interfacial stress. Although one widely accepted bond - slip constitutive model is planned in this chapter, the following questions still exist at current stage.

Although a lot of experimental research has done about this bond - slip constitutive model, it is not enough to build an accurate numerical model to embody the internal mechanism of debonding failure.

It is tough to measure interfacial bond - slip relationship in the in-plane shear test [23], and the results are of large dispersion, so the accuracy of the measured bond - slip model is under doubt.

CHAPTER 4. BENDING REINFORCEMENT

4.1. Introduction

The adhesion of FRP plate to concrete beam is important to ensure the cooperation of two components. Generally believed that, in the FRP-reinforced concrete structures, the bonding stress along FRP-concrete interface is mainly on account of shear stress. It can be illustrated in the bending reinforcement and in the shear reinforcement. For example, in the bending reinforcement, the bottom-pasted FRP plate (Figure 9) bears part of the cross-section moment and improves the flexural capacity because of the tensile force generated by the shear stress along the FRP-concrete interface.

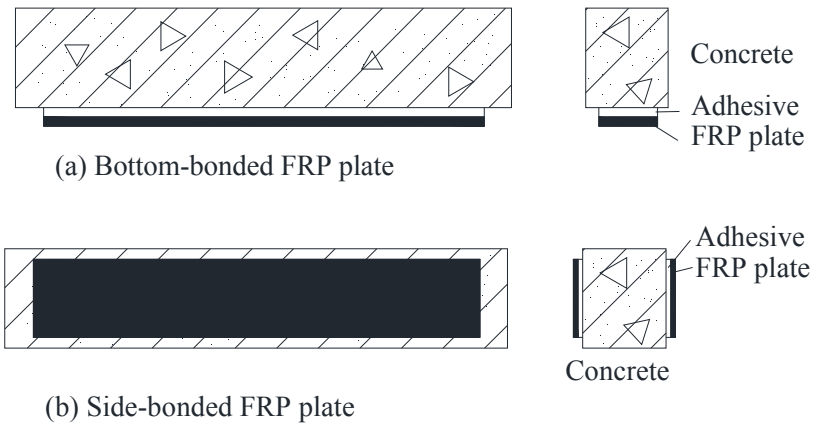

Figure 9. FRP plate bonding types

In the shear reinforcement, the side-pasted FRP plate (Figure 9) bears part of the shear tension through the shear stress along the FRP-concrete interface, prevents the development of inclined cracks and improves the component shear strength. Only in rare cases, the interfacial normal stress will have a major impact. For instance, in the bending reinforcement, a mutation of

the cross-section flexural stiffness occurs at the end of FRP component, and a force concentration leads the bond joint into a severely peeling situation. Also, the normal stress results from rigid dislocation of the inclined cracks greatly aggravate the peeling damage.

In practical engineering applications, since the adverse effects of the interfacial normal stress can be avoided by arranging FRP U-type clamps or mechanical anchoring, etc, the mechanical research properties are focused on the interfacial shear stress and the resulting peeling debonding, rather than the interfacial normal stress.

4.2. Failure Types of the Bottom-Reinforced FRP Plates

Using outwardly pasted FRP plate to improve the flexural strength of the concrete is one of the main technologies for concrete reinforcement. In the bending reinforcement, FRP plate is affixed to the bottom of beam bears the cross-section tensile stress with tensile steel.

As we stated above, the mechanical property of FRP-reinforced structure is mainly characterized by the bond quality. In addition to two common failure cases: tensile ruptures of FRP plate and crushes of concrete, the debonding of concrete beam and FRP component are often seen and subject to the following possible cases [28].

1) Plate end debonding firstly induces at the plate end, and then propagates to the middle along the beam-plate interface (Figure 10b).
2) Flexural crack debonding starts at the high-moment area and derived from the generated point to the both ends of the plate (Figure 10c).
3) Concrete cover debonding (Figure 10d).

4) Critical diagonal crack debonding， generated near plate end by a shear crack, expands from the crack to each end of the components (Figure 10e).

5) Combination of the above four modes.

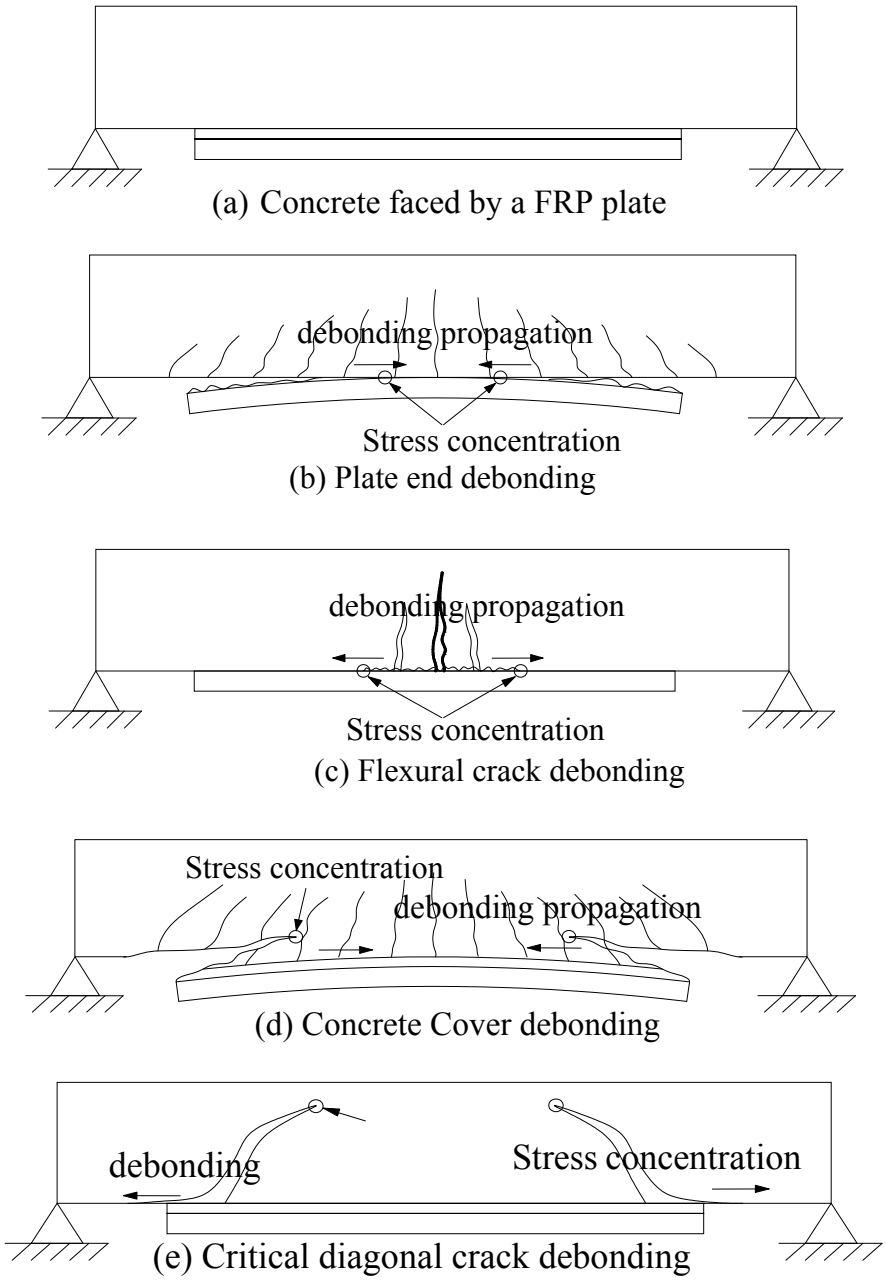

Figure 10. Failure types of the FRP plates

The above four types of debonding failure can be divided into two categories: one is stress-induced debonding failure, generated by the force concentration at the FRP sheet end, including the FRP plate end debonding (Figure 10b) and the concrete cover debonding (Figure 10d); the other is crack-induced debonding failure, caused by the development of bottom cracks, including the flexural crack debonding (Figure 10c) and the critical diagonal crack debonding (Figure 10e). The author summaries the reasons and the protection measures for above various flexural debonding failure in Table 3. Currently, for each type of debonding, there are corresponding measures to avoid its appearance.

Table 3. The reasons and the protection measures for various flexural debonding failure

Category	Types	Reason	Measures
Stress - induced Debongding failure	FRP plate end (Figure 10b)	Because of the truncation of FRP plate, the stress concentrates and the cross-section flexural stiffness is not continuous at the FRP sheet end. Stress-induced debonding is closely in connection with the stiffness of FRP plate; the greater rigidity the FRP plate has, the more possibly the joint debonds.	Currently, this category of spin-off has been handled by attaching U-shaped hoop at the end of FRP plate or taking other mechanically anchoring measures. [29][30][31]
	Concrete cover (Figure 10d);		
Crack - induced Debonding failure	Flexural crack (Figure 10c)	Once formed a large bending crack, stress is sectionally concentrated at the adjunct areas. It is common in the FRP flexural reinforcement. This is on account of the much lower strength of concrete. Due to the property limitation, concrete yields prior to FRP plate, and cracks firstly appear in the concrete rather than in the FRP plate.	This peeling failure is depended on the trend of concrete flexural cracks. U-shaped hoop or other anchoring measures is not completely useful at this situation. , so it is necessary for this form of in-depth study of debonding.
	Critical diagonal crack (Figure 10e)	In this type of debonding failure, appearance of a large diagonal shear crack is a siginficant sign. It is due to the inadequate resistance to shear of the reinforced concrete. After that, the structures on both sides of the crack detach and dislocate from each other.	In the actual engineering, the general requirement “strong shear, weak bending” effectively avoids the lack of shear strength, and this type of failure is not persuasive.

4.3. Factors Affecting the Bond Strength

In the major applications of reinforced concrete over the past several decades, steel-strengthening bars are widely employed because of their outstanding characters -- economic benefit and efficiency. The similar ability of elongtation of these bars makes them match with reinforcing concrete. Unfortunately, the enormous cost for maintenance might be a great challenge due to marked corrosion of steel, when it exposed to severe environments. Consequently, various new techniques have been utilized to lengthen the service lifetime of structures and to slow the deterioration of steel reinforcing bars, such as using synthetic membranes. Among them, fiber-reinforced polymer (FRP) is acting as the most outstanding alternate for reinforcing materials successfully reduce the weight and size of concrete, and to greatly improve the long-term performance of civil construction facilities.

A polymer with various agents added to enhance its material properties is referred to as a plastic. After the combination process, a final product in seized of reliable material properties is composite plastics, by bonding two or three homogeneous plastics together. [32]. Due to its low material and productions costs, global polymer production began in the mid-20th century, along with the emergence of new production technologies and new product categories, and lastly in the late 1970's, full-grew when its productions world-widely used in FRP: glass, carbon, and aramid. From the first utilization of GFPR at the end of World War II, to the application of CFRP in the late 1950's, and to the stage of omnipresent material today, these fibers have gained a lot of progress and achievement in the investigation of strength and elasticity. To comprehensively understand the

properties of FRP and its contribution to current society, this thesis reviews a class of structural materials involving the influence factors of FRP bond strength in every aspect.

4.3.1. Type of FRP reinforcement

The demands for FRPs in the field of construction have considerably increased, especially for the two major construction types: CFRP and GFRP as in Figure 11. Due to its strength and elasticity, FRP, as a pretty charming material, has been world widely accepted. To efficiently improve the properties of structural materials, the influence of the FRP types on the bond strength and adhesive expresses an open issue requiring analysis in further detail [33].

The prime mechanisms of the joint bond can be concluded into the following three parts: adhesive force, frictional force, and engage force.

For traditional steel rebars, the engage force is the major origin of the bond due to its surface characteristics: high shear strength, rib geometry, high rigidity, and so on. However, that engage force is also the major limitation for bond strength of FRP sheets. While steel rebars are outstanding of lateral confinement owing to their unique rib bearing, FRPs attribute their bond strength to the adhesion and the friction. Different mechanical ways of two materials directly lead to distinct results that bond-strength values of steel rebars present markedly higher than that of FRP sheets [34]. For exterior FRP systems, Marianovella Leone et al. have done some experiments about this and present a paper to detailedly illustrate his opinion.[33]. The experimental results shown in Table 4 prove that the maximum bond stresses vary with the type of reinforcement according to the mechanical properties [33].

(a) CFRP rebar

(b) GFRP rebar with screw thread

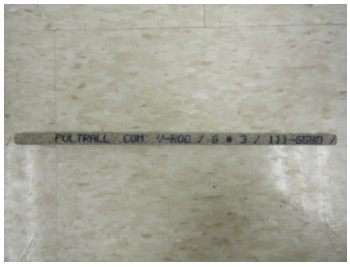

(c) GFRP bar

(d) Steel

(e) CFRP Tape

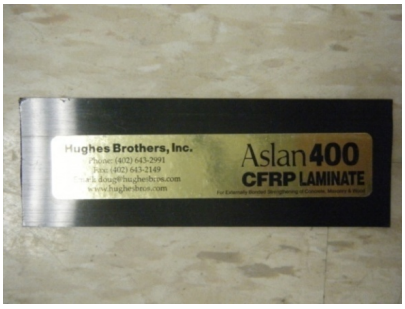

(f) CFRP Laminate

Figure 11. Types of FRP reinforcement

In particular, samples faced with the CFRP laminates have the highest value of the maximum bond stress. Compared with sheets, the factory production of laminates reacts positively on the utmost bond stress, which greatly improves the quality of the reinforcement. The instinct gaps of maximum bond stresses between CFRP-faced samples and GFRP-faced samples proves

that the mechanical properties of CFRP are much better than GFRP according as reduced imperfections.

Table 4. Maximum bond stresses with types of reinforcement [33]

Specimens	Temperature (0)	Maximum bond stress (Mpa)
CFRP sheet	20	4.22
CFRP laminate		5.65
GFRP sheet		3.41
CFRP sheet	80	1.96
CFRP laminate		4.21
GFRP sheet		0.96

Also, in other literature, the relationship between the utmost bond stress and the type of FRP plate is analyzed. [33].

4.3.2. Bonding length

The most important parameter to measure the performance of FRP-concrete interface is the effective anchorage length Le [35]. If the actual bonding length L is smaller than Le, the peeling capacity will be increase with the increase of bonding length; if FRP bond length is bigger than if Le, the peeling capacity will not be effected by the bonding length.

4.3.3. Concrete strength

Several specialists have found that the bond strength occupies a heavily dependent on concrete strength. Marta Baena et al. did a tests based on this assumption and show us a relationship between the concrete strength and the bond strength. His experimental results are illustrated in Table 5 [36].

In Table 5, the C2's bond strength of (high-stress concrete) is almost 1.5 times than C1's (low stress concrete), and the ratio is vitiating up to 2.1. Obviously, the positive influence of concrete strength is clear exhibited.

Table 5. Bond stresses change with concrete strength

Concrete type	Concrete Strength	Location of Bond Failure	Restraint Factor
C1(low strength concrete)	15 Mpa	At the surface of the FRP sheet	Value of concrete strength
C2(high strength concrete)	> 30 Mpa	At the concrete matrix	FRP's properties

4.3.4. Temperature

Compared to only 30% decrease of steel strength in the scope of 150–200°C, the bond reduces approximately 90% at the same temperature range. The temperature impact on the joint along the interface of concrete and FRP rebars was discussed by Amnon Katz and Neta Berman in their paper. Besides the test, they also developed a semi-empirical model to present that a rise in temperature accompanies a decrease in bond strength in Table 6 [37].

Table 6. Temperature affects bond behavior [36].

Specimens	Temperature	Maximum bond stress	Calculated slip	Experimental
CFRP sheet	20	4.22	0.181	0.661
	80	1.96	0.116	0.078
CFRP laminate	20	5.65	0.087	0.270
	80	4.21	0.237	0.866
GFRP sheet	20	3.41	0.186	0.645
	80	0.96	0.182	0.221

Besides, Marta Baena et al experiments also give us some ideas that temperature affects bond behavior [36].

Finally, the results can be obtained that two parameters are affecting the bond-strength reduction: crosslinking and glass transition temperature [37].

1) The critical point where the polymer loses its mechanical property is controlled by the glass transition temperature of the polymer layer at the surface of the rod.
2) The quantity of crosslinks is related to the degrading rate of the polymer's property after the glass transition temperature has been attained.

4.4. Interfacial Stress Analysis Model

Normally, the behavior of the concrete and FRP interface is the critical parameter that affects the FRP-reinforced structures. As far back as the 1970's, the interfacial stress between concrete and the plate received great attention. Numerous studies were conducted to measure the mechanism property of FRP-strengthened concrete structures. Quantitatively characterizing the kinetics of debond growth is becoming the most pressing matter of the moment [17]. To deeply understand the mechanical stress analysis of this advanced material, several methods and models were proposed to evaluate the accurate bond strength.

4.4.1. Closed-form rigorous method

In simply supported FRP plated-bonded beams, A. Benachour et al. initially worked out a closed-form rigorous solution under three load cases: an arbitrarily positioned, single-point and a uniformly distributed load. Their model is outstanding, classical, which is general essentially, but applicable to various load cases. Their general solutions of adhesive for all three load cases are shown below [38]:

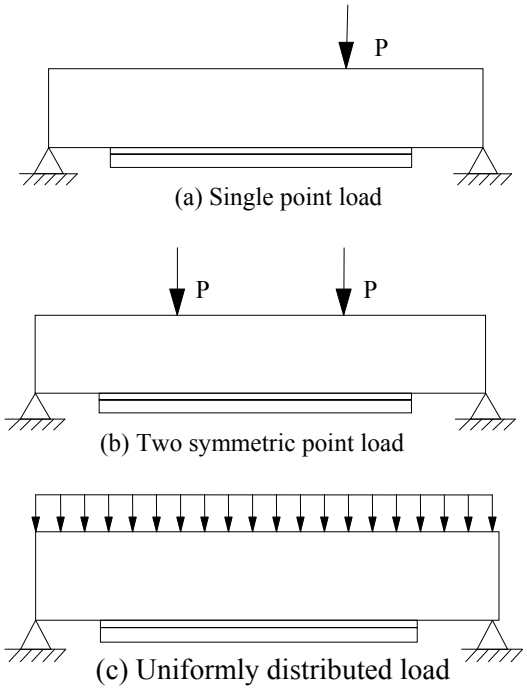

Figure 12. Three load cases of imply supported FRP plated-bonded beams

In their model, the stress is related to the properties of the plated beams such as width, height and the shear modulus.

$$\tau(x) = B_1 \cosh\left(\sqrt{\frac{G_a}{t_a}\left(A_{11}^x + \frac{b_l h^2}{4E_s I_s} + \frac{b_l}{A_s E_s}\right)}x\right) + B_2 \sinh\left(\sqrt{\frac{G_a}{t_a}\left(A_{11}^x + \frac{b_l h^2}{4E_s I_s} + \frac{b_l}{A_s E_s}\right)}x\right) + \frac{G_a h}{2\lambda^2 t_a E_s I_s} V_s(x) \tag{3}$$

And the normal stresses is

$$\sigma(x) = e^{-\beta x}\left[C_1 \cos\left(\sqrt[4]{\frac{E_a}{4t_a}\left(D_{11}^x + \frac{b_l}{E_s I_s}\right)} \bullet x\right) + C_2 \sin\left(\sqrt[4]{\frac{E_a}{4t_a}\left(D_{11}^x + \frac{b_l}{E_s I_s}\right)} \bullet x\right)\right] - \frac{b_l(h/2) - D_{11}^x E_s I_s (t_l/2)}{D_{11}^x E_s I_s + b_l}\frac{d\tau(x)}{dx} - \frac{1}{D_{11}^x E_s I_s + b_l} q \tag{4}$$

Where, G is the shear modulus, and the b, h are the width, height separately.

Different load cases lead to various interfacial stresses. With the help of three boundary conditions, A. Benachour et al. separately count the interfacial stresses subjected to various load cases. In addition, the high concentrations of normal stress and shear stress are also taken into consideration in the process of applying the boundary condition. To better catch the parameters that affect the interface behavior, such as the thickness of plate, the fiber orientations, and the adhesive stiffness, A. Benachour and his coworkers conduct a parametric study and compare the results with other existing solutions

1) There exist high shear force and normal force concentration at the boundary.
2) With the increase of beam's longitudinal fiber, the effective modulus of FRP enhanced.
3) The higher E-modulus plated has a lower interfacial stress concentration at the boundary.
4) The G-modulus is taken into account in evaluating the peak interfacial stress at the boundary.

4.4.2. Fourier series: minimization of complementary energy

For FRP-faced beam, to solve the interfacial stress problem, J. Yang et al. present the Fourier series and the minimization of complementary energy yielding thermal loads and arbitrary loads.[39]. This method is outstanding in accounting the interfacial normal stress has a dramatic difference between the two adherent-adhesive interfaces. What is more, in this paper, the stress distribution is non-uniform, and the boundary condition is stress free. Same as the closed-form rigorous solution, J. Yang et al. method is also set up for various load cases, not only the three

basic-load cases: pure bending, pure tension, and partial distributed loading. Their analytical predictions can be given as the following main conclusions.

1) The normal stresses and the shear stresses influence the interfacial stresses at the close-by areas together while the former takes more contribution.
2) When coming to the two types of peak interfacial stresses, they are in proportion to axial stiffness' square root.
3) Interfacial stresses caused by a uniform temperature can be represented as axial loads which are accordingly equivalent, and the temperature gradient caused interfacial stresses are relative to bending moment.

4.4.3. Linear elastic theory

To solve the interfacial stresses, Boucif Guenaneche et al. use a relatively simple linear elastic theory in the FRP-strengthened concrete. Then, on the structural performance, the interface slip, which is generated by the time-dependent shear deformations (such as concrete creep and shrinkage) and the adherent shear deformations, is seriously considered [40].

Compared with other solutions, the difference this unique method has is that it innovatively uses only one differential equation to express the normal and shear stresses rather than two differential equations. Besides, Boucif Guenaneche et al., like some other researchers, also conduct a parametric study showing the effects of relative variables to the interface behavior, for example, the adhesive stiffness and thickness. Their solutions are very serviceable in the numerical studies and experimental research.

4.4.4. Higher-order beam theory

By using higher-order beam theory, Frostig and Rabinovitch presented a 2D linear elastic continuous medium to describe the adhesive layer[41]. The model's governing equations, derived from a high-order, closed-form analytical method, are used to characterize the behavior of the FRP-bonded beam under the conditions of appropriate continuity and boundary. Although the high-order theory is relatively complex in calculation, its dominance in evaluating the concentration distribution of shear stress at the boundary cannot be ignored. What is more, it is amazing for the ability to be transferred to the simpler theories by omitting the appropriate terms. The same as the above methods, Rabinovitch and Frostig are also parametrically studying the governing factors that affect the intensity and magnitude of concentrated edge stresses.

CHAPTER 5. ANALYTICAL MODEL

5.1. Basic Assumptions

The simplified model of a beam plated with an external FRP is usually met in the research of harbor, wharf, highway and so on. Figure 13 is the basic simplified model for these types of beams, and Figure 14 shows the basic geometry and notation for them.

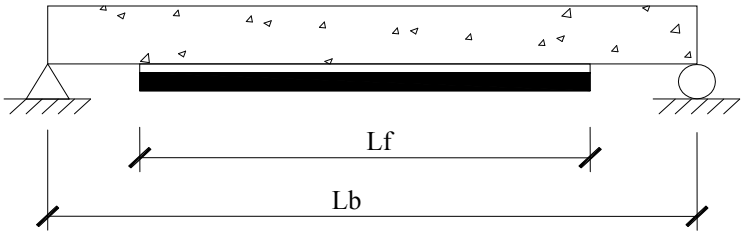

Figure 13. Simple supported beam placed by FRP

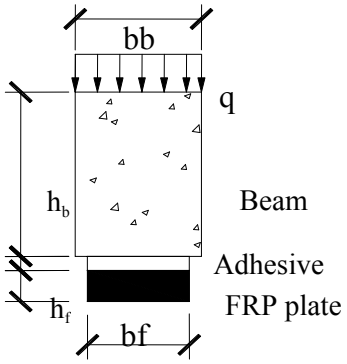

Figure 14. Geometry and notation of a strengthened beam

5.1.1. Continuous beam assumption

It is assumed that the substance is fully filled in the entire volume without voids; in simple terms, the material is dense. Under this assumption, we can pick up any unit of the adhesively bonded structures to process stress analysis. It is worth mentioning that, under normal operating conditions, the deformed solid should still maintain its continuity. Therefore, the deformation of

the solid deformable body must meet the geometric compatibility; that is, neither “gap” nor “squeeze” happens after deformation.

5.1.2. Homogeneity assumption

Any volume element of the structure can represent the entire object for the mechanical properties. Obviously, this representation varies with different materials. For example, the size of a representative unit for concrete is almost ten times that for metal. The minimum size of the selected unit is restrictive in order to maintain the average statistics of materials’ mechanical properties at a constant value.

5.1.3. The assumption of isotropy

Along all directions of the materials, the mechanical properties are same. For metal, the statistic is an average value from all oriented crystals. For the FPR materials, due to the re-arrangement of the crystal in the rolling process, there is some discrepancy of mechanical properties between the rolling direction and perpendicular rolling direction. Also, this small discrepancy varies with the type of materials and the degree of rolling, which have little effect on the beam’s stress analysis. To simplify the problem, scientists usually adopt the assumption of isotropy, so does this thesis’s calculation.

5.2. One-Parameter Elastic Foundation Model

So far, most beam research is based on the classical Euler-Bernoulli theory, a simple and practical tool used to calculate the beam deflection, but the theory is only suitable for a laterally loaded beam without taking the shear deformation into consideration. The Euler-Bernoulli beam

theory, discovered by Jacob Bernoulli, is also called classical beam theory, engineering's beam theory, or beam theory. After the generations of the Ferris wheel, it is widely spreading because it creatively hypothesizes that cross sections keep plane and perpendicular to the beam's central axis. However, while this theory contributes a lot to the slender beams' case, the error in shear force and moment distribution caused by neglecting transverse shear deformations is a fatal factor for thick beams with discrete loads [42]. Therefore, most current mechanical analyses are based on the Timoshenko beam theory.

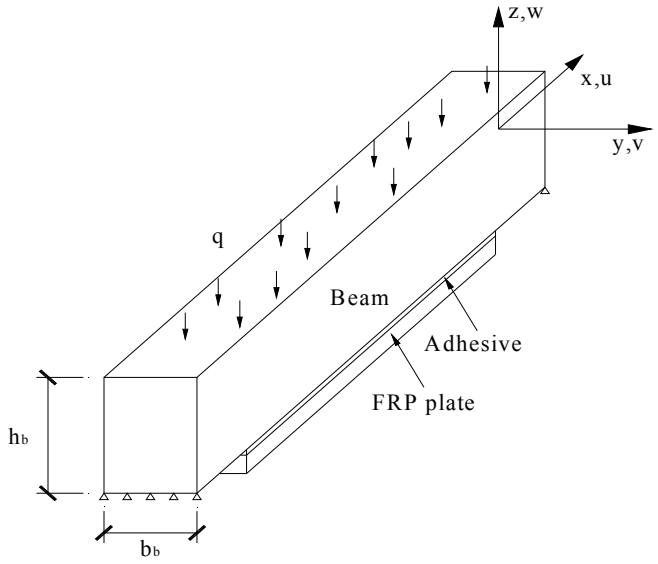

Figure 15. Simply supported sandwich plate subjected to a lateral pressure load

Winkler's elastic foundation model (Figure 15), as the most classical mechanical model, assumes a linear force-deflection relationship between the beam and the jointed FPR plate. In this model, the mechanical interaction of the two parts can be represented by several vertical mutually independent springs with a stiffness parameter k to resist beam's deformation, and these linear springs are closely spaced.

Within a representative adhesive joint, two adherents of concrete and the FPR plate are linked by an adhesive of latex-based layer. Two adherents are built as Winkler's beam with thickness h1 and h2 and with width b. Based on Winkler's elastic foundation model, the slide along the connecting interface is neglected. We take the vertical displacement into consideration.

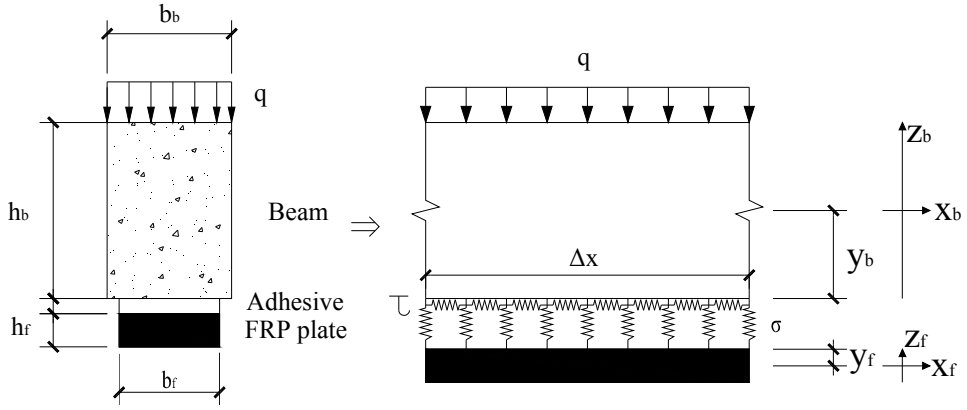

Figure 16. Cross section of FRP-reinforced concrete

Serials of equilibrium equations can be derived from the force diagram in Figure 16. The adhesive layer is thinner when compared with the joint adherents, then through the layers thickness, the stresses of which could be deemed as constant.

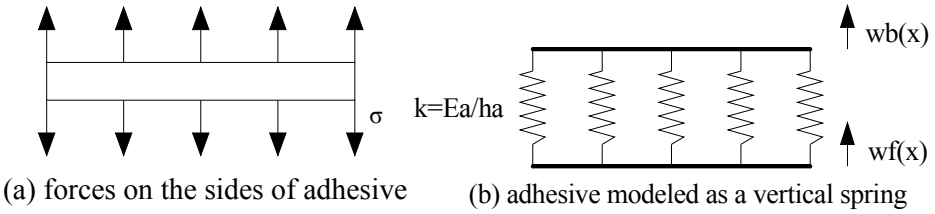

Figure 17. Adhesive modeled as a vertical spring

In this one-parameter model, the separation of two adherents generated an interfacial normal stress, which is the stress normal to the FPR-concrete interface, represented by $\sigma(x)$ in Figure 17 [43] [44] [45].

5.2.1. Applying continuative equations

The relationship between stress and strain can be written as following:

$$\left.\begin{array}{l} \sigma = E\varepsilon \;\Rightarrow\; \sigma = E\dfrac{\Delta w(x)}{h_a} \\ \sigma = k_a \Delta w(x) \end{array}\right\} \;\Rightarrow\; k_a = \frac{E}{h_a} \tag{5}$$

In equation (5), the adhesive is built as a liner-vertical spring with a stiffness of $\frac{E}{h_a}$

$$\sigma(x) = \frac{E}{h_a}\Delta w(x) = \frac{E}{h_a}\left(w_f(x) - w_b(x)\right) \tag{6}$$

The curvature is determined by the moment in the cross section

$$w'' = -\frac{M(x)}{EI} \;\Rightarrow\; \frac{dw_b^2(x)}{dx^2} = -\frac{M_b(x)}{E_b I_b}, \qquad \frac{dw_f^2(x)}{dx^2} = -\frac{M_f(x)}{E_f I_f} \tag{7}$$

EI is the bending rigidity.

5.2.2. Applying equilibrium equations

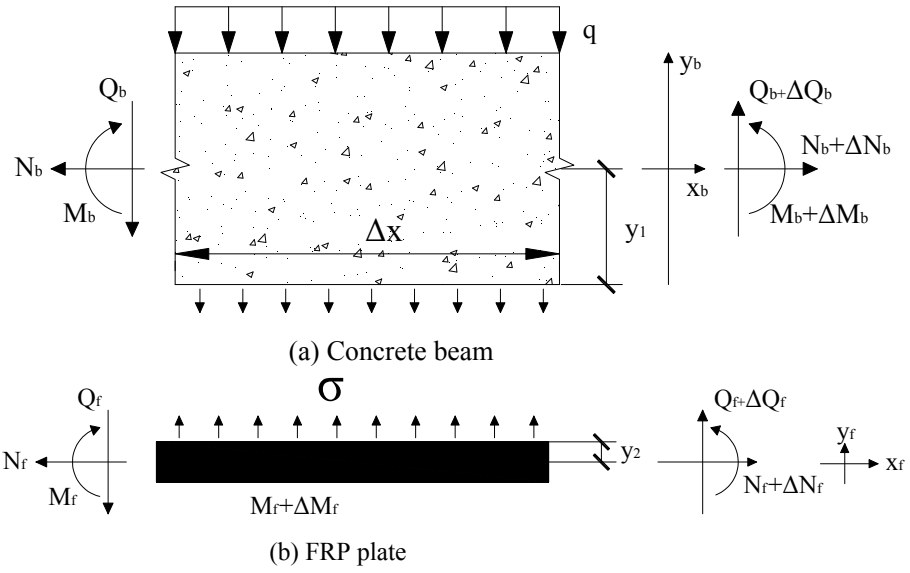

(a) Concrete beam

(b) FRP plate

Figure 18. Free-body diagram for one-parameter model

With the help of equilibrium equations, the relationship of moments, shear forces, axial forces can be built showing in Figure 18.

Forces are balanced in x direction.

$$\frac{dN_b}{dx}=0, \qquad \frac{dN_f}{dx}=0 \tag{8}$$

Forces are balanced in y direction

$$\Delta Q_b = q(x)\Delta x+\sigma(x)b_f\Delta x, \qquad \Delta Q_f=-\sigma(x)b_f\Delta x \tag{9}$$

$$\frac{dQ_b}{dx}=q(x)+\sigma(x)b_f, \qquad \frac{dQ_f}{dx}=-\sigma(x)b_f \tag{10}$$

Moments are balanced round the right bottom point.

$$\begin{aligned}&\Delta M_b+Q_b\times\Delta x-q(x)\times\frac{1}{2}(\Delta x)^2-\sigma(x)b_f\times\frac{1}{2}(\Delta x)^2=0,\\&\Delta M_f+Q_f\times\Delta x+\sigma(x)\times\frac{1}{2}(\Delta x)^2=0\end{aligned} \tag{11}$$

$$\frac{dM_b}{dx}=-Q_b+\frac{1}{2}q(x)dx+\frac{1}{2}\sigma(x)b_f dx, \qquad \frac{dM_f}{dx}=-Q_f-\frac{1}{2}\sigma(x)b_f dx \tag{12}$$

dx is very small, $\frac{1}{2}q(x)dx\approx 0, \frac{1}{2}\sigma(x)b_f dx\approx 0$ (13)

Then $\frac{dM_b}{dx}=-Q_b, \qquad \frac{dM_f}{dx}=-Q_f$ (14)

Summarizing the relationship

$$\begin{cases}\dfrac{dN_b}{dx}=0, & \dfrac{dN_f}{dx}=0\\ \dfrac{dQ_b}{dx}=q(x)+\sigma(x)b_f, & \dfrac{dQ_f}{dx}=-\sigma(x)b_f\\ \dfrac{dM_b}{dx}=-Q_b, & \dfrac{dM_f}{dx}=-Q_f\end{cases} \tag{15}$$

5.2.3. Calculating $\sigma(x)$

Differentiating equation (6) on both side and combining the above-mentioned equations, equation (12) can be expressed on the basis of $\sigma(x)$ as follows:

$$\frac{dw_b^4(x)}{dx^4} = -\frac{1}{E_b I_b}\frac{dM_b^2(x)}{dx^2} = \frac{1}{E_b I_b}\frac{dQ_b}{dx} = \frac{1}{E_b I_b}\left(q(x)+\sigma(x)b_f\right) \tag{16}$$

$$\frac{dw_f^4(x)}{dx^4} = -\frac{1}{E_f I_f}\frac{dM_f^2(x)}{dx^2} = \frac{1}{E_f I_f}\frac{dQ_f}{dx} = -\frac{1}{E_f I_f}\sigma(x)b_f \tag{17}$$

And substituting equation (16) and (17) into equation (6), the differential equation of $\sigma(x)$ can be achieved in terms of external force.

$$\frac{d\sigma^4(x)}{dx^4} = \frac{E_a}{h_a}\left(\frac{dw_f^4(x)}{dx^4} - \frac{dw_b^4(x)}{dx^4}\right) = -\frac{E_a}{h_a}\left(\frac{1}{E_b I_b}\left(q(x)+\sigma(x)b_f\right) + \frac{1}{E_f I_f}\sigma(x)b_f\right) \tag{18}$$

Simplifying the above equation can get

$$\frac{d\sigma^4(x)}{dx^4} + \frac{E_a b_f}{h_a}\left(\frac{1}{E_b I_b} + \frac{1}{E_f I_f}\right)\sigma(x) = -\frac{E_a}{h_a E_b I_b}q(x) \tag{19}$$

Assuming $A_1 = \frac{E_a b_f}{h_a}\left(\frac{1}{E_b I_b} + \frac{1}{E_f I_f}\right)$ and $A_2 = \frac{E_a}{h_a E_b I_b}$, the governing equation changes into $\frac{d\sigma^4(x)}{dx^4} + A_1\sigma(x) = -A_2 q(x)$ (20)

The corresponding homogeneous equation is $\frac{d\sigma^4(x)}{dx^4} + A\sigma(x) = 0$ (21)

The characteristic equation corresponding to the above governing differential equation is

$$r^{(4)} + A_1 = 0 \tag{22}$$

And the corresponding characteristic root

$$r_1 = \sqrt[4]{\frac{A}{4}} + \sqrt[4]{\frac{A}{4}}i, \quad r_2 = \sqrt[4]{\frac{A_1}{4}} - \sqrt[4]{\frac{A_1}{4}}i, \quad r_3 = -\sqrt[4]{\frac{A_1}{4}} + \sqrt[4]{\frac{A_1}{4}}i, \quad r_4 = -\sqrt[4]{\frac{A_1}{4}} - \sqrt[4]{\frac{A_1}{4}} \tag{23}$$

Assume $\lambda = \sqrt[4]{\frac{A_1}{4}} = \sqrt[4]{\frac{E_a b}{4h_a}\left(\frac{1}{E_b I_b} + \frac{1}{E_f I_f}\right)}$ (24)

$$r_1 = \lambda + \lambda i, \quad r_2 = \lambda - \lambda i, \quad r_3 = -\lambda + \lambda i, \quad r_4 = -\lambda - \lambda i \tag{25}$$

Then, the solution of the corresponding homogeneous equation

$$\sigma(x) = e^{\lambda x}(C_{11}\cos\lambda x + C_{12}\sin\lambda x) + e^{-\lambda x}\left(C_{13}\cos\lambda x + C_{14}\sin\lambda x\right) + \sigma_{11}(x) \tag{26}$$

C11, C12, C13and C14 are arbitrarily constant coefficients determined by the boundary.

$\sigma_{11}(x) = -\frac{A_2}{A_1}q(x)$ is one special solution of equation (20) corresponding to $-A_2 q(x)$

With the increase of x, the normal stress is approaching to zero. When x is large enough, $C_{11} = C_{12} = 0$. The general result then becomes $\sigma(x) = e^{-\lambda x}\left(C_{13}\cos\lambda x + C_{14}\sin\lambda x\right) - \frac{A_2}{A_1}q(x)$

5.2.4. Applying boundary conditions

At x=0, the moment of FRP plate is boundary free with zero moment $M_{f(x=0)} = 0$ and zero axial force $Q_{f(x=0)} = 0$. Between the plate end and the beam end, the moment in this section is only resisted by the concrete beam.

$$x = 0: \quad Q_{f(x=0)} = 0, \quad Q_{b(x=0)} = Q_{T(x=0)}, M_{f(x=0)} = 0, \quad M_{b(x=0)} = M_{T(x=0)} \tag{27}$$

$$\sigma(x) = \frac{E_a}{h_a}\Delta w(x) = \frac{E_a}{h_a}\left(w_f(x) - w_b(x)\right) \tag{28}$$

Where, $w'' = -\frac{M(x)}{EI} \Rightarrow \frac{dw_b^2(x)}{dx^2} = -\frac{M_b(x)}{E_b I_b}, \qquad \frac{dw_f^2(x)}{dx^2} = -\frac{M_f(x)}{E_f I_f}$ (29)

Differentiating equation (28) on both sides, and input equation (29),

$$\frac{d^2\sigma(x)}{dx}=\frac{E_a}{h_a}\left(w_f^{"}(x)-w_b^{"}(x)\right)=\frac{E_a}{h_a}\left(-\frac{M_f(x)}{E_fI_f}+\frac{M_b(x)}{E_bI_b}\right) \tag{30}$$

When x=0, the above equation (30) changes into

$$\left.\frac{d^2\sigma(x)}{dx}\right|_{x=0}=\frac{E_a}{h_a}\left(\frac{M_b(0)}{E_bI_b}\right)=\frac{E_a}{h_a}\frac{M_b(0)}{E_bI_b} \tag{31}$$

Substituting equation (26) into equation (31), the express changes as:

$$\frac{d^2\sigma(x)}{dx}=-2\lambda^2C_{14}e^{-\lambda x}\cos\lambda x+2\lambda^2C_{13}e^{-\lambda x}\sin\lambda x-\left.\frac{A_2}{A_1}\frac{dq^2(x)}{dx}\right|_{x=0}=\frac{E_a}{h_a}\frac{M_T(0)}{E_bI_b} \tag{32}$$

Where, $C_{14}=-\frac{1}{2\lambda^2}\frac{E_a}{h_a}\frac{M_T(0)}{E_bI_b}-\frac{1}{2\lambda^2}\left.\frac{A_2}{A_1}\frac{dq^2(x)}{dx}\right|_{x=0}$ (33)

Continuing to differentiate on both sides of equation (32)

$$\frac{d^3\sigma(x)}{dx}=\frac{E_a}{h_a}\frac{1}{E_bI_b}\left(Q_f-Q_b\right) \tag{34}$$

$$\frac{d^3\sigma(x)}{dx}=2\lambda^3e^{-\lambda x}\cos\lambda x\left(C_{34}+C_{33}\right)+2\lambda^3e^{-\lambda x}\sin\lambda x\left(C_{34}-C_{33}\right) \tag{35}$$

$$-\frac{A_2}{A_1}\frac{dq^3(x)}{dx^3}=\frac{E_a}{h_a}\frac{1}{E_fI_f}Q_f-\frac{E_a}{h_a}\frac{1}{E_bI_b}Q_b \tag{36}$$

$$\left.\frac{d^3\sigma(x)}{dx}\right|_{x=0}=2\lambda^3\left(C_{14}+C_{13}\right)-\left.\frac{A_2}{A_1}\frac{dq^3(x)}{dx^3}\right|_{x=0}=-\frac{E_a}{h_a}\frac{1}{E_bI_b}Q_T(0) \tag{37}$$

By calculating equation (37) and C14, C13 is easy to be answered.

$$\begin{aligned}C_{13}=&-\frac{1}{2\lambda^3}\frac{E_a}{h_a}\frac{1}{E_bI_b}Q_T(0)+\frac{1}{2\lambda^3}\left.\frac{A_2}{A_1}\frac{dq^3(x)}{dx^3}\right|_{x=0}-C_{14}=\frac{1}{2\lambda^2}\frac{E_a}{h_a}\frac{M_T(0)}{E_bI_b}\\&-\frac{1}{2\lambda^3}\frac{E_a}{h_a}\frac{1}{E_bI_b}Q_T(0)+\frac{1}{2\lambda^3}\left.\frac{A_2}{A_1}\frac{dq^3(x)}{dx^3}\right|_{x=0}+\frac{1}{2\lambda^2}\left.\frac{A_2}{A_1}\frac{dq^2(x)}{dx}\right|_{x=0}\end{aligned} \tag{38}$$

5.3. Two-Parameter Elastic Foundation Model

As is stated above, though the one-parameter model is simple and easy to use by representing the stiffness of the vertical springs with a parameter, k, the inability to take the shear force and the shear strain along the adhesive layers into account makes the one-parameter theory clearly less precise. To confront this shortage, the improved two-parameter elastic foundation theory, in which various types of interactions between Winkler's independent springs are closer to reality, is introduced and developed by Filonenko-Borodich, Hetényi, Pasternak, Kerr, Vlasov and Leontievt (Figure 19).

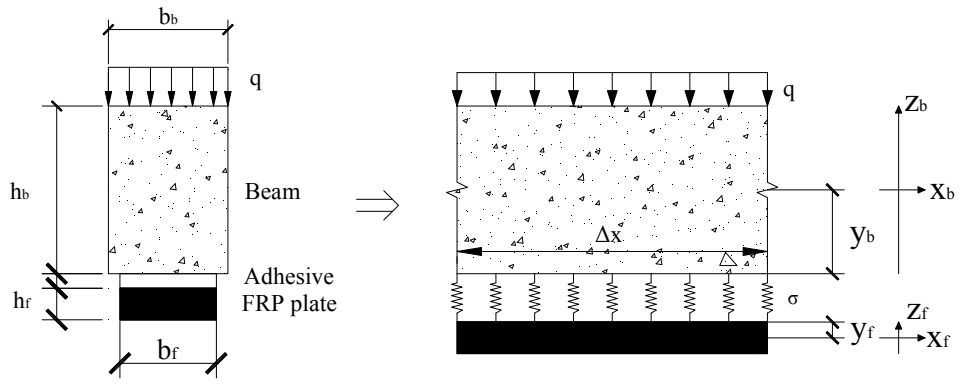

Figure 19. Free body diagram for two-parameter

$$\begin{Bmatrix}\sigma_{xx}\\ \sigma_{zz}\\ \sigma_{xz}\end{Bmatrix}=\begin{bmatrix}\frac{E}{1-v^2} & \frac{vE}{1-v^2} & 0\\ \frac{vE}{1-v^2} & \frac{E}{1-v^2} & 0\\ 0 & 0 & \frac{(1-v)E}{2(1-v^2)}\end{bmatrix}\begin{Bmatrix}\varepsilon_{xx}\\ \varepsilon_{zz}\\ r_{xz}\end{Bmatrix}=\frac{E}{1-v^2}\begin{bmatrix}1 & v & 0\\ v & 1 & 0\\ 0 & 0 & \frac{1-v}{2}\end{bmatrix}\begin{Bmatrix}\frac{\partial u}{\partial x}\\ \frac{\partial w}{\partial z}\\ \frac{\partial u}{\partial z}+\frac{\partial w}{\partial x}\end{Bmatrix} \quad (39)$$

Both theories have been used to find an applicable and simple model of representing a joint adhesive. Two-parameter elastic foundation models are much more acceptable. While one of the

two parameters is allocated, as in Winkler's model, to the rigidity of normal springs, the other one is assigned to interfacial shear force of the joint bond [1][2].

$$\left\{\varepsilon_f\right\}=\begin{Bmatrix}\varepsilon_{f-xx}\\ \varepsilon_{f-zz}\\ r_{f-xz}\end{Bmatrix}=\begin{Bmatrix}\dfrac{\partial u_f}{\partial x}\\ \dfrac{\partial w_f}{\partial z}\\ \dfrac{\partial u_f}{\partial z}+\dfrac{\partial w_f}{\partial x}\end{Bmatrix}=\begin{bmatrix}\partial/\partial x & 0\\ 0 & \partial/\partial y\\ \partial/\partial y & \partial/\partial x\end{bmatrix}\begin{Bmatrix}u_f\\ w_f\end{Bmatrix}=\begin{Bmatrix}\varepsilon_{f-xx}^{M}+\varepsilon_{f-xx}^{N}+\varepsilon_{f-xx}^{T}\\ \dfrac{\partial w_f}{\partial z}\\ \dfrac{\partial u_f}{\partial z}+\dfrac{\partial w_f}{\partial x}\end{Bmatrix}$$

$$=\begin{Bmatrix}\pm\dfrac{y_b}{E_f I_f}M_f(x)+\dfrac{\partial {u_f}^{N}}{\partial x}+\alpha_f\Delta t\\ \dfrac{\partial w_f}{\partial z}\\ \dfrac{\partial {u_f}^{N}}{\partial z}+\dfrac{\partial {w_f}^{N}}{\partial x}\end{Bmatrix} \tag{40}$$

5.3.1. Applying equilibrium equations

With the help of equilibrium equations, the relationship of moments, shear forces, axial forces can be built showing in Figure 20.

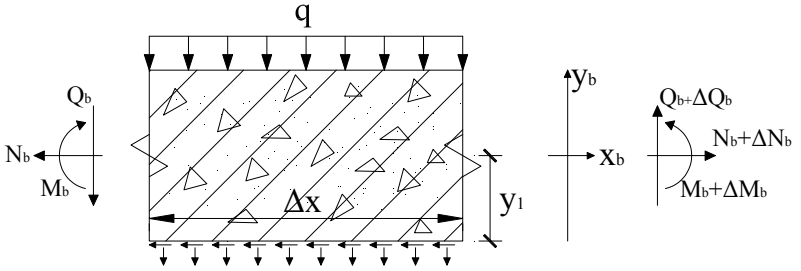

(a) concrete beam

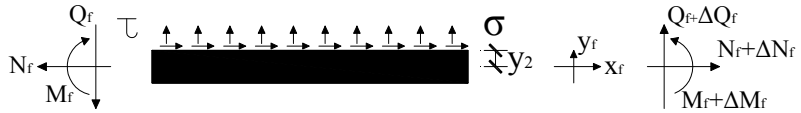

(b) FRP plate

Figure 20. Free-body diagram for two-parameter model

Differential axial force can be calculated by tracking the balance of force in x direction.

$$\Delta N_b = \tau_{xx} b_f \Delta x, \qquad \Delta N_f = -\tau_{xx} b_f \Delta x \tag{41}$$

$$\frac{dN_b}{dx} = \tau_{xx} b_f, \qquad \frac{dN_f}{dx} = -\tau_{xx} b_f \tag{42}$$

Differential shear force can be calculated by tracking the balance of force in y direction.

$$\Delta Q_b = q(x)\Delta x + \sigma(x) b_f \Delta x, \qquad \Delta Q_f = -\sigma(x) b_f \Delta x \tag{43}$$

$$\frac{dQ_b}{dx} = q(x) + \sigma(x) b_f, \qquad \frac{dQ_f}{dx} = -\sigma(x) b_f \tag{44}$$

Differential shear force can be calculated by tracking the balance of moment at the right bottom of each component.

$$\begin{aligned} &\Delta M_b + Q_b \times \frac{\Delta x}{2} + (Q_b + \Delta Q_b) \times \frac{\Delta x}{2} - \tau_{xx} b_f \Delta x y_1 = 0, \\ &\Delta M_f + Q_f \times \frac{\Delta x}{2} + (Q_f + \Delta Q_f) \times \frac{\Delta x}{2} - \tau_{xx} b_f \Delta x y_2 = 0 \end{aligned} \tag{45}$$

yi(i=a,b) is the distance from interface of the bond joint to the centroidal principal axis of the respective adherent.

Therefore,

$$\begin{aligned} &\frac{dM_b}{dx} = -Q_b - \frac{\Delta Q_b}{2} + \tau_{xx} b_f y_1, \\ &\frac{dM_f}{dx} = -Q_f - \frac{\Delta Q_f}{2} + \tau_{xx} b_f y_2 \end{aligned} \tag{46}$$

Δx is very small, $\frac{\Delta Q_b}{2} \approx 0, \frac{\Delta Q_f}{2} \approx 0$

Then $\frac{dM_b}{dx} = -Q_b + \frac{1}{2} b_f h_b \tau_{xx}, \qquad \frac{dM_f}{dx} = -Q_f + \frac{1}{2} b_f h_f \tau_{xx}$ (47)

Summarizing the relationship as bellow

$$\begin{cases} \dfrac{dN_b}{dx}=\tau_{xx}b_f, \qquad \dfrac{dN_f}{dx}=-\dfrac{dN_b}{dx}=-\tau_{xx}b_f \\ \dfrac{dQ_b}{dx}=q(x)+\sigma(x)b_f, \qquad \dfrac{dQ_f}{dx}=-\sigma(x)b_f \\ \dfrac{dM_b}{dx}=-Q_b+b_f y_1\tau_{xx}, \qquad \dfrac{dM_f}{dx}=-Q_f+b_f y_2\tau_{xx} \end{cases} \tag{48}$$

5.3.2. Applying continuative equations

In the continuative equations, the strains of components takes consider in all three deformations: axial, bending and shear. Figure 21 takes part of the FRP plate under consideration. Firstly to separately consider the moment effects, it is assumed that the FRP-reinforced is subjected to pure bending.

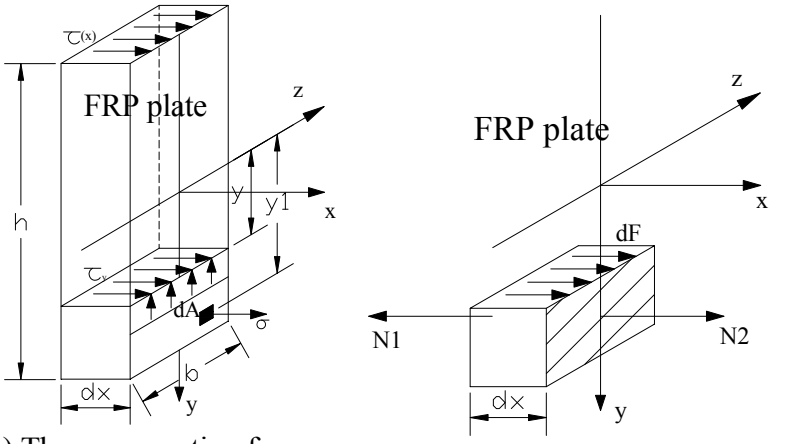

(a) The cross-section force of the concrete beam

(b) Differential segment

Figure 21. Differential segment of partial FRP plate

Under pure bending, the force can be worked out through integration

$$\begin{aligned} N_1&=\int_A\sigma_1 dA=\int_A\frac{My_1}{I_z}dA=\frac{M}{I_z}\int_A y_1 dA=\frac{M}{I_z}\int_y^{\frac{h}{2}} y_1 dby_1=\frac{M}{I_z}\frac{b}{2}\left(\frac{h^2}{4}-y^2\right) \\ N_2&=\int_A\sigma_2 dA=\int_A\frac{(M+dM)y_1}{I_z}dA=\frac{(M+dM)}{I_z}\int_A y_1 dA=\frac{(M+dM)}{I_z}\frac{b}{2}\left(\frac{h^2}{4}-y^2\right) \end{aligned} \tag{49}$$

σ_1 and σ_2 are the normal stress at $y = y_1$. In the longitudinal direction, $dF = \tau_y b dx$,

Assuming that τ_y remains same at the same y, and neglecting the change of τ_y in *dx*.

For the concrete beam,

The equilibrium equation for dx is $N_{2b} - N_{1b} + dF_b - \tau(x) b_b dx = 0$ (50)

$$dF_b = N_{1b} - N_{2b} + \tau(x) b_b dx = \tau_{yb} b_b dx \tag{51}$$

$$\tau_{yb} b_b dx = N_{1b} - N_{2b} + \tau(x) b_b dx = -\frac{dM_b}{I_z} \frac{b_b}{2} \left(\frac{h_b^2}{4} - y_b^2 \right) + \tau(x) b_b dx \tag{52}$$

$$\tau_{yb} = -\frac{dM_b}{dx I_z} \frac{1}{2} \left(\frac{h_b^2}{4} - y_b^2 \right) + \tau(x) \tag{53}$$

Inserting the beam equilibrim equation, $\frac{dM_b}{dx} = -Q_b + b_f y_b \tau(x)$

$$\begin{aligned} \tau_{yb} &= -\frac{\left(-Q_b + b_f y_b \tau(x)\right)}{dx I_z} \frac{1}{2} \left(\frac{h_b^2}{4} - y_b^2 \right) + \tau(x) \\ &= \frac{1}{I_z} \frac{1}{2} \left(\frac{h_b^2}{4} - y_b^2 \right) Q_b - \frac{b_f y_b}{I_z} \frac{1}{2} \left(\frac{h_b^2}{4} - y_b^2 \right) \tau(x) + \tau(x) \end{aligned} \tag{54}$$

With the reciprocal law of shear stress $\tau = \tau_y$

$$\tau_b = \frac{1}{I_z} \frac{1}{2} \left(\frac{h_b^2}{4} - y_b^2 \right) Q_b - \frac{b_f y_b}{I_z} \frac{1}{2} \left(\frac{h_b^2}{4} - y_b^2 \right) \tau(x) + \tau(x) \tag{55}$$

In this equation, Q_b and τ_b have the same direction

Q_b is the shear stress,

I_{zb} is the moment of inertia,

b_b is the width of the concrete beam,

h_b is the height of the concrete beam.

The shear strain generated by the shear force is

$$\gamma=\frac{\tau_b}{G_b}=\frac{1}{I_z}\frac{1}{2G_b}\left(\frac{h_b{}^2}{4}-y_b{}^2\right)Q_b-\frac{b_f y_b}{I_z}\frac{1}{2G_b}\left(\frac{h_b{}^2}{4}-y_b{}^2\right)\tau(x)+\frac{1}{G_b}\tau(x)=\frac{\partial u_b}{\partial y}+\frac{\partial w_b}{\partial x} \quad (56)$$

G is the shear modulus, *u,w* are the displacements in the x, y direction.

Assuming there is no deformation in the cross-section, w and y are independent.

$$u_b=-y_b\frac{\partial w_b}{\partial x}+\frac{1}{I_z}\frac{y_b}{2G_b}\left(\frac{h_b{}^2}{4}-\frac{1}{3}y_b{}^2\right)Q_b-\frac{b_f y_b^2}{I_z}\frac{1}{8G_b}\left(h_b{}^2-2y_b{}^2\right)\tau(x)+\frac{y_b}{G_b}\tau(x)+C(x) \quad (57)$$

At the neutral axis, there is no longitude displacement.

$$u_b\big|_{y_b=0}=0\,,\qquad u_b\big|_{y_b=0}=C(x)=0$$

$$\varepsilon_{xb}=\frac{du_b}{dx}=-y_b\frac{d^2w_b}{\partial x^2}+\frac{1}{I_z}\frac{y_b}{2G_b}\left(\frac{h_b{}^2}{4}-\frac{1}{3}y_b{}^2\right)\frac{dQ_b}{dx}$$
$$-\frac{b_f y_b^2}{I_z}\frac{1}{8G_b}\left(h_b{}^2-2y_b{}^2\right)\frac{d\tau(x)}{dx}+\frac{y_b}{G_b}\frac{d\tau(x)}{dx} \quad (58)$$

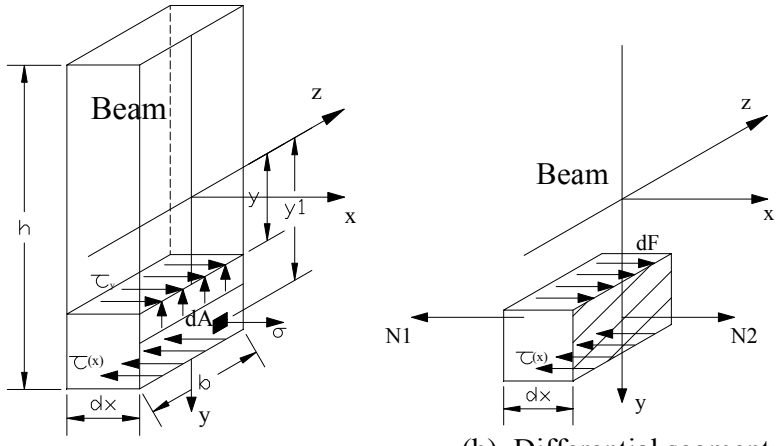

(a) The cross-section force of the concrete beam

(b) Differential segment

Figure 22. Differential segment of partial concrete beam

Substituting $w''=-\frac{M(x)}{EI}$ into ε_{xb}

$$\varepsilon_{xb} = y_b \frac{M_b(x)}{E_b I_b} + \frac{1}{I_z}\frac{y_b}{2G_b}\left(\frac{h_b^{\,2}}{4} - \frac{1}{3}y_b^{\,2}\right)\frac{dQ_b}{dx} - \frac{b_f y_b^2}{I_z}\frac{1}{8G_b}\left(h_b^{\,2} - 2y_b^{\,2}\right)\frac{d\tau(x)}{dx} + \frac{y_b}{G_b}\frac{d\tau(x)}{dx} \tag{59}$$

Following the same steps above, ε_{xf} is calculated as:

$$\varepsilon_{xf} = \frac{du_f}{dx} = y_f \frac{M_f(x)}{E_f I_f} + \frac{1}{I_f}\frac{y_f}{2G_f}\left(\frac{h_f^{\,2}}{4} - \frac{1}{3}y_f^{\,2}\right)\frac{dQ_f}{dx} - \frac{b_f y_f^2}{I_f}\frac{1}{8G_b}\left(h_f^{\,2} - 2y_f^{\,2}\right)\frac{d\tau(x)}{dx} \tag{60}$$

The adhesive layer is subjected to uniform shear stresses, and then across the thickness of adhesive, *u* remains linear. The above analysis are all based on the pure bending, to get the whole strain, the strain generated by axial deformation are added into the equation (59) and (60).

$$\varepsilon_{xb}\left(x, \frac{h_f}{2}\right) = \frac{h_b}{2}\frac{M_b(x)}{E_b I_b} + \frac{N_b(x)}{E_b A_b} + \frac{1}{I_{zb}}\frac{h_b^3}{24G_b}\frac{dQ_b}{dx} - \frac{b_f h_b^4}{I_{zb}}\frac{1}{64G_b}\frac{d\tau(x)}{dx} + \frac{h_b}{2G_b}\frac{d\tau(x)}{dx} \tag{61}$$

$$\varepsilon_f\left(x, -\frac{h_f}{2}\right) = -\frac{h_f}{2}\frac{M_f(x)}{E_f I_f} + \frac{N_f(x)}{E_f A_f} - \frac{1}{I_{zf}}\frac{h_f^3}{24G_f}\frac{dQ_f}{dx} - \frac{b_f}{I_{zf}}\frac{1}{64G_f}h_f^{\,4}\frac{d\tau(x)}{dx} \tag{62}$$

5.3.3. Calculating $\tau(x)$

In this analysis, τ_{xx} is assumedly uniform and the $u(x,y)$ can be deemed to change linearly across the adhesive height.

$$\frac{du_a}{dy} = \frac{1}{h_a}\left(u_b(x,y) - u_f(x,y)\right) \tag{63}$$

$$\frac{d\tau(x)}{dx} = G_a\left(\frac{d^2u_a(x,y)}{dxdy} + \frac{d^2w_a(x,y)}{dx^2}\right) \tag{64}$$

$$\begin{aligned}
&\frac{d^2u_a}{dxdy}=\frac{1}{h_a}\left(\frac{du_b(x,y)}{dx}-\frac{du_f(x,y)}{dx}\right)=\frac{1}{h_a}\left(\varepsilon_b\left(x,\frac{h_b}{2}\right)-\varepsilon_f\left(x,-\frac{h_f}{2}\right)\right)\\
&\frac{d^2w_a(x,y)}{dx^2}=-\frac{M_a(x)}{E_aI_a}\approx 0
\end{aligned} \tag{65}$$

$$\frac{d\tau(x)}{dx}\approx G_a\frac{d^2u_a(x,y)}{dxdy}=\frac{G_a}{h_a}\left(\varepsilon_b\left(x,\frac{h_b}{2}\right)-\varepsilon_f\left(x,-\frac{h_f}{2}\right)\right) \tag{66}$$

Inputting the equation (61) and the equation (62) into (64), it is the governing differential equation of $\tau(x)$

$$\begin{aligned}
&\frac{d\tau(x)}{dx}\\
&=\frac{G_a}{h_a}\left(\begin{array}{l}\left(\frac{h_b}{2}\frac{M_b(x)}{E_bI_b}+\frac{N_b(x)}{E_bA_b}+\frac{1}{I_{zb}}\frac{h_b^3}{24G_b}\frac{dQ_b}{dx}-\frac{b_fh_b^4}{I_{zb}}\frac{1}{64G_b}\frac{d\tau(x)}{dx}+\frac{h_b}{2G_b}\frac{d\tau(x)}{dx}\right)\\ -\left(-\frac{h_f}{2}\frac{M_f(x)}{E_fI_f}+\frac{N_f(x)}{E_fA_f}-\frac{1}{I_{zf}}\frac{h_f^3}{24G_f}\frac{dQ_f}{dx}-\frac{b_fh_f^4}{I_{zf}}\frac{1}{64G_f}\frac{d\tau(x)}{dx}\right)\end{array}\right)\\
&=\frac{G_a}{h_a}\left(\begin{array}{l}\frac{h_f}{2}\frac{M_f(x)}{E_fI_f}-\frac{N_f(x)}{E_fA_f}+\frac{h_b}{2}\frac{M_b(x)}{E_bI_b}+\frac{N_b(x)}{E_bA_b}+\frac{1}{I_{zf}}\frac{h_f^3}{24G_f}\frac{dQ_f}{dx}\\ +\frac{1}{I_{zb}}\frac{h_b^3}{24G_b}\frac{dQ_b}{dx}+\frac{b_fh_f^4}{I_{zf}}\frac{1}{64G_f}\frac{d\tau(x)}{dx}-\frac{b_fh_b^4}{I_{zb}}\frac{1}{64G_b}\frac{d\tau(x)}{dx}+\frac{h_b}{2G_b}\frac{d\tau(x)}{dx}\end{array}\right)
\end{aligned} \tag{67}$$

Since the deflections are small, by approximately assuming they have same curvature, the relationship between the moments could be written as $M_b(x)=\frac{E_bI_b}{E_fI_f}M_f(x)$, the Amir M. Malek et al.[46] listed the equations of bending moment, but they omitted the affection of peeling stress. So their answers are not applicable.

$$M_T=M_b(x)+M_f(x)+N_f\left(\frac{h_b}{2}+\frac{h_f}{2}+h_a\right) \tag{68}$$

Where,

$$M_f(x)=\frac{E_fI_f}{E_bI_b+E_fI_f}\left(M_T-N_f\left(\frac{h_b}{2}+\frac{h_f}{2}+h_a\right)\right)$$
$$M_b(x)=\frac{E_bI_b}{E_bI_b+E_fI_f}\left(M_T+N_b\left(\frac{h_b}{2}+\frac{h_f}{2}+h_a\right)\right) \tag{69}$$

Inputting equation (68) into equation (67), the governing differential equation is

$$\frac{d\tau(x)}{dx}=-B_3M_T-\frac{1}{B_2}\frac{G_a}{h_a}\frac{\left(\frac{h_b}{2}+\frac{h_f}{2}+h_a\right)}{2\left(E_bI_b+E_fI_f\right)}\left(h_fN_f-h_bN_b\right)$$
$$-\frac{1}{B_2}\frac{G_a}{h_a}\frac{N_f(x)}{E_fA_f}+\frac{G_a}{h_a}\frac{N_b(x)}{E_bA_b}+B_4\sigma(x)-B_5q(x) \tag{70}$$

$$\frac{d\tau^2(x)}{dx^2}-B_1\tau(x)=-B_3\frac{dM_T}{dx}+B_4\frac{d\sigma(x)}{dx}-B_5\frac{dq(x)}{dx} \tag{71}$$

$$\text{Where } B_1=b_f\frac{G_a}{h_a}\left(\frac{\left(\frac{h_b}{2}+\frac{h_f}{2}+h_a\right)}{2\left(E_bI_b+E_fI_f\right)}\left(h_f+h_b\right)+\frac{1}{E_fA_f}+\frac{1}{E_bA_b}\right)\frac{1}{B_2} \tag{72}$$

$$B_2=1-\frac{G_a}{h_a}\left(\frac{b_fh_b^4}{I_{zb}}\frac{1}{64G_b}-\frac{b_fh_f^4}{I_{zf}}\frac{1}{64G_f}-\frac{h_b}{2G_b}\right)\quad B_3=-\frac{1}{B_2}\frac{G_a}{h_a}\frac{\left(h_f+h_b\right)}{2\left(E_bI_b+E_fI_f\right)} \tag{73}$$

$$B_4=-\frac{1}{B_2}\frac{G_a}{h_a}\frac{b_f}{24}\left(\frac{1}{I_{zf}}\frac{h_f^3}{G_f}-\frac{1}{I_{zb}}\frac{h_b^3}{G_b}\right),\quad B_5=-\frac{1}{B_2}\frac{G_a}{h_a}\frac{1}{I_{zb}}\frac{h_b^3}{24G_b} \tag{74}$$

The general solution to equation (70) and (71) is given by

$$\tau(x)=C_{21}\times e^{\sqrt{B_1}x}+C_{22}\times e^{-\sqrt{B_1}x}+\frac{B_3}{B_1}\frac{dM_T}{dx}-\frac{B_4}{B_1}\frac{d\sigma(x)}{dx}+\frac{B_5}{B_1}\frac{dq(x)}{dx} \tag{75}$$

5.3.4. Calculating $\sigma(x)$

Based on the above one-parameter analysis, we can get the normal stress first.

The stiffness of the vertical spring is $k_a = \frac{E_a}{h_a}$

$$\sigma(x) = \frac{E_a}{h_a}\Delta w(x) = \frac{E_a}{h_a}\left(w_f(x) - w_b(x)\right) \tag{76}$$

For a differential element, its curvature can be indicated by its applied moment $M(x)$

$$w'' = -\frac{M(x)}{EI} \quad \Rightarrow \quad \frac{dw_b^2(x)}{dx^2} = -\frac{M_b(x)}{E_b I_b}, \frac{dw_f^2(x)}{dx^2} = -\frac{M_f(x)}{E_f I_f} \tag{77}$$

Here, EI is the flexural stiffness for each component.

Differentiating equation (77) on both side twice, the differential equations are changed into follows in the light of $\sigma(x)$,

$$\frac{dw_b^4(x)}{dx^4} = -\frac{1}{E_b I_b}\frac{dM_b^2(x)}{dx^2} = \frac{1}{E_b I_b}\left(q(x) + \sigma(x)b_f - b_f y_1 \frac{d\tau_{xx}}{dx}\right) \tag{78}$$

$$\frac{dw_f^4(x)}{dx^4} = -\frac{1}{E_f I_f}\frac{dM_f^2(x)}{dx^2} = -\frac{1}{E_f I_f}\left(\sigma(x)b_f + b_f y_2 \frac{d\tau_{xx}}{dx}\right) \tag{79}$$

Substituting (78) and (79) into (76)

$$\begin{aligned}\frac{d\sigma^4(x)}{dx^4} &= \frac{E_a}{h_a}\left(\frac{dw_f^4(x)}{dx^4} - \frac{dw_b^4(x)}{dx^4}\right) = \frac{E_a}{h_a}\begin{pmatrix} -\frac{1}{E_f I_f}\left(\sigma(x)b_f + b_f y_2 \frac{d\tau(x)}{dx}\right) \\ -\frac{1}{E_b I_b}\left(q(x) + \sigma(x)b_f - b_f y_1 \frac{d\tau(x)}{dx}\right)\end{pmatrix} \\ &= \frac{E_a}{h_a}\begin{pmatrix} -\frac{1}{E_f I_f}\sigma(x)b_f - \frac{1}{E_f I_f}b_f y_2 \frac{d\tau(x)}{dx} \\ -\frac{1}{E_b I_b}q(x) - \frac{1}{E_b I_b}\sigma(x)b_f + \frac{1}{E_b I_b}b_f y_1 \frac{d\tau(x)}{dx}\end{pmatrix} \\ &= -\frac{E_a}{h_a}\left(\frac{1}{E_f I_f} + \frac{1}{E_b I_b}\right)\sigma(x)b_f + \frac{E_a}{h_a}\left(\frac{b_f y_1}{E_b I_b} - \frac{b_f y_2}{E_f I_f}\right)\frac{d\tau(x)}{dx}\end{aligned} \tag{80}$$

$\sigma(x)$ and $\tau(x)$ are coupled in this differential equations and difficult to solve this equations set. In order to simple this problem, the author neglect the influence of shear deformations in both structures.

Then $\tau(x)$ change into $\tau(x) = C_{21} \times e^{\sqrt{B_1}x} + C_{22} \times e^{-\sqrt{B_1}x} + \frac{B_3}{B_1}\frac{dM_T}{dx} + \frac{B_5}{B_1}\frac{dq(x)}{dx}$

The governing equation changes into

$$\frac{d\sigma^4(x)}{dx^4} + F_1\sigma(x) = \frac{F_2}{\sqrt{B_1}}\frac{d\tau(x)}{dx} \tag{81}$$

$$\frac{d\sigma^4(x)}{dx^4} + F_1\sigma(x) = F_2C_{21} \times e^{\sqrt{B_1}x} - F_3C_{22} \times e^{-\sqrt{B_1}x} + \frac{F_2}{\sqrt{B_1}}\frac{B_3}{B_1}\frac{d^2M_T}{dx^2} + \frac{F_2}{\sqrt{B_1}}\frac{B_5}{B_1}\frac{d^2q(x)}{dx^2} \tag{82}$$

Where, $F_1 = \frac{E_a b_f}{h_a}\left(\frac{1}{E_f I_f} + \frac{1}{E_b I_b}\right)$, $F_2 = \sqrt{B_1}\frac{E_a}{h_a}b_f\left(\frac{y_1}{E_b I_b} - \frac{y_2}{E_f I_f}\right)$, $F_3 = F_2$,

$$F_4 = \frac{B_3}{B_1\sqrt{B_1}}F_2,\ F_5 = \frac{B_5}{B_1\sqrt{B_1}}F_2 \tag{83}$$

Using the same method in the one-parameter medal, the general solution of the corresponding homogeneous equation is

$$\begin{aligned}\sigma(x) = {} & e^{\beta x}(C_{31}\cos\beta x + C_{32}\sin\beta x) + e^{-\beta x}\left(C_{33}\cos\beta x + C_{34}\sin\beta x\right) \\ & + \sigma_{31}(x) + \sigma_{32}(x) + \sigma_{33}(x) + \sigma_{34}(x)\end{aligned} \tag{84}$$

Where $\beta = \sqrt[4]{\frac{F_1}{4}}$

C31, C32, C33, and C34 are arbitrarily constant coefficients decided by boundary conditions

$\sigma_{31}(x)=\frac{F_2}{F_1}C_{21}e^{\sqrt{B_1}x}$ is one special solution corresponding to $F_2C_{21}\times e^{\sqrt{B_1}x}$

$\sigma_{32}(x)=-\frac{F_3}{F_1}C_{22}\times e^{-\sqrt{B_1}x}$ is one special solution corresponding to $-F_3C_{22}\times e^{-\sqrt{B_1}x}$

$\sigma_{33}(x)=-\frac{F_4}{F_1}\frac{d^2M_T}{dx^2}$ is one special solution corresponding to $F_4\frac{d^2M_T}{dx^2}$

$\sigma_{35}=\frac{F_5}{F_1}\frac{d^2q(x)}{dx^2}$ is one special solution corresponding to $F_5\frac{d^2q(x)}{dx^2}$

x is starting from the left intersection of concrete beam and FRP plate, in another word, x is always positive. With the increase of x, the normal stress is approaching zero, and as a result $C_{31}=C_{32}=0$ for large x.

$$\sigma(x)=e^{-\beta x}\left(C_{33}\cos\beta x+C_{34}\sin\beta x\right)+\frac{F_2}{F_1}C_{21}e^{\sqrt{B_1}x}-\frac{F_3}{F_1}C_{22}e^{-\sqrt{B_1}x}+\frac{F_4}{F_1}\frac{d^2M_T}{dx^2}+\frac{F_5}{F}\frac{d^2q(x)}{dx^2} \tag{85}$$

Substituting $\sigma(x)$ into $\tau(x)$, the expression of $\tau(x)$ is given

$$\begin{aligned}\tau(x)=&\left(1-\frac{B_4}{B_1}\frac{F_2}{F_1}\sqrt{B_1}\right)\left(C_{21}e^{\sqrt{B_1}x}+C_{22}e^{-\sqrt{B_1}x}\right)+\frac{B_4}{B_1}\beta e^{-\beta x}C_{33}\left(\cos\beta x+\sin\beta x\right)\\&+\frac{B_4}{B_1}\beta C_{34}\left(\sin\beta x-\cos\beta x\right)-\frac{B_4}{B_1}\frac{1}{F_1}\left(F_4\frac{d^3M_T}{dx^3}+F_5\frac{d^3q(x)}{dx^3}\right)\\&+\frac{1}{B_1}\left(B_3\frac{dM_T}{dx}+B_5\frac{dq(x)}{dx}\right)\end{aligned} \tag{86}$$

5.3.5. Using the boundary conditions

The moment of FRP plate is boundary free at x=0 with zero moment $M_{f(x=0)}=0$ and zero axial force $Q_{f(x=0)}=0$. Between the plate end and the beam end, the moment in this section is only

resisted by the concrete beam.The secondary boundary condition is at $x = L_s$, where shear force and stress are both zero.

$$\text{X=0,} \qquad N_f(0) = N_b(0) = 0, \qquad Q_f(0) = 0 \qquad M_f(0) = 0 \tag{87}$$

$$x = L_s \qquad \tau(L_s) = 0 \tag{88}$$

Assuming L_s is the length from left end of FRP plate (x=0) to the point of zero shear force.

The equation (70) at the plate end yields:

$$\begin{aligned}
\left.\frac{d\tau(x)}{dx}\right|_{x=0} &= \sqrt{B_1}C_{21} - \sqrt{B_1}C_{22} + \frac{B_3}{B_1}\left.\frac{d^2M_T}{dx^2}\right|_{x=0} + \frac{B_5}{B_1}\left.\frac{d^2q(x)}{dx^2}\right|_{x=0} \\
&\quad - \frac{B_4}{B_1}\left(-2\beta^2 C_{34} + \frac{F_2}{F_1}B_1C_{21} - B_1\frac{F_3}{F_1}C_{22} + \frac{F_4}{F_1}\left.\frac{d^4M_T}{dx^4}\right|_{x=0} + \frac{F_5}{F}\left.\frac{d^4q(x)}{dx^4}\right|_{x=0}\right) \\
&= -B_3M_T(0) + B_4C_{33} + B_4\frac{F_2}{F_1}C_{21} - B_4\frac{F_3}{F_1}C_{22} \\
&\quad + B_4\frac{F_4}{F_1}\left.\frac{d^2M_T}{dx^2}\right|_{x=0} + B_4\frac{F_5}{F}\left.\frac{d^2q(x)}{dx^2}\right|_{x=0} - B_5q(0)
\end{aligned} \tag{89}$$

$$\begin{aligned}
C_{21} &= C_{22} + F_7B_4C_{33} - 2F_7\frac{B_4}{B_1}\beta^2C_{34} + F_7\left(B_4\frac{F_4}{F_1} - \frac{1}{B_1}B_3 + \right)\left.\frac{d^2M_T}{dx^2}\right|_{x=0} \\
&\quad + F_7\left(B_4\frac{F_5}{F} - \frac{1}{B_1}B_5\right)\left.\frac{d^2q(x)}{dx^2}\right|_{x=0} \\
&\quad - F_7\left(B_5q(0) + B_3M_T(0)\right) + F_7\left(\frac{B_4}{B_1}\frac{F_4}{F_1}\left.\frac{d^4M_T}{dx^4}\right|_{x=0} + \frac{B_4}{B_1}\frac{F_5}{F_1}\left.\frac{d^4q(x)}{dx^4}\right|_{x=0}\right)
\end{aligned} \tag{90}$$

Where,

$$F_7 = \frac{1}{\left(\sqrt{B_1} - 2B_4\frac{F_2}{F_1}\right)}$$

$$\tau(L_s) = C_{21}\times e^{\sqrt{B_1}L_s} + C_{22}\times e^{-\sqrt{B_1}L_s} + \frac{B_3}{B_1}\left.\frac{dM_T}{dx}\right|_{x=L_s} + \frac{B_5}{B_1}\left.\frac{dq(x)}{dx}\right|_{x=L_s} = 0 \tag{91}$$

$$
\begin{aligned}
C_{22} = & -\frac{e^{\sqrt{B_1}L_s}}{\left(e^{-\sqrt{B_1}L_s}+e^{\sqrt{B_1}L_s}\right)}F_7B_4C_{33}+2\frac{e^{\sqrt{B_1}L_s}}{\left(e^{-\sqrt{B_1}L_s}+e^{\sqrt{B_1}L_s}\right)}F_7\frac{B_4}{B_1}\beta^2C_{34} \\
& -F_7\frac{e^{\sqrt{B_1}L_s}}{\left(e^{-\sqrt{B_1}L_s}+e^{\sqrt{B_1}L_s}\right)}\left(\frac{B_4}{B_1}\frac{F_4}{F_1}\frac{d^4M_T}{dx^4}\bigg|_{x=0}+\frac{B_4}{B_1}\frac{F_5}{F_1}\frac{d^4q(x)}{dx^4}\bigg|_{x=0}\right) \\
& -F_7\frac{e^{\sqrt{B_1}L_s}}{\left(e^{-\sqrt{B_1}L_s}+e^{\sqrt{B_1}L_s}\right)}\left(B_4\frac{F_4}{F_1}-\frac{1}{B_1}B_3+\right)\frac{d^2M_T}{dx^2}\bigg|_{x=0} \\
& -F_7\frac{e^{\sqrt{B_1}L_s}}{\left(e^{-\sqrt{B_1}L_s}+e^{\sqrt{B_1}L_s}\right)}\left(B_4\frac{F_5}{F}-\frac{1}{B_1}B_5\right)\frac{d^2q(x)}{dx^2}\bigg|_{x=0} \\
& +F_7\frac{e^{\sqrt{B_1}L_s}}{\left(e^{-\sqrt{B_1}L_s}+e^{\sqrt{B_1}L_s}\right)}\left(B_5q(0)+B_3M_T(0)\right) \\
& -\frac{1}{\left(e^{-\sqrt{B_1}L_s}+e^{\sqrt{B_1}L_s}\right)}\frac{B_3}{B_1}\frac{dM_T}{dx}\bigg|_{x=L_s}-\frac{1}{\left(e^{-\sqrt{B_1}L_s}+e^{\sqrt{B_1}L_s}\right)}\frac{B_5}{B_1}\frac{dq(x)}{dx}\bigg|_{x=L_s}
\end{aligned}
\tag{92}
$$

Inputting C_{22} into equation (89) and (90), C_{21} is expressed in term of C_{33}, C_{34}

$$
\begin{aligned}
C_{21} = & \frac{e^{-\sqrt{B_1}L_s}}{\left(e^{-\sqrt{B_1}L_s}+e^{\sqrt{B_1}L_s}\right)}F_7B_4C_{33}-2\frac{e^{-\sqrt{B_1}L_s}}{\left(e^{-\sqrt{B_1}L_s}+e^{\sqrt{B_1}L_s}\right)}F_7\frac{B_4}{B_1}\beta^2C_{34} \\
& +F_7\frac{e^{-\sqrt{B_1}L_s}}{\left(e^{-\sqrt{B_1}L_s}+e^{\sqrt{B_1}L_s}\right)}\left(\frac{B_4}{B_1}\frac{F_4}{F_1}\frac{d^4M_T}{dx^4}\bigg|_{x=0}+\frac{B_4}{B_1}\frac{F_5}{F_1}\frac{d^4q(x)}{dx^4}\bigg|_{x=0}\right) \\
& +F_7\frac{e^{-\sqrt{B_1}L_s}}{\left(e^{-\sqrt{B_1}L_s}+e^{\sqrt{B_1}L_s}\right)}\left(B_4\frac{F_4}{F_1}-\frac{1}{B_1}B_3\right)\frac{d^2M_T}{dx^2}\bigg|_{x=0} \\
& +F_7\frac{e^{-\sqrt{B_1}L_s}}{\left(e^{-\sqrt{B_1}L_s}+e^{\sqrt{B_1}L_s}\right)}\left(B_4\frac{F_5}{F}-\frac{1}{B_1}B_5\right)\frac{d^2q(x)}{dx^2}\bigg|_{x=0} \\
& -F_7\frac{e^{-\sqrt{B_1}L_s}}{\left(e^{-\sqrt{B_1}L_s}+e^{\sqrt{B_1}L_s}\right)}\left(B_5q(0)+B_3M_T(0)\right) \\
& -\frac{1}{\left(e^{-\sqrt{B_1}L_s}+e^{\sqrt{B_1}L_s}\right)}\frac{1}{B_1}\left(B_3\frac{dM_T}{dx}\bigg|_{x=L_s}+B_5\frac{dq(x)}{dx}\bigg|_{x=L_s}\right)
\end{aligned}
\tag{93}
$$

Differentiating equation (76) and putting equation (67) (85) into the results lead to

$$\left.\frac{d^2\sigma(x)}{dx}\right|_{x=0} = -2\beta^2 C_{34} + \frac{F_2}{F_1} B_1 C_{21} - B_1 \frac{F_3}{F_1} C_{22} + \left.\frac{F_4}{F_1}\frac{d^4 M_T}{dx^4}\right|_{x=0} + \left.\frac{F_5}{F_1}\frac{d^4 q(x)}{dx^4}\right|_{x=0} = \frac{E_a}{h_a}\frac{M_T(0)}{E_b I_b} \tag{94}$$

$$C_{34} = \frac{F_2}{F_1\sqrt{F_1}} B_1 (C_{21} - C_{22}) + \left.\frac{F_4}{F_1\sqrt{F_1}}\frac{d^4 M_T}{dx^4}\right|_{x=0} + \left.\frac{F_5}{F_1\sqrt{F_1}}\frac{d^4 q(x)}{dx^4}\right|_{x=0} - \frac{1}{\sqrt{F_1}}\frac{E_a}{h_a}\frac{M_T(0)}{E_b I_b} \tag{95}$$

Substituting equation (92) and (81) into the above equation,

$$\begin{aligned} C_{34} = & -\frac{F_7 F_2}{F_8 F_1\sqrt{F_1}} B_1 B_4 C_{33} + \frac{1}{F_1\sqrt{F_1}}\left(F_4 \left.\frac{d^4 M_T}{dx^4}\right|_{x=0} + F_5 \left.\frac{d^4 q(x)}{dx^4}\right|_{x=0} \right) \\ & - \frac{F_2}{F_8 F_1\sqrt{F_1}} B_1 F_7 \left(\left(B_4 \frac{F_4}{F_1} + \frac{B_3}{B_1} \right) \left.\frac{d^2 M_T}{dx^2}\right|_{x=0} + \left(B_4 \frac{F_5}{F_1} + \frac{B_5}{B_1} \right) \left.\frac{d^2 q(x)}{dx^2}\right|_{x=0} \right) \\ & + \frac{F_2}{F_8 F_1\sqrt{F_1}} B_1 F_7 \left(B_3 M_T(0) + B_5 q(0) \right) - \frac{1}{F_8\sqrt{F_1}} \frac{E_a}{h_a} \frac{M_T(0)}{E_b I_b} \end{aligned} \tag{96}$$

Where, $F_8 = 1 + \frac{F_2}{F_1} B_1 F_7 \frac{B_4}{B_1}$

Continuing to differentiate equation (94) once again, substituted by the equation (85) and applying $N_f(0) = N_b(0) = 0, Q_f(0) = 0, M_f(0) = 0$ at the plate end, the boundary condition is:

$$\begin{aligned} \frac{d^3\sigma(x)}{dx^3} &= \frac{E_a}{h_a}\left(-\frac{1}{E_f I_f}\frac{dM_f(x)}{dx} + \frac{1}{E_b I_b}\frac{dM_b(x)}{dx} \right) \\ &= \frac{E_a}{h_a}\frac{1}{E_f I_f} Q_f - \frac{E_a}{h_a}\frac{1}{E_b I_b} Q_b + \frac{E_a}{h_a}\left(\frac{1}{E_b I_b} b_f y_b - \frac{1}{E_f I_f} b_f y_f \right) \tau(x) \end{aligned} \tag{97}$$

$$\begin{aligned} & 2\beta^3 (C_{34} + C_{33}) + \frac{F_4}{F_1}\left.\frac{d^5 M_T}{dx^5}\right|_{x=0} + \left.\frac{F_5}{F}\frac{d^5 q(x)}{dx^5}\right|_{x=0} \\ & = -\frac{E_a}{h_a}\frac{1}{E_b I_b} Q_T(0) + (C_{21} + C_{22})\left(\frac{E_a}{h_a} b_f \left(\frac{y_b}{E_b I_b} - \frac{y_f}{E_f I_f} \right) - B_1 \frac{F_2}{F_1}\sqrt{B_1} \right) \\ & + \frac{E_a}{h_a} b_f \left(\frac{y_b}{E_b I_b} - \frac{y_f}{E_f I_f} \right) \frac{B_3}{B_1} \left.\frac{dM_T}{dx}\right|_{x=0} + \frac{E_a}{h_a} b_f \left(\frac{y_b}{E_b I_b} - \frac{y_f}{E_f I_f} \right) \frac{B_5}{B_1} \left.\frac{dq(x)}{dx}\right|_{x=0} \end{aligned} \tag{98}$$

Substituting equation (92) (93) and (84) into above equations, C_{33} is finally worked out.

$$
\begin{aligned}
C_{33} = & -\frac{1}{F_{11}}\frac{1}{F_1}\left(F_4 \left.\frac{d^5 M_T}{dx^5}\right|_{x=0} + F_5 \left.\frac{d^5 q(x)}{dx^5}\right|_{x=0} \right) \\
& + \frac{1}{F_{11}}\left(F_6 F_7 F_{10}\frac{B_4}{B_1} - F_9 \frac{1}{\sqrt{F_1}} \right)\frac{1}{F_1}\left(F_4 \left.\frac{d^4 M_T}{dx^4}\right|_{x=0} + F_5 \left.\frac{d^4 q(x)}{dx^4}\right|_{x=0} \right) \\
& + \frac{1}{F_{11}}\frac{1}{B_1} F_7 \left(F_9 \frac{F_2}{F_8 F_1 \sqrt{F_1}} B_1 - F_6 F_{10} \right)\left(B_3 \left.\frac{d^2 M_T}{dx^2}\right|_{x=0} + B_5 \left.\frac{d^2 q(x)}{dx^2}\right|_{x=0} \right) \\
& + \frac{1}{F_{11}}\left(F_9 \frac{F_2}{F_8 F_1 \sqrt{F_1}} B_1 + F_6 F_{10} \right) F_7 B_4 \frac{1}{F_1}\left(F_4 \left.\frac{d^2 M_T}{dx^2}\right|_{x=0} + F_5 \left.\frac{d^2 q(x)}{dx^2}\right|_{x=0} \right) \\
& + \frac{1}{F_{11}}\frac{E_a}{h_a} b_f \left(\frac{y_b}{E_b I_b} - \frac{y_f}{E_f I_f} \right)\frac{1}{B_1}\left(B_3 \left.\frac{dM_T}{dx}\right|_{x=0} + B_5 \left.\frac{dq(x)}{dx}\right|_{x=0} \right) \\
& - \frac{1}{F_{11}}\left(F_9 \frac{F_2}{F_8 F_1 \sqrt{F_1}} B_1 + F_6 F_{10} \right) F_7 \left(B_3 M_T(0) + B_5 q(0) \right) \\
& + \frac{1}{F_{11}} F_9 \frac{1}{F_8 \sqrt{F_1}} \frac{E_a}{h_a} \frac{M_T(0)}{E_b I_b} - \frac{1}{F_{11}}\frac{E_a}{h_a}\frac{1}{E_b I_b} Q_T(0) \\
& - \frac{1}{F_{11}} F_6 \frac{2}{\left(e^{-\sqrt{B_1}L_s} + e^{\sqrt{B_1}L_s} \right)}\frac{1}{B_1}\left(B_3 \left.\frac{dM_T}{dx}\right|_{x=L_s} + B_5 \left.\frac{dq(x)}{dx}\right|_{x=L_s} \right)
\end{aligned}
\tag{99}
$$

Where, $F_6 = \dfrac{E_a}{h_a} b_f \left(\dfrac{y_b}{E_b I_b} - \dfrac{y_f}{E_f I_f} \right) - B_1 \dfrac{F_2}{F_1}\sqrt{B_1}$, $F_9 = 2\left(F_6 F_{10} F_7 \dfrac{B_4}{B_1} + \beta \right)\beta^2$,

$$
F_{10} = \frac{e^{-\sqrt{B_1}L_s} - e^{\sqrt{B_1}L_s}}{e^{\sqrt{B_1}L_s} + e^{-\sqrt{B_1}L_s}},\quad F_{11} = \left(2\beta^3 - F_6 F_{10} F_7 B_4 - F_9 \frac{F_7 F_2}{F_8 F_1 \sqrt{F_1}} B_1 B_4 \right) \tag{100}
$$

5.4. Three-Parameter Elastic Foundation Model

As is mentioned before, the one-parameter model is obviously simple and easy to use by representing the stiffness of the vertical springs with a parameter, k, the inability to take the shear force and the shear strain along the adhesive layers into account makes the one-parameter theory

clearly less precise. To confront this shortage, the improved two-parameter elastic foundation theory, in which various types of interactions between Winkler's independent springs are closer to reality, is introduced and developed by Filonenko-Borodich; Hetényi, Pasternak, Kerr, Vlasov and Leontiev. Both theories have been used to find an applicable and simple model of representing a joint adhesive. Two-parameter elastic foundation models are much more acceptable. While one of the two parameters is allocated to the rigidity of normal springs, the other one is assigned to interfacial shear force of the joint bond.

As this thesis stated above, serious continuous shear springs and distributed normal springs are used to modelthe adhesive is built as without any interactions between this two types of springs. This kind of adhesive layer simulation is a called two-parameter foundation model, and is elaborated in Goland and Reissner's paper [47]. Although the closed-form formula of interfacial stresses from the two-parameter foundation model is rather acceptable and its accuracy is proven by other continuum methods such as FEM, there are still small deviations at the small area close to the edge of the adhesive layer. In other words, the two-parameter foundation model is deficient in satisfying the boundary conditions: no shear stress generated at the adhesive border with free boundary condition. To achieve more accurate interfacial stresses of the bond, this thesis refines the model by developing the two-parameter foundation model into a three-parameter, elastic foundation model. In the two-parameter model, there is a rudimental flaw with the adhesive layer. The peel stresses in the beam, adhesive and FRP system are assumed the same; however, they are not. Then, the equilibrium equations of the adhesive are not met. The advanced, three-parameter

foundation model revises this problem by drawing an additional parameter to separate the two interfacial peel stresses. At this stage, the existing interfacial stresses can be cataloged into three categories: the peel stresses along the beam-adhesive interface $\sigma_1(x)$, along the adhesive-FRP plate interface $\sigma_2(x)$, and the shear stress of the adhesive layer $\tau(x)$. Accordingly, to fulfill this idea, this adhesive layer can be modeled as one shear spring layers plus two interconnected normal spring layers, one more normal spring layer when compared with the two-parameter foundation model. Because of this additional spring layer, the three-parameter foundation model is much stricter in measuring the debonding situations and the crack conditions. From this developed model, the closed-form expressions of interfacial stresses are simple and clear to work out to meet the boundary conditions. Based on the statement above, we can draw the free-body diagram for Figure 23.

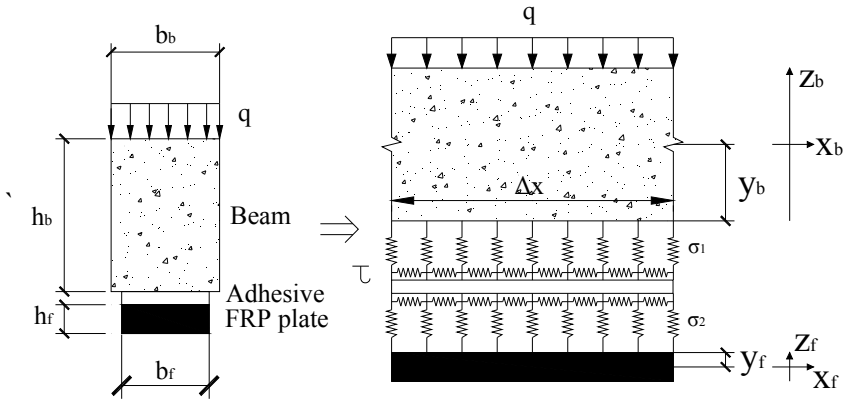

Figure 23. Cross section of RFP-reinforce concrete in three-parameter

5.4.1. Applying equilibrium equations

Repeating steps in the two-parameter model, the equations for the three-parameter model showing the relationship of moments, shear forces, axial forces in Figure 24 be built:

$$\begin{cases} \dfrac{dN_b(x)}{dx}=\tau(x)b_f, \qquad \dfrac{dN_f(x)}{dx}=-\tau(x)b_f \\ \dfrac{dQ_b(x)}{dx}=q(x)+\sigma_1(x)b_f, \qquad \dfrac{dQ_f(x)}{dx}=-\sigma_2(x)b_f \\ \dfrac{dM_b(x)}{dx}=-Q_b+b_2y_b\tau(x), \qquad \dfrac{dM_f(x)}{dx}=-Q_f+b_fy_1\tau(x) \\ \dfrac{d\tau(x)}{dx}=\dfrac{\sigma_2-\sigma_1}{h_a} \end{cases} \tag{101}$$

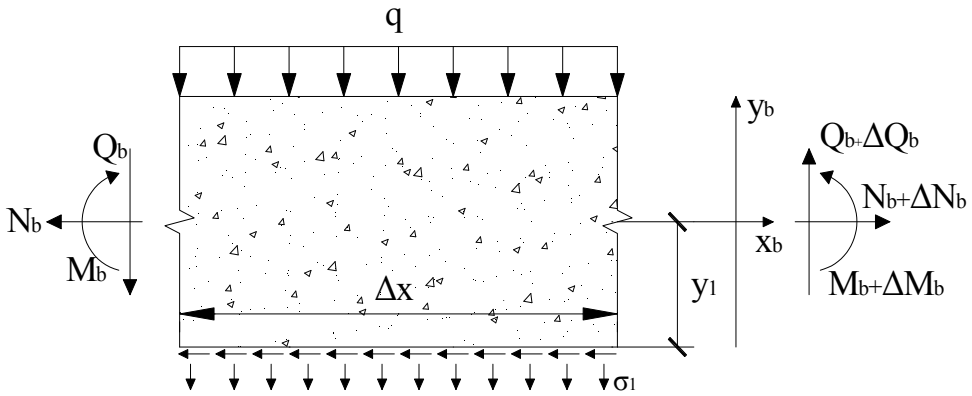

(a) concrete beam

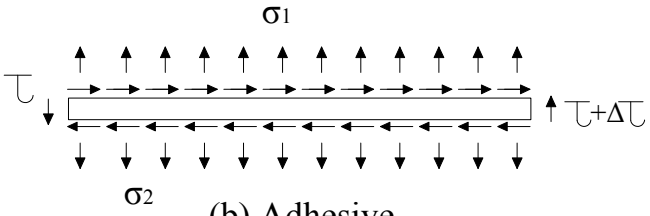

(b) Adhesive

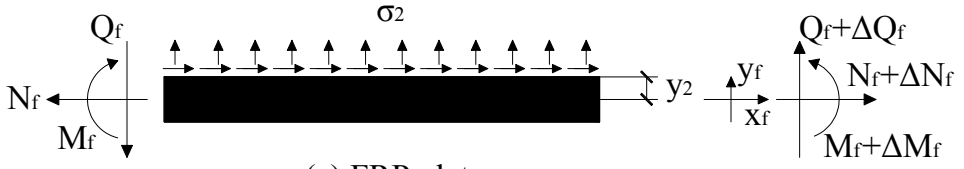

(c) FRP plate

Figure 24. Free-body diagram for three-parameter model. (a) concrete beam (b) adhesive (c) FRP plate

5.4.2. Calculating $\tau(x)$

Redoing calculations in the two-parameter model, the governing differential equation of $\tau(x)$ can be expressed on the basis of the axial force, the shear force and the moment.

$$\frac{d\tau(x)}{dx}\left(1-\frac{G_a}{h_a}\left(\frac{b_f h_b^4}{I_{zb}}\frac{1}{64G_b}-\frac{b_f h_f^4}{I_{zf}}\frac{1}{64G_f}-\frac{h_b}{2G_b}\right)\right)$$
$$=\frac{G_a}{h_a}\left(\begin{array}{l}\dfrac{\left(h_f+h_b\right)}{2\left(E_bI_b+E_fI_f\right)}M_T-\dfrac{1}{I_{zf}}\dfrac{h_f^3}{24G_f}b_f\sigma_2(x)+\dfrac{1}{I_{zb}}\dfrac{h_b^3}{24G_b}b_f\sigma_1(x)\\ -\left(\dfrac{N_f}{E_fA_f}-\dfrac{N_b}{E_bA_b}\right)-\dfrac{\left(\frac{h_b}{2}+\frac{h_f}{2}+h_a\right)}{2\left(E_bI_b+E_fI_f\right)}\left(h_fN_f-h_bN_b\right)+\dfrac{1}{I_{zb}}\dfrac{h_b^3}{24G_b}q(x)\end{array}\right) \quad (102)$$

$$\frac{d\tau(x)}{dx}=-R_3M_T-\frac{1}{R_2}\frac{G_a}{h_a}\frac{\left(\frac{h_b}{2}+\frac{h_f}{2}+h_a\right)}{2\left(E_bI_b+E_fI_f\right)}\left(h_fN_f-h_bN_b\right)-\frac{1}{R_2}\frac{G_a}{h_a}\left(\frac{N_f}{E_fA_f}-\frac{N_b}{E_bA_b}\right) \quad (103)$$
$$-R_6\sigma_2(x)+R_7\sigma_1(x)-R_5q(x)$$

Differentiating once on both size of equation and substituted by equation (36), the governing differential equation is

$$\frac{d^2\tau(x)}{dx^2}-R_1\tau(x)=-R_3\frac{dM_T}{dx}-R_6\sigma_2(x)+R_7\sigma_1(x)-R_5q(x) \quad (104)$$

Where, $R_1=b_f\dfrac{1}{R_2}\dfrac{G_a}{h_a}\left(\dfrac{\left(\frac{h_b}{2}+\frac{h_f}{2}+h_a\right)}{2\left(E_bI_b+E_fI_f\right)}\left(h_f+h_b\right)+\dfrac{1}{E_fA_f}+\dfrac{1}{E_bA_b}\right)$,

$R_2=1-\dfrac{G_a}{h_a}\left(\dfrac{b_f h_b^4}{I_{zb}}\dfrac{1}{64G_b}-\dfrac{b_f h_f^4}{I_{zf}}\dfrac{1}{64G_f}-\dfrac{h_b}{2G_b}\right)$,

$R_3=-\dfrac{1}{R_2}\dfrac{G_a}{h_a}\dfrac{\left(h_f+h_b\right)}{2\left(E_bI_b+E_fI_f\right)}$,

$$R_4 = -\frac{1}{R_2}\frac{G_a}{h_a}\frac{b_f}{24}\left(\frac{1}{I_{zf}}\frac{h_f^3}{G_f} - \frac{1}{I_{zb}}\frac{h_b^3}{G_b}\right), \quad R_5 = -\frac{1}{R_2}\frac{G_a}{h_a}\frac{1}{I_{zb}}\frac{h_b^3}{24G_b},$$

$$R_6 = -\frac{1}{R_2}\frac{G_a}{h_a}\frac{1}{I_{zf}}\frac{h_f^3}{24G_f}b_f, \; R_7 = -\frac{1}{R_2}\frac{G_a}{h_a}\frac{1}{I_{zb}}\frac{h_b^3}{24G_b}b_f$$

$$R_4 = -\left(R_6 - R_7\right) \tag{105}$$

5.4.3. Calculating $\sigma_1(x)$ and $\sigma_2(x)$

The vertical stress is represented by a serial of vertical spring with stiffness $k_a = 2\frac{E_a}{h_a}$

$$\tau(x) = G_a r_a = G_a \frac{u_{b(z_b=0)} - u_{f(z_f=h_f)}}{h_a}, \quad \sigma_1(x) + \sigma_2(x) = \frac{2E}{h_a}\left(w_f(x) - w_b(x)\right) \tag{106}$$

$$\text{Where, } \begin{cases} \sigma_1(x) = \dfrac{2E}{h_a}\Delta w_1(x) = \dfrac{2E}{h_a}\left(w_a(x) - w_b(x)\right) \\ \sigma_2(x) = \dfrac{2E}{h_a}\Delta w_2(x) = \dfrac{2E}{h_a}\left(w_f(x) - w_a(x)\right) \end{cases} \tag{107}$$

$$\sigma_2 + \sigma_1 = \frac{2E}{h_a}\left(w_f(x) - w_a(x)\right) - \frac{2E}{h_a}\left(w_a(x) - w_b(x)\right) = \frac{2E}{h_a}\left(w_f(x) - w_b(x)\right) \tag{108}$$

According to the Euler–Bernoulli beam theory [48], the curvature is given by

$$w'' = -\frac{M(x)}{EI} \quad \Rightarrow \quad \frac{dw_b^2(x)}{dx^2} = -\frac{M_b(x)}{E_b I_b}, \qquad \frac{dw_f^2(x)}{dx^2} = -\frac{M_f(x)}{E_f I_f} \tag{109}$$

Where E is the Young's modulus, EI is the bending stiffness.

Differentiating equation four times are

$$\begin{aligned} \frac{dw_b^4(x)}{dx^4} &= -\frac{1}{E_b I_b}\frac{dM_b^2(x)}{dx^2} = \frac{1}{E_b I_b}\left(\frac{dQ_b(x)}{dx} - b_f y_b \frac{d\tau(x)}{dx}\right) \\ &= \frac{1}{E_b I_b}\left(q(x) + \sigma_1(x) b_f - b_f y_1 \frac{d\tau(x)}{dx}\right) \end{aligned} \tag{110}$$

$$\begin{aligned}\frac{dw_f^4(x)}{dx^4} &= -\frac{1}{E_f I_f}\frac{dM_f^2(x)}{dx^2} = \frac{1}{E_f I_f}\left(\frac{dQ_f(x)}{dx} - b_f y_f \frac{d\tau(x)}{dx}\right) \\ &= -\frac{1}{E_f I_f}\left(\sigma_2(x) b_f + b_f y_2 \frac{d\tau(x)}{dx}\right)\end{aligned} \tag{111}$$

Combine equations (109) and (110) (111) together, the governing equation, on the basis of the component deflections, is

$$\begin{aligned}\frac{d\sigma_1^4(x)}{dx^4} + \frac{d\sigma_2^4(x)}{dx^4} &= \frac{2E_a}{h_a}\left(\frac{dw_f^4(x)}{dx^4} - \frac{dw_b^4(x)}{dx^4}\right) \\ &= -\frac{2E_a}{h_a}\left(\begin{array}{l}\dfrac{1}{E_b I_b}\left(q(x) + \sigma_1(x) b_f - b_f y_1 \dfrac{d\tau(x)}{dx}\right) \\ + \dfrac{1}{E_f I_f}\left(\sigma_2(x) b_f + b_f y_2 \dfrac{d\tau(x)}{dx}\right)\end{array}\right)\end{aligned} \tag{112}$$

$$\frac{d\tau(x)}{dx} = \frac{\sigma_2 - \sigma_1}{h_a} \tag{113}$$

Substituting $\sigma_2 = \frac{d\tau(x)}{dx}\mathrm{h}_a + \sigma_1$ into the above equation, the governing equation changes into

$$\begin{aligned}&\frac{d\sigma_1^4(x)}{dx^4} + \frac{E_a}{h_a}\left(\frac{1}{E_b I_b} + \frac{1}{E_f I_f}\right)\sigma_1(x) b_f \\ &= -\frac{d\tau^5(x)}{dx^5}\frac{\mathrm{h}_a}{2} - \frac{E_a}{h_a}\frac{1}{E_b I_b} q(x) + \frac{E_a}{h_a} b_f \left(\frac{y_1}{E_b I_b} - \frac{\mathrm{h}_a + y_2}{E_f I_f}\right)\frac{d\tau(x)}{dx}\end{aligned} \tag{114}$$

The governing equations are coupled and difficult to solve this equations set. In order to simple this problem, the author neglect the influence of shear deformations in both structures.

Then $\tau(x)$ change into $\tau(x) = C_{41} \times e^{\sqrt{R_1}x} + C_{42} \times e^{-\sqrt{R_1}x} + \frac{R_3}{R_1}\frac{dM_T}{dx} + \frac{R_5}{R_1}\frac{dq(x)}{dx}$ (115)

$$\frac{d\sigma_1^4(x)}{dx^4}+S_1\sigma_1(x)=\left(S_2-\frac{h_a}{2}R_1^2\right)\sqrt{R_1}\left(C_{41}\times e^{\sqrt{R_1}x}-C_{42}\times e^{-\sqrt{R_1}x}\right)$$
$$-\frac{h_a}{2R_1}\left(R_3\frac{d^6M_T}{dx^6}+B_5\frac{d^6q(x)}{dx^6}\right)+\frac{S_2}{R_1}\left(R_3\frac{d^2M_T}{dx^2}+R_5\frac{d^2q(x)}{dx^2}\right)-\frac{E_a}{h_a}\frac{1}{E_bI_b}q(x) \quad (116)$$

Where, $S_1=\frac{E_a}{h_a}\left(\frac{1}{E_bI_b}+\frac{1}{E_fI_f}\right)b_f$, $S_2=\frac{E_a}{h_a}b_f\left(\frac{y_1}{E_bI_b}-\frac{h_a+y_2}{E_fI_f}\right)$ (117)

Using the same method in the one-parameter medal, the solution of the corresponding homogeneous equation is

$$\sigma_1(x)=e^{\gamma x}(C_{51}\cos\gamma x+C_{52}\sin\gamma x)+e^{-\gamma x}\left(C_{53}\cos\gamma x+C_{54}\sin\gamma x\right)$$
$$+\sigma_{51}(x)+\sigma_{52}(x)+\sigma_{53}(x)+\sigma_{54}(x) \quad (118)$$

Where $\gamma=\sqrt[4]{\frac{S_1}{4}}$ (119)

Take the boundary conditions into consideration, is easy to get the arbitrarily constant coefficients C51, C52, C53and C54.

$$\sigma_{51}(x)=\left(S_2-\frac{h_a}{2}R_1^2\right)\frac{\sqrt{R_1}}{S_1}\left(C_{41}\times e^{\sqrt{R_1}x}-_{42}\times e^{-\sqrt{R_1}x}\right) \quad (120)$$

is the special solution corresponding to $\left(S_2-\frac{h_a}{2}R_1^2\right)\sqrt{R_1}\left(C_{41}\times e^{\sqrt{R_1}x}-_{42}\times e^{-\sqrt{R_1}x}\right)$

$$\sigma_{52}(x)=-\frac{h_a}{2R_1S_1}\left(B_3\frac{d^6M_T}{dx^6}+B_5\frac{d^6q(x)}{dx^6}\right) \quad (121)$$

is the special solution corresponding to $-\frac{h_a}{2R_1}\left(R_3\frac{d^6M_T}{dx^6}+R_5\frac{d^6q(x)}{dx^6}\right)$

$$\sigma_{53}(x)=\frac{S_2}{R_1S_1}\left(R_3\frac{d^2M_T}{dx^2}+R_5\frac{d^2q(x)}{dx^2}\right) \quad (122)$$

is the special solution corresponding to $\frac{S_2}{R_1}\left(R_3\frac{d^2M_T}{dx^2}+R_5\frac{d^2q(x)}{dx^2}\right)$

$$\sigma_{54}(x) = -\frac{S_2}{S_1}\frac{E_a}{h_a}\frac{1}{E_b I_b}q(x) \tag{123}$$

is the special solution corresponding to $-S_2\frac{E_a}{h_a}\frac{1}{E_b I_b}q(x)$

Since x is starting from the left intersection of concrete beam and FRP plate, in another word, x is always positive. With the increase of x, the normal stress is approaching zero. In the next calculation for C33 and C34, to simple the problem, for x at large, it is deemed to be zero, and as a result C31=C32=0

$$\begin{aligned}\sigma_1(x) &= e^{-\gamma x}\left(C_{53}\cos\gamma x + C_{54}\sin\gamma x\right)\\ &+\left(S_2 - \frac{\mathrm{h}_a}{2}B_1^2\right)\frac{\sqrt{R_1}}{S_1}\left(C_{41}\times e^{\sqrt{R_1}x} - C_{42}\times e^{-\sqrt{R_1}x}\right) - \frac{S_2}{S_1}\frac{E_a}{h_a}\frac{1}{E_b I_b}q(x)\\ &-\frac{\mathrm{h}_a}{2R_1S_1}\left(R_3\frac{d^6M_T}{dx^6} + R_5\frac{d^6q(x)}{dx^6}\right) + \frac{S_2}{R_1S_1}\left(R_3\frac{d^2M_T}{dx^2} + R_5\frac{d^2q(x)}{dx^2}\right)\end{aligned} \tag{124}$$

$$\begin{aligned}\sigma_2 &= e^{-\gamma x}\left(C_{53}\cos\gamma x + C_{54}\sin\gamma x\right)\\ &+\left(\left(S_2 - \frac{\mathrm{h}_a}{2}R_1^2\right)\frac{1}{S_1} + \mathrm{h}_a\right)\sqrt{R_1}\left(C_{41}\times e^{\sqrt{R_1}x} - C_{42}\times e^{-\sqrt{R_1}x}\right)\\ &-\frac{\mathrm{h}_a}{2R_1S_1}\left(B_3\frac{d^6M_T}{dx^6} + B_5\frac{d^6q(x)}{dx^6}\right) - \frac{S_2}{S_1}\frac{E_a}{h_a}\frac{1}{E_b I_b}q(x)\\ &+\left(\frac{S_2}{R_1S_1} + \frac{\mathrm{h}_a}{R_1}\right)\left(R_3\frac{d^2M_T}{dx^2} + R_5\frac{d^2q(x)}{dx^2}\right)\end{aligned} \tag{125}$$

Where $R_6 = -\frac{1}{R_2}\frac{G_a}{h_a}\frac{1}{I_{zf}}\frac{h_f^3}{24G_f}b_f$, $R_7 = -\frac{1}{R_2}\frac{G_a}{h_a}\frac{1}{I_{zb}}\frac{h_b^3}{24G_b}b_f$

$$R_4 = R_7 - R_6 \tag{126}$$

$$\tau(x) = C_{41}\times e^{\sqrt{R_1}x} + C_{42}\times e^{-\sqrt{R_1}x} + \frac{R_3}{R_1}\frac{dM_T}{dx} + \frac{R_6}{R_1}\frac{d\sigma_2(x)}{dx} - \frac{R_7}{R_1}\frac{d\sigma_1(x)}{dx} + \frac{R_5}{R_1}\frac{dq(x)}{dx} \tag{127}$$

$$\tau(x)=\left(1+R_6 \mathrm{h}_a-R_4\left(S_2-\frac{\mathrm{h}_a}{2}R_1^2\right)\frac{1}{S_1}\right)\left(C_{41}\times e^{\sqrt{R_1}x}+C_{42}\times e^{-\sqrt{R_1}x}\right)+\frac{R_4}{R_1}\phi e^{-\gamma x}$$
$$+\frac{R_4}{R_1}\gamma e^{-\gamma x}C_{53}\left(\cos\gamma x+\sin\gamma x\right)+\frac{R_4}{R_1}\gamma e^{-\gamma x}C_{54}\left(\sin\beta x-\cos\beta x\right)$$
$$+\frac{R_4}{R_1}\frac{\mathrm{h}_a}{2R_1S_1}\left(R_3\frac{d^7M_T}{dx^7}+R_5\frac{d^7q(x)}{dx^7}\right) \tag{128}$$
$$+\left(\frac{R_6}{R_1^2}\mathrm{h}_a-\frac{R_4}{R_1}\frac{S_2}{R_1S_1}\right)\left(R_3\frac{d^3M_T}{dx^3}+R_5\frac{d^3q(x)}{dx^3}\right)$$
$$+\frac{1}{R_1}\left(R_3\frac{dM_T}{dx}+R_5\frac{dq(x)}{dx}\right)+\frac{R_4}{R_1}\frac{S_2}{S_1}\frac{E_a}{h_a}\frac{1}{E_bI_b}\frac{dq(x)}{dx}$$

5.4.4. Using the following two boundary conditions

The 1st one is at x=0. Here, FRP plate is boundary free with $M_{f(x=0)}=0$ and zero axial force $Q_{f(x=0)}=0$. Between the plate end and the beam end, the moment in this section is only resisted by the concrete beam.

The 2nd one is at $x=L_s$, where shear force and shear stress are zero.

X=0, $N_f(0)=N_b(0)=0$, $Q_f(0)=0$, $M_f(0)$, $\tau(0)=0$

$x=L_s$ $\tau(L_s)=0$ (129)

Assuming L_s is the distance from x=0 to the location of zero shear force.

To simple this problem, assuming that the external load are distributed load or point load, so the high order of M(x) and q(x) can be neglected.

$$\tau(x)=C_{41}\times e^{\sqrt{R_1}x}+C_{42}\times e^{-\sqrt{R_1}x}+\frac{R_3}{R_1}\frac{dM_T}{dx}+\frac{R_6}{R_1}\frac{d\sigma_2(x)}{dx}-\frac{R_7}{R_1}\frac{d\sigma_1(x)}{dx}+\frac{R_5}{R_1}\frac{dq(x)}{dx} \tag{130}$$

The equation (103) at the plate end yields:

$$\tau(x)=\left(1+R_6\mathrm{h}_a-R_4\left(S_2-\frac{\mathrm{h}_a}{2}R_1^2\right)\frac{1}{S_1}\right)\left(C_{41}\times e^{\sqrt{R_1}x}+C_{42}\times e^{-\sqrt{R_1}x}\right)+\frac{R_4}{R_1}\phi e^{-\gamma x}$$
$$+\frac{R_4}{R_1}\gamma e^{-\gamma x}C_{53}\left(\cos\gamma x+\sin\gamma x\right)+\frac{R_4}{R_1}\gamma e^{-\gamma x}C_{54}\left(\sin\beta x-\cos\beta x\right)$$
$$+\frac{R_4}{R_1}\frac{\mathrm{h}_a}{2R_1S_1}\left(R_3\frac{d^7M_T}{dx^7}+R_5\frac{d^7q(x)}{dx^7}\right)+\left(\frac{R_6}{R_1^2}\mathrm{h}_a-\frac{R_4}{R_1}\frac{S_2}{R_1S_1}\right)\left(R_3\frac{d^3M_T}{dx^3}+R_5\frac{d^3q(x)}{dx^3}\right)$$
$$+\frac{1}{R_1}\left(R_3\frac{dM_T}{dx}+R_5\frac{dq(x)}{dx}\right)+\frac{R_4}{R_1}\frac{S_2}{S_1}\frac{E_a}{h_a}\frac{1}{E_bI_b}\frac{dq(x)}{dx} \tag{131}$$

$$S_4=\left(1+R_6\mathrm{h}_a-R_4\left(S_2-\frac{\mathrm{h}_a}{2}B_1^2\right)\frac{1}{S_1}\right)\sqrt{R_1} \tag{132}$$

$$\tau(0)=0 \qquad \begin{aligned}\phi=&-\frac{\sqrt{R_1}}{R_4}S_4\left(C_{41}+C_{42}\right)-\gamma C_{53}+\gamma C_{54}\\&-\frac{1}{R_4}\left(R_3\frac{dM_T}{dx}+R_5\frac{dq(x)}{dx}\right)-\frac{S_2}{S_1}\frac{E_a}{h_a}\frac{1}{E_bI_b}\frac{dq(x)}{dx}\end{aligned} \tag{133}$$

$$\left.\frac{d\tau(x)}{dx}\right|_{x=0}=\sqrt{R_1}\left(C_{41}-C_{42}\right)+\frac{1}{R_1}\left(R_5\frac{d^2q(x)}{dx^2}+R_3\frac{d^2M_T}{dx^2}\right)$$
$$=-\left(R_3M_T+R_5q(x)\right)+R_4C_{53}+\left(R_4\left(S_2-\frac{\mathrm{h}_a}{2}B_1^2\right)\frac{1}{S_1}-R_6\mathrm{h}_a\right)\sqrt{R_1}\left(C_{41}-C_{42}\right) \tag{134}$$
$$+R_4\frac{S_2}{R_1S_1}\left(R_3\frac{d^2M_T}{dx^2}+R_5\frac{d^2q(x)}{dx^2}\right)-R_4\frac{S_2}{S_1}\frac{E_a}{h_a}\frac{1}{E_bI_b}q(x)$$

$$\begin{aligned}C_{41}=&C_{42}+\frac{1}{S_4}R_4C_{53}-\frac{1}{S_4}\left(R_3M_T+R_5q(x)\right)-\frac{1}{S_4}R_4\frac{S_2}{S_1}\frac{E_a}{h_a}\frac{1}{E_bI_b}q(x)\\&+\frac{1}{S_4}\frac{1}{R_1}\left(R_4\frac{S_2}{S_1}-1\right)\left(R_3\frac{d^2M_T}{dx^2}+R_5\frac{d^2q(x)}{dx^2}\right)\end{aligned} \tag{135}$$

Where $S_4=\left(1+R_6\mathrm{h}_a-R_4\left(S_2-\frac{\mathrm{h}_a}{2}B_1^2\right)\frac{1}{S_1}\right)\sqrt{R_1}$,

$$S_3=\frac{1}{\sqrt{S_1}}\left(\left(S_2-\frac{\mathrm{h}_a}{2}R_1^2\right)\frac{1}{S_1}+\frac{\mathrm{h}_a}{2}\right)R_1\sqrt{R_1} \tag{136}$$

$$\tau(L_s) = C_{41} \times e^{\sqrt{R_1}L_s} + C_{42} \times e^{-\sqrt{R_1}L_s} + \frac{R_3}{R_1}\frac{dM_T}{dx}\bigg|_{x=L_s} + \frac{R_5}{R_1}\frac{dq(x)}{dx}\bigg|_{x=L_s} = 0 \tag{137}$$

$$\begin{aligned} C_{42} = & -\frac{e^{\sqrt{R_1}L_s}}{\left(e^{-\sqrt{R_1}L_s} + e^{\sqrt{R_1}L_s}\right)}\frac{1}{S_4}R_4 C_{53} \\ & -\frac{e^{\sqrt{R_1}L_s}}{\left(e^{-\sqrt{R_1}L_s} + e^{\sqrt{R_1}L_s}\right)}\frac{1}{S_4}\frac{1}{R_1}\left(R_4\frac{S_2}{S_1} - 1\right)\left(R_3\frac{d^2M_T}{dx^2} + R_5\frac{d^2q(x)}{dx^2}\right) \\ & +\frac{e^{\sqrt{R_1}L_s}}{\left(e^{-\sqrt{R_1}L_s} + e^{\sqrt{R_1}L_s}\right)S_4}\left(R_3M_T + R_5q(x)\right) + \frac{e^{\sqrt{R_1}L_s}}{\left(e^{-\sqrt{R_1}L_s} + e^{\sqrt{R_1}L_s}\right)}\frac{R_4}{S_4}\frac{S_2}{S_1}\frac{E_a}{h_a}\frac{1}{E_bI_b}q(x) \\ & -\frac{1}{\left(e^{-\sqrt{R_1}L_s} + e^{\sqrt{R_1}L_s}\right)}\frac{1}{R_1}\left(R_3\frac{dM_T}{dx}\bigg|_{x=L_s} + R_5\frac{dq(x)}{dx}\bigg|_{x=L_s}\right) \end{aligned} \tag{138}$$

Inputting C_{42} into equation (132), (133), (134) , (135), C_{41} is expressed by C_{53} and C_{54}

$$\begin{aligned} C_{41} = & \frac{e^{-\sqrt{R_1}L_s}}{\left(e^{-\sqrt{R_1}L_s} + e^{\sqrt{R_1}L_s}\right)}\frac{1}{S_4}R_4 C_{53} \\ & +\frac{e^{-\sqrt{R_1}L_s}}{\left(e^{-\sqrt{R_1}L_s} + e^{\sqrt{R_1}L_s}\right)}\frac{1}{S_4}\frac{1}{R_1}\left(R_4\frac{S_2}{S_1} - 1\right)\left(R_3\frac{d^2M_T}{dx^2} + R_5\frac{d^2q(x)}{dx^2}\right) \\ & -\frac{e^{-\sqrt{R_1}L_s}}{\left(e^{-\sqrt{R_1}L_s} + e^{\sqrt{R_1}L_s}\right)}\frac{1}{S_4}\left(R_3M_T + R_5q(x)\right) \\ & -\frac{e^{-\sqrt{R_1}L_s}}{\left(e^{-\sqrt{R_1}L_s} + e^{\sqrt{R_1}L_s}\right)}\frac{1}{S_4}R_4\frac{S_2}{S_1}\frac{E_a}{h_a}\frac{1}{E_bI_b}q(x) \\ & -\frac{1}{\left(e^{-\sqrt{R_1}L_s} + e^{\sqrt{R_1}L_s}\right)}\frac{1}{R_1}\left(R_3\frac{dM_T}{dx}\bigg|_{x=L_s} + R_5\frac{dq(x)}{dx}\bigg|_{x=L_s}\right) \end{aligned} \tag{139}$$

$$S_{12} = \frac{e^{-\sqrt{R_1}L_s} - e^{\sqrt{R_1}L_s}}{\left(e^{\sqrt{R_1}L_s} + e^{-\sqrt{R_1}L_s}\right)} \tag{140}$$

Since x is starting from the left intersection of concrete beam and FRP plate, in another word, x is always positive. With the increase of x, the normal stress is approaching zero. In the next

calculation for C_{53} and C_{54}, to simple the problem, for x at large, it is deemed to be zero, and as a result $C_{51}=C_{52}=0$

$$\sigma_2(x)+\sigma_1(x)=\frac{2E}{h_a}\left(w_f(x)-w_a(x)\right)-\frac{2E}{h_a}\left(w_a(x)-w_b(x)\right)=\frac{2E}{h_a}\left(w_f(x)-w_b(x)\right) \quad (141)$$

$$w''=-\frac{M(x)}{EI} \quad \Rightarrow \quad \frac{dw_b^2(x)}{dx^2}=-\frac{M_b(x)}{E_bI_b}, \qquad \frac{dw_f^2(x)}{dx^2}=-\frac{M_f(x)}{E_fI_f} \quad (142)$$

Differentiating equation (108) twice and substituting (109) into (141),(142) gives

$$\frac{d\sigma_1^2(x)}{dx^2}+\frac{d\sigma_1^2(x)}{dx^2}=\frac{2E}{h_a}\left(-\frac{M_f(x)}{E_fI_f}+\frac{M_b(x)}{E_bI_b}\right) \quad (143)$$

$$\begin{aligned}\frac{d^2\sigma_1(x)}{dx^2}&=\left(S_2-\frac{h_a}{2}R_1^2\right)\frac{R_1}{S_1}\sqrt{R_1}\left(C_{41}\times e^{\sqrt{R_1}x}-C_{42}\times e^{-\sqrt{R_1}x}\right)\\&\quad-2\gamma^2C_{54}e^{-\gamma x}\cos\gamma x+2\gamma^2C_{53}e^{-\gamma x}\sin\gamma x-\frac{S_2}{S_1}\frac{E_a}{h_a}\frac{1}{E_bI_b}\frac{dq(x)}{dx}\end{aligned} \quad (144)$$

$$\begin{aligned}\frac{d^2\sigma_2(x)}{dx^2}&=\left(\left(S_2-\frac{h_a}{2}R_1^2\right)\frac{1}{S_1}+h_a\right)R_1\sqrt{R_1}\left(C_{41}\times e^{\sqrt{R_1}x}-C_{42}\times e^{-\sqrt{R_1}x}\right)\\&\quad-2\gamma^2C_{54}e^{-\gamma x}\cos\gamma x+2\gamma^2C_{53}e^{-\gamma x}\sin\gamma x-\frac{S_2}{S_1}\frac{E_a}{h_a}\frac{1}{E_bI_b}\frac{dq(x)}{dx}\end{aligned} \quad (145)$$

$$\begin{aligned}&\left.\frac{d^2\sigma_1(x)}{dx^2}\right|_{x=0}+\left.\frac{d^2\sigma_2(x)}{dx^2}\right|_{x=0}\\&\quad=-4\gamma^2C_{54}-2\frac{S_2}{S_1}\frac{E_a}{h_a}\frac{1}{E_bI_b}\left.\frac{dq(x)}{dx}\right|_{x=0}+2S_3\sqrt{S_1}\left(C_{41}-C_{42}\right)=\frac{2E_a}{h_a}\frac{M_T(0)}{E_bI_b}\end{aligned} \quad (146)$$

$$C_{54}=-\frac{1}{\sqrt{S_1}}\frac{S_2}{S_1}\frac{E_a}{h_a}\frac{1}{E_bI_b}\left.\frac{dq(x)}{dx}\right|_{x=0}+S_3\left(C_{41}-C_{42}\right)-\frac{1}{\sqrt{S_1}}\frac{E_a}{h_a}\frac{M_T(0)}{E_bI_b} \quad (147)$$

Where, $S_3=\frac{1}{\sqrt{S_1}}\left(\left(S_2-\frac{h_a}{2}R_1^2\right)\frac{1}{S_1}+\frac{h_a}{2}\right)R_1\sqrt{R_1}$ (148)

Substituting equation (138) and (139) into the above equation (147)

$$
\begin{aligned}
C_{54} = {} & \frac{S_3}{S_8}\frac{1}{S_4}R_4C_{53} + \frac{1}{S_8}S_3\frac{1}{S_4R_1}\left(R_4\frac{S_2}{S_1}-1\right)\left(R_3\left.\frac{d^2M_T}{dx^2}\right|_{x=0} + R_5\left.\frac{d^2q(x)}{dx^2}\right|_{x=0}\right) \\
& -\frac{1}{S_8}\left(S_3\frac{1}{S_4}\frac{R_4}{R_1}+\frac{1}{\sqrt{S_1}}\right)\frac{S_2}{S_1}\frac{E_a}{h_a}\frac{1}{E_bI_b}\left.\frac{dq(x)}{dx}\right|_{x=0} \\
& -\frac{1}{S_8}S_3\frac{1}{S_4}R_4\frac{S_2}{S_1}\frac{E_a}{h_a}\frac{1}{E_bI_b}q(0) \\
& -\frac{1}{S_8}\frac{1}{\sqrt{S_1}}\frac{E_a}{h_a}\frac{M_T(0)}{E_bI_b} - \frac{1}{S_8}S_3\frac{1}{S_4}\left(R_3M_T + R_5q(0)\right)
\end{aligned}
\tag{149}
$$

$$
\text{Where } S_8 = \left(1 + S_3\frac{1}{S_4}\frac{R_4}{R_1}2\gamma^2\right) \tag{150}
$$

Continuing to differentiate equation (143) once again, and applying the equilibrium equation, the results lead to

$$
\begin{aligned}
\frac{d\sigma_1^3(x)}{dx^3} + \frac{d\sigma_1^3(x)}{dx^3} &= \frac{2E}{h_a}\left(-\frac{-Q_f + b_f y_2\tau(x)}{E_fI_f} + \frac{-Q_b + b_f y_1\tau(x)}{E_bI_b}\right) \\
&= \frac{2E}{h_a}\left(\frac{Q_f}{E_bI_b} - \frac{b_f y_2}{E_fI_f}\tau(x) - \frac{Q_b}{E_fI_f} + \frac{b_f y_1}{E_bI_b}\tau(x)\right)
\end{aligned}
\tag{151}
$$

$$
\begin{aligned}
\frac{d^3\sigma_1(x)}{dx^3} + \frac{d^3\sigma_2(x)}{dx^3} &= 4\gamma^3e^{-\gamma x}\cos\gamma x\left(C_{54}+C_{53}\right) + 4\gamma^3e^{-\gamma x}\sin\gamma x\left(C_{54}-C_{53}\right) \\
&\quad + 2\sqrt{S_1}S_3\sqrt{R_1}\left(C_{41}\times e^{\sqrt{R_1}x} + C_{42}\times e^{-\sqrt{R_1}x}\right) \\
&= 2\frac{E_a}{h_a}\frac{1}{E_fI_f}Q_f - 2\frac{E_a}{h_a}\frac{1}{E_bI_b}Q_b + 2S_6S_5\left(C_{41}\times e^{\sqrt{R_1}x} + C_{42}\times e^{-\sqrt{R_1}x}\right) \\
&\quad + 2S_6\frac{R_4}{R_1}\gamma e^{-\gamma x}C_{53}\left(\cos\gamma x + \sin\gamma x\right) + 2S_6\frac{R_4}{R_1}\gamma e^{-\gamma x}C_{54}\left(\sin\beta x - \cos\beta x\right) \\
&\quad + 2S_6\frac{1}{R_1}\left(R_3\frac{dM_T}{dx} + R_5\frac{dq(x)}{dx}\right) + 2S_6\frac{R_4}{R_1}\frac{S_2}{S_1}\frac{E_a}{h_a}\frac{1}{E_bI_b}\frac{dq(x)}{dx}
\end{aligned}
\tag{152}
$$

$$
\text{Where, } S_5 = \left(1 + R_6h_a - R_4\left(S_2 - \frac{h_a}{2}R_1^2\right)\frac{1}{S_1}\right), \quad S_6 = \frac{E_a}{h_a}\left(\frac{1}{E_bI_b}b_fy_b - \frac{1}{E_fI_f}b_fy_f\right) \tag{153}
$$

$$2\gamma^3\left(C_{54}+C_{53}\right)=-\frac{E_a}{h_a}\frac{1}{E_bI_b}Q_b+\left(S_6S_5-\sqrt{S_1}S_3\sqrt{R_1}\right)\left(C_{41}+C_{42}\right)+S_6\frac{R_4}{R_1}\gamma C_{53}$$
$$-S_6\frac{R_4}{R_1}\gamma C_{54}+S_6\frac{1}{R_1}\left(R_3\frac{dM_T}{dx}+R_5\frac{dq(x)}{dx}\right)+S_6\frac{R_4}{R_1}\frac{S_2}{S_1}\frac{E_a}{h_a}\frac{1}{E_bI_b}\frac{dq(x)}{dx} \quad (154)$$

Assuming $S_7=\left(S_6S_5-\sqrt{S_1}S_3\sqrt{R_1}\right)$,

$$2\gamma^3\left(C_{54}+C_{53}\right)=S_7\left(C_{41}+C_{42}\right)+S_6\frac{R_4}{R_1}\gamma C_{53}-S_6\frac{R_4}{R_1}\gamma C_{54}$$
$$+S_6\frac{R_4}{R_1}\frac{S_2}{S_1}\frac{E_a}{h_a}\frac{1}{E_bI_b}\frac{dq(x)}{dx}-\frac{E_a}{h_a}\frac{1}{E_bI_b}Q_b+S_6\frac{1}{R_1}\left(R_3\frac{dM_T}{dx}+R_5\frac{dq(x)}{dx}\right) \quad (155)$$

Substituting equation (138), (139) and (149) into equation (153), (154), all the coefficients are finally worked out.

$$C_{53}=\frac{1}{S_{11}}\left(S_9\frac{1}{S_8}S_3+S_7S_{12}\right)\frac{1}{S_4}\frac{1}{R_1}\left(R_4\frac{S_2}{S_1}-1\right)\left(R_3\frac{d^2M_T}{dx^2}\bigg|_{x=0}+R_5\frac{d^2q(x)}{dx^2}\bigg|_{x=0}\right)$$
$$+\frac{1}{S_{11}}S_6\frac{1}{R_1}\left(R_3\frac{dM_T}{dx}+R_5\frac{dq(x)}{dx}\right)-\frac{1}{S_{11}}\frac{E_a}{h_a}\frac{1}{E_bI_b}Q_b$$
$$-\frac{1}{S_{11}}\left(S_9\frac{1}{S_8}S_3+S_7S_{12}\right)\frac{1}{S_4}\left(R_3M_T+R_5q(0)\right)$$
$$-\frac{1}{S_{11}}\left(\frac{S_9}{S_8}\left(\frac{S_3}{S_4}\frac{R_4}{R_1}+\frac{1}{\sqrt{S_1}}\right)+\left(S_7S_{12}\frac{1}{S_4}-S_6\right)\frac{R_4}{R_1}\right)\frac{S_2}{S_1}\frac{E_a}{h_a}\frac{1}{E_bI_b}\frac{dq(x)}{dx}\bigg|_{x=0} \quad (156)$$
$$-\frac{1}{S_{11}}\left(S_9\frac{1}{S_8}S_3+S_7S_{12}\right)R_4\frac{S_2}{S_4S_1}\frac{E_a}{h_a}\frac{1}{E_bI_b}q(0)-\frac{S_9}{S_{11}S_8}\frac{1}{\sqrt{S_1}}\frac{E_a}{h_a}\frac{M_T(0)}{E_bI_b}$$
$$-\frac{1}{S_{11}}S_7\frac{2}{\left(e^{-\sqrt{R_1}L_s}+e^{\sqrt{R_1}L_s}\right)}\frac{1}{R_1}\left(R_3\frac{dM_T}{dx}\bigg|_{x=L_s}+R_5\frac{dq(x)}{dx}\bigg|_{x=L_s}\right)$$

$$S_9=-\left(\gamma S_6\frac{R_4}{R_1}+2\gamma^3\right),\quad S_{10}=\left(2\gamma^3-S_7S_{12}\frac{1}{S_4}R_4-S_6\frac{R_4}{R_1}\gamma\right),\quad S_{11}=\left(S_{10}-S_9\frac{1}{S_8}S_3\frac{1}{S_4}R_4\right),$$

$$S_{12}=\frac{e^{-\sqrt{R_1}L_s}-e^{\sqrt{R_1}L_s}}{\left(e^{\sqrt{R_1}L_s}+e^{-\sqrt{R_1}L_s}\right)} \quad (157)$$

5.5. Summary

In this chapter, there elastic foundation models are gradually developed to analysis the stresses of FRP-reinforced concrete. In the progress from one-parameter model to three-parameter model, the model is becoming more complicated and completed. Three-parameter model not only overcomes the neglection of shear stress in the one-parameter model, but also solves the boundary problem.

CHAPTER 6. NUMERICAL VERIFICATION

6.1. Shear Stress and Peeling Stress under Point Load

For the FRP-reinforce concrete under point load as shown in Figure 12, the shear force $V_T(x=0)$ at the left-end point of FRP plate and the moment $M_T(x=0)$ at this point are:

$$q(x) = a_1 x + a_2 = 0 \tag{158}$$

$$Q_T(x=0) = -R = -\frac{P(L_0 - L_1 - L_P)}{L_0} \tag{159}$$

$$M_0 = RL_1 \quad \left.\frac{dM_T}{dx}\right|_{x=0} = -Q_T(x=0) = R \tag{160}$$

R is the left reaction force at support, Lp is the distance from the load to the left FRP end.

If p is more than one, using the moment balance and the force balance equations to find a invented force and its distance to the plate end.

As shown above, under point load, the solutions of three parameter models are greatly simplified. Substituting the shear stress, moment and the distributed force into the results, the calculated equation is changed into Table 7 and Table 8.

Table 7. Solution of one-parameter model under point load

Solutions	$\sigma(x) = e^{-\lambda x}\left(C_{13}\cos\lambda x + C_{14}\sin\lambda x\right)$
Coefficients	$\lambda = \sqrt[4]{\frac{A_1}{4}} = \sqrt[4]{\frac{E_a b}{4h_a}\left(\frac{1}{E_b I_b} + \frac{1}{E_f I_f}\right)}$ $C_{14} = -\frac{1}{2\lambda^2}\frac{E_a}{h_a}\frac{RL_1}{E_b I_b}$ $C_{13} = \frac{1}{2\lambda^2}\frac{E_a}{h_a}\frac{RL_1}{E_b I_b} + \frac{1}{2\lambda^3}\frac{E_a}{h_a}\frac{1}{E_b I_b}R$

Table 8. Solution of two-parameter model under point load

Solutions	$\tau(x)=C_{21}\times e^{\sqrt{B_1}x}+C_{22}\times e^{-\sqrt{B_1}x}-\frac{B_4}{B_1}\frac{d\sigma(x)}{dx}$ $\sigma(x)=e^{-\beta x}\left(C_{33}\cos\beta x+C_{34}\sin\beta x\right)+\frac{F_2}{F_1}C_{21}e^{\sqrt{B_1}x}-\frac{F_3}{F_1}C_{22}e^{-\sqrt{B_1}x}$
Coefficients	C_{21} $=\frac{e^{-\sqrt{B_1}L_s}}{\left(e^{-\sqrt{B_1}L_s}+e^{\sqrt{B_1}L_s}\right)}F_7B_4C_{33}-2\frac{e^{-\sqrt{B_1}L_s}}{\left(e^{-\sqrt{B_1}L_s}+e^{\sqrt{B_1}L_s}\right)}F_7\frac{B_4}{B_1}\beta^2C_{34}-F_7\frac{e^{-\sqrt{B_1}L_s}}{\left(e^{-\sqrt{B_1}L_s}+e^{\sqrt{B_1}L_s}\right)}(B_3RL_1)$ C_{22} $=-\frac{e^{\sqrt{B_1}L_s}}{\left(e^{-\sqrt{B_1}L_s}+e^{\sqrt{B_1}L_s}\right)}F_7B_4C_{33}+2\frac{e^{\sqrt{B_1}L_s}}{\left(e^{-\sqrt{B_1}L_s}+e^{\sqrt{B_1}L_s}\right)}F_7\frac{B_4}{B_1}\beta^2C_{34}+F_7\frac{e^{\sqrt{B_1}L_s}}{\left(e^{-\sqrt{B_1}L_s}+e^{\sqrt{B_1}L_s}\right)}(B_3RL_1)$ $C_{33}=\frac{1}{F_{11}}\frac{E_a}{h_a}b_f\left(\frac{y_b}{E_bI_b}-\frac{y_f}{E_fI_f}\right)\frac{1}{B_1}(B_3R)$ $-\frac{1}{F_{11}}\left(F_9\frac{F_2}{F_8F_1\sqrt{F_1}}B_1+F_6F_{10}\right)F_7(B_3RL_1)+\frac{1}{F_{11}}\left(\frac{F_9L_1}{F_8\sqrt{F_1}}+1\right)\frac{E_a}{h_a}\frac{R}{E_bI_b}$ $C_{34}=-\frac{F_7F_2}{F_8F_1\sqrt{F_1}}B_1B_4C_{33}+\frac{F_2}{F_8F_1\sqrt{F_1}}B_1F_7(B_3RL_1)-\frac{1}{F_8\sqrt{F_1}}\frac{E_a}{h_a}\frac{RL_1}{E_bI_b}$

Table 9. Solution of three-parameter model under point load

Solutions	$\tau(x)=C_{41}\times e^{\sqrt{R_1}x}+C_{42}\times e^{-\sqrt{R_1}x}+\frac{R_3}{R_1}R+\frac{R_6}{R_1}\frac{d\sigma_2(x)}{dx}-\frac{R_7}{R_1}\frac{d\sigma_1(x)}{dx}$
Coefficients	$C_{41}=\frac{e^{-\sqrt{R_1}L_s}}{\left(e^{-\sqrt{R_1}L_s}+e^{\sqrt{R_1}L_s}\right)}\left(\frac{1}{S_4}R_4C_{53}-\frac{1}{S_4}\frac{R_4}{R_1}2\gamma^2C_{54}-\frac{1}{S_4}(R_3RL_1)\right)$ $C_{42}=\frac{e^{\sqrt{R_1}L_s}}{\left(e^{-\sqrt{R_1}L_s}+e^{\sqrt{R_1}L_s}\right)}\left(\frac{1}{S_4}\frac{R_4}{R_1}2\gamma^2C_{54}+\frac{1}{S_4}(R_3RL_1)-\frac{1}{S_4}R_4C_{53}\right)$ $C_{53}=\frac{1}{S_{11}}\frac{E_a}{h_a}\frac{1}{E_bI_b}R+\frac{1}{S_{11}}S_6\frac{1}{R_1}(R_3R)-\frac{1}{S_{11}}\left(S_9\frac{1}{S_8}S_3+S_7S_{12}\right)\frac{1}{S_4}(R_3RL_1)-\frac{1}{S_{11}}S_9\frac{1}{S_8}\frac{1}{\sqrt{S_1}}\frac{E_a}{h_a}\frac{RL_1}{E_bI_b}$ $C_{54}=\frac{1}{S_8}S_3\frac{1}{S_4}R_4C_{53}-\frac{1}{S_8}\frac{1}{\sqrt{S_1}}\frac{E_a}{h_a}\frac{RL_1}{E_bI_b}-\frac{1}{S_8}S_3\frac{1}{S_4}(R_3RL_1)$

6.2. Simplified Formula under Point Load

In practical engineering, $\sqrt{R_1}L_s >> 4$, $e^{-\sqrt{R_1}L_s} \approx 0$, and the item with $\sqrt{R_1}L_s$ is much larger than others, so in this simplified formula, it is logic to define

$$C_{21} = C_{41} = 0 \tag{161}$$

Therefore, the peeling stress and shearing stress can be simplified, and the whole set of equations changes into Table 10, Table 11, and Table 12.

Table 10. Simplified formula of one-parameter model under point load

Solutions	$\sigma(x) = e^{-\lambda x}\left(C_{13}\cos\lambda x + C_{14}\sin\lambda x\right)$
Coefficients	$\lambda = \sqrt[4]{\frac{A_1}{4}} = \sqrt[4]{\frac{E_a b}{4h_a}\left(\frac{1}{E_b I_b} + \frac{1}{E_f I_f}\right)}$ $C_{14} = -\frac{1}{2\lambda^2}\frac{E_a}{h_a}\frac{RL_1}{E_b I_b}$ $C_{13} = \frac{1}{2\lambda^2}\frac{E_a}{h_a}\frac{RL_1}{E_b I_b} + \frac{1}{2\lambda^3}\frac{E_a}{h_a}\frac{1}{E_b I_b}R$

Table 11. Simplified formula of two-parameter model under point load

Solutions	$\tau(x) = C_{22}\times e^{-\sqrt{B_1}x} - \frac{B_4}{B_1}\frac{d\sigma(x)}{dx}$ $\sigma(x) = e^{-\beta x}\left(C_{33}\cos\beta x + C_{34}\sin\beta x\right) - \frac{F_3}{F_1}C_{22}e^{-\sqrt{B_1}x}$
Coefficients	$C_{22} = -\frac{e^{\sqrt{B_1}L_s}}{\left(e^{-\sqrt{B_1}L_s} + e^{\sqrt{B_1}L_s}\right)}F_7 B_4 C_{33} + 2\frac{e^{\sqrt{B_1}L_s}}{\left(e^{-\sqrt{B_1}L_s} + e^{\sqrt{B_1}L_s}\right)}F_7\frac{B_4}{B_1}\beta^2 C_{34}$ $+ F_7\frac{e^{\sqrt{B_1}L_s}}{\left(e^{-\sqrt{B_1}L_s} + e^{\sqrt{B_1}L_s}\right)}\left(B_3 RL_1\right)$ $C_{33} = \frac{1}{F_{11}}\frac{E_a}{h_a}b_f\left(\frac{y_b}{E_b I_b} - \frac{y_f}{E_f I_f}\right)\frac{1}{B_1}\left(B_3 R\right)$ $-\frac{1}{F_{11}}\left(F_9\frac{F_2}{F_8 F_1\sqrt{F_1}}B_1 + F_6 F_{10}\right)F_7\left(B_3 RL_1\right) + \frac{1}{F_{11}}\left(\frac{F_9 L_1}{F_8\sqrt{F_1}} + 1\right)\frac{E_a}{h_a}\frac{R}{E_b I_b}$ $C_{34} = -\frac{F_7 F_2}{F_8 F_1\sqrt{F_1}}B_1 B_4 C_{33} + \frac{F_2}{F_8 F_1\sqrt{F_1}}B_1 F_7\left(B_3 RL_1\right) - \frac{1}{F_8\sqrt{F_1}}\frac{E_a}{h_a}\frac{RL_1}{E_b I_b}$

Table 12. Simplified formula of three-parameter model under point load

Solutions	$\tau(x)=C_{42}\times e^{-\sqrt{R_1}x}+\frac{R_3}{R_1}R+\frac{R_6}{R_1}\frac{d\sigma_2(x)}{dx}-\frac{R_7}{R_1}\frac{d\sigma_1(x)}{dx}$ $\sigma_1(x)=e^{-\gamma x}\left(C_{53}\cos\gamma x+C_{54}\sin\gamma x\right)+\left(S_2-\frac{h_a}{2}B_1^2\right)\frac{\sqrt{R_1}}{S_1}\left(-C_{42}\times e^{-\sqrt{R_1}x}\right)$ $\sigma_2=e^{-\gamma x}\left(C_{53}\cos\gamma x+C_{54}\sin\gamma x\right)$ $+\left(\left(S_2-\frac{h_a}{2}R_1^2\right)\frac{1}{S_1}+h_a\right)\sqrt{R_1}\left(-C_{42}\times e^{-\sqrt{R_1}x}\right)$
Coefficients	$C_{42}=-\frac{e^{\sqrt{R_1}L_s}}{\left(e^{-\sqrt{R_1}L_s}+e^{\sqrt{R_1}L_s}\right)}\frac{1}{S_4}R_4C_{53}+\frac{e^{\sqrt{R_1}L_s}}{\left(e^{-\sqrt{R_1}L_s}+e^{\sqrt{R_1}L_s}\right)}\frac{1}{S_4}\frac{R_4}{R_1}2\gamma^2C_{54}$ $+\frac{e^{\sqrt{R_1}L_s}}{\left(e^{-\sqrt{R_1}L_s}+e^{\sqrt{R_1}L_s}\right)}\frac{1}{S_4}(R_3RL_1)$ $C_{53}=\frac{1}{S_{11}}\frac{E_a}{h_a}\frac{1}{E_bI_b}R+\frac{1}{S_{11}}S_6\frac{1}{R_1}(R_3R)$ $-\frac{1}{S_{11}}\left(S_9\frac{1}{S_8}S_3+S_7S_{12}\right)\frac{1}{S_4}(R_3RL_1)-\frac{1}{S_{11}}S_9\frac{1}{S_8}\frac{1}{\sqrt{S_1}}\frac{E_a}{h_a}\frac{RL_1}{E_bI_b}$ $C_{54}=\frac{1}{S_8}S_3\frac{1}{S_4}R_4C_{53}-\frac{1}{S_8}\frac{1}{\sqrt{S_1}}\frac{E_a}{h_a}\frac{RL_1}{E_bI_b}-\frac{1}{S_8}S_3\frac{1}{S_4}(R_3RL_1)$

6.3. Finite Element Method Validation and Parameter Analysis

6.3.1. Theoretical analysis and comparison of finite element results

The calculated stresses from three models have been compared with the result from finite element method. The dimensions, the mechanical behaviors, and the loading case of the specimen showing in Figure 25 are obtained from the experiments by Hamid Saadatmanesh [46] and the closed-form high-order analysis by O. Rabinovich and Y. Frostig. T. [42]. The load for this test is P=100kN.

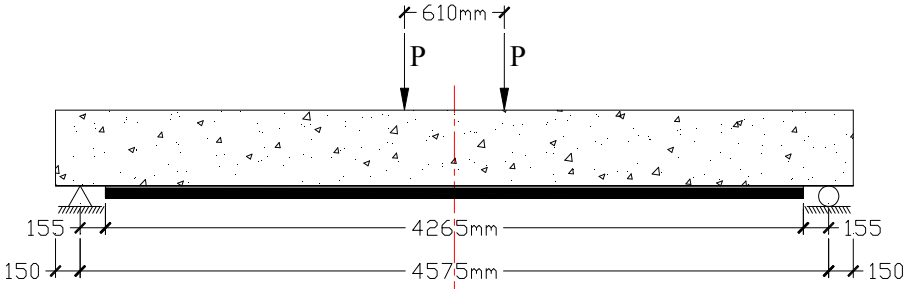

(a) Loading Case of the FRP-strengthened Beam

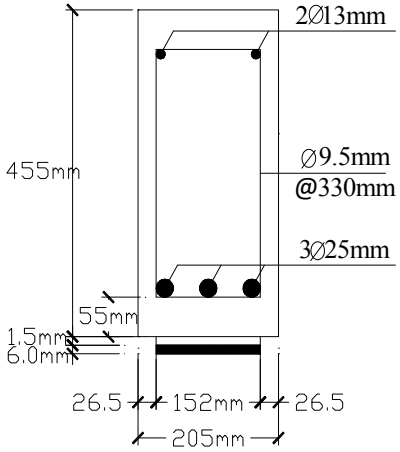

(b) Geometry, Mechanical Propertiesof
the FRP-strengthened Beam

Figure 25. Mechanical Properties of the FRP-strengthened Beam

The elastic modulus of the total concrete beam can be calculated using the following equations.

$$E_b = E_c\left(1+\mu\frac{E_s-E_c}{E_c}\right) = 27,990\left(1+0.018634\frac{200,000-27,990}{27,990}\right) = 31195.23(MPa) \quad (162)$$

$$\mu = \frac{A_s}{A_b} = \frac{2\times 6.5^2\pi + 3\times 12.5^2\pi}{0.093275\times 10^6} = 0.018634 = 1.86\% \quad (163)$$

The cross-sectional attributes of this system are concluded in [46] and Table 13.

Table 13. The cross-sectional attributes

	Area (m2)	Elastic modulus (MPa)	Inertia moment (m4)	v	Shear modulus (MPa)	y (m)
Beam	0.09328	31,195	31,195	0.18	11,860	0.2275
Adhesive	0.00023	814	814	0.37	297	
FRP plate	0.00091	37230	37,230	0.35	13,788	0.003

Y -- the distance between neutral axis and interface.

As verifications, in this section, the interfacial stress along the interface of FRP-reinforced concrete is obtained by four methods: one-parameter, two-parameter, three-parameter, and finite element method (FEM). Shown in Figure 26, the FRP-strengthened concrete beam is modeled linearity and meshed with eight-node, isoperimetric elements in Figure 27. Since there is a concentration of stress at FRP plate end, to achieve more accurate results, a very fine mesh is adopted at this area than automatic one [21].

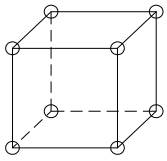

Figure 26. Finite element mesh

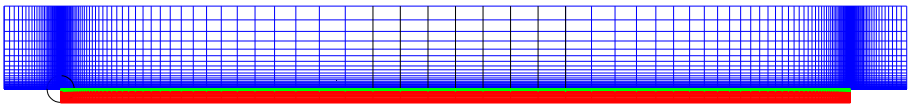

(a) Overall view

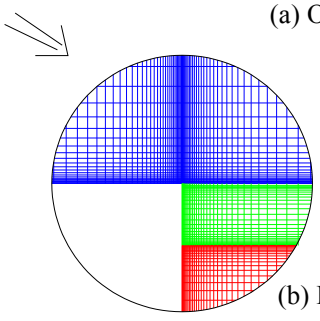

(b) Detailed view at the FRP plate end

Figure 27. Finite elment model of FRP-reinforced concrete under two-point load: (a) overall mesh; (b) detailed mesh at FRP plate end

The comparison results from the two-parameter, three-parameter and FEM are concluded in the following Table 14.

Table 14. Numerical comparison of three different models

	Models		Maximum standard stress(MPa)	relative error
shear stress	two-parameter		0.3525	-12.09%
	three-parameter		0.361	-9.98%
	FEM		0.401	--
normal stress	one-parameter		0.0062	-97.69%
	two-parameter		0.2279	-15.08%
	Three -parameter	beam-adhesive	0.2229	-16.95%
		adhesive-FRP	0.2284	-14.91%
	FEM		0.2684	--

In the section, the interfacial stresses are calculated for three different models and compared with the FEM results. As shown in Figure 28, the maximum shear stress happens almost at the FRP plate end, and then finally reaches a fixed value.

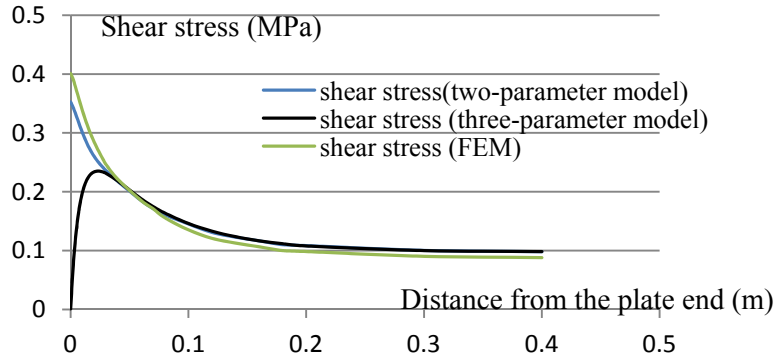

Figure 28. Interfacial shear stress of three different models along the whole beam

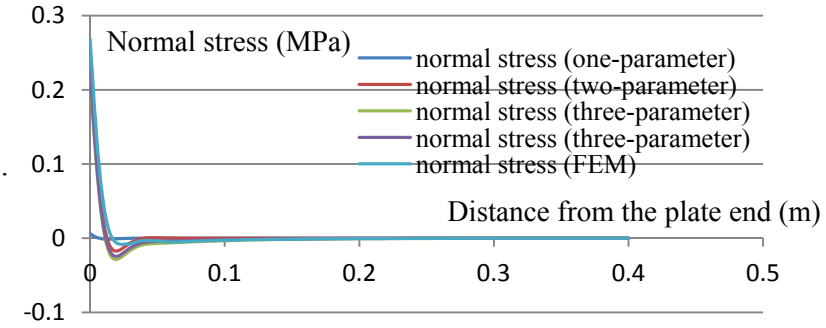

Figure 29. Interfacial normal stress of three different models along the whole beam

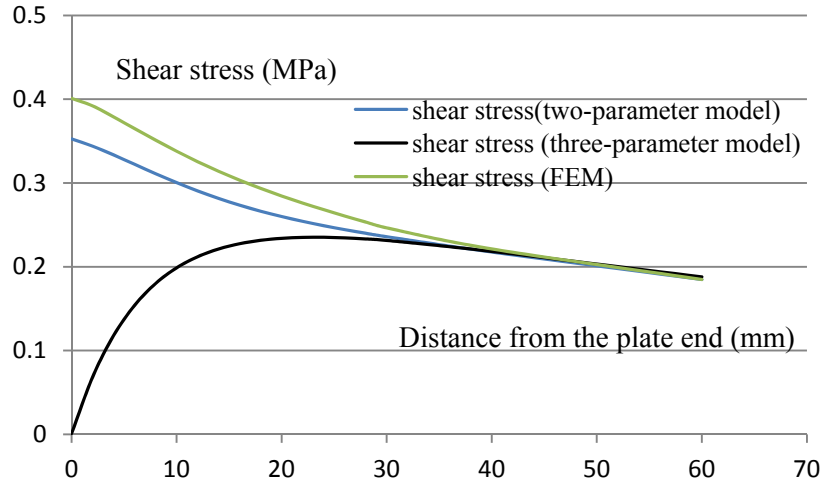

Figure 30. Interfacial shear stress at the FRP plate end

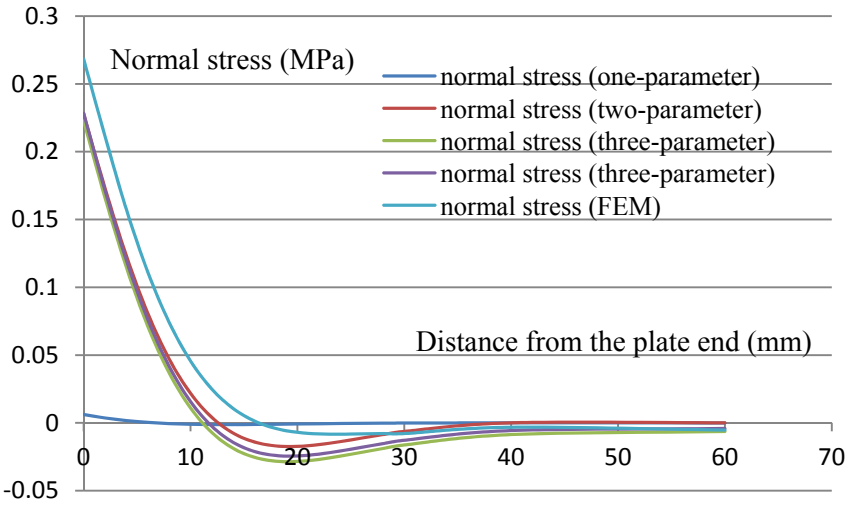

Figure 31. Interfacial normal stress at the FRP plate end

From the above calculation, results in the two-parameter models and the three-parameter models are almost matched with the calculation of finite element method. As shown in Figure 28, Figure 29, Figure 30, and Figure 31 from the FRP end to the middle cross, shear stress is subjected to nonlinear distribution. It reduces sharply near the end, and then changes to flat decrease until zero at the middle span. The peeling stress is quickly dropping to zero.

6.3.2. Parameter analysis of maximum shear stress and peeling stress

The following figures are based on the same data verified by the finite element method in section 6.3.1. This section uses three-parameter model as a representative to analyze the relationship between maximum shear stress τ_{max}, maximum peeling stress σ_{max} and several parameters, as shown in the following figures.

1) Thickness of adhesive layer

In Figure 32, thickness of adhesive h_a has an important impact on τ_{max}. It is approximate that τ_{max} reduces linearly with the increase of h_a. In the practical engineering, thickness of adhesive layer ranges from 1mm to 3mm mostly. In this calculation, when ha = 1, 2, 3mm, τ_{max} is 0.3763MPa, 0.34818MPa, 0.3276MPa accordingly. When comparing with τ_{max} at ha = 1mm, τ_{max} at ha = 1mm decrease 7.47% and τ_{max} at 3mm decrease 12.93%.

The same as τ_{max}, σ_{max} varies with the change of adhesive thickness, especially sharp when ha < 1mm. For the common used value 1mm – 3mm, σ_{max} at the beam-adhesive interface changes from 0.2572037 MPa to 0.199658617 MPa to 0.168669837 MPa when ha = 1, 2, 3mm. When comparing with σ_{max} at ha = 1mm, σ_{max} at ha = 1mm decrease -22.37%and σ_{max} at 3mm decrease -34.42% separately.

Therefore, in the FRP reinforcing technologies, thickness of adhesive layers affects the value of τ_{max} and σ_{max} greatly, and should be under serious consideration. In order to ensure the safety of reinforced concrete, design code should set up a limit for the adhesive thickness to reduce the maximum shear stress and maximum peeling stress.

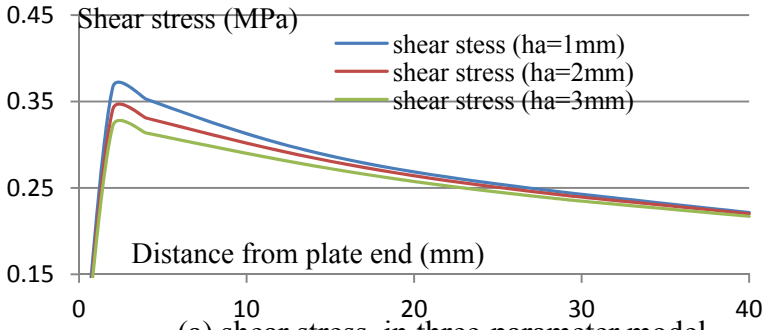

(a) shear stress in three-parameter model

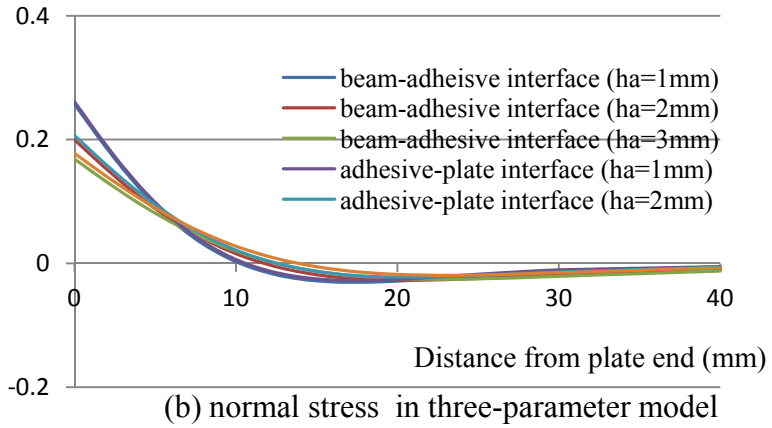

(b) normal stress in three-parameter model

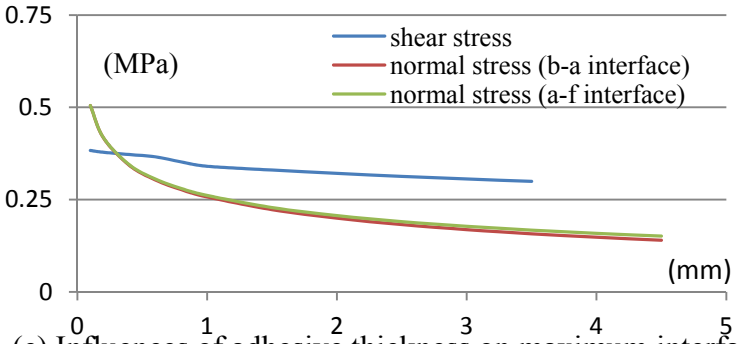

(c) Influences of adhesive thickness on maximum interfacial stress

Figure 32. Influences of adhesive thickness on stress

To avoid local shear failure of concrete, increasing adhesive thickness is a useful way. But on the other hand, high adhesive thickness will lead to huge shrinkage of concrete in the curing process, which results in failed bond by separating the concrete and FRP plate one from the other. Therefore, an appropriate adhesive thickness is essential in the FRP pasted concrete. Besides,

reducing the elastic modulus, shear modulus are also convictive ways to minish the maximum shear stress $\tau_{\max}$.

2) Elastic modulus of adhesive layer

In Figure 33, the maximum peeling stress $\sigma_{\max}$ and the maximum shear stress $\tau_{\max}$ are basically subjected to linear relation with the shear modulus of adhesive layer E_a. $\tau_{\max}$ grows smoothly with the increase of E_a while $\sigma_{\max}$ reduces sharply. It is easy to capture in the figure that a difference of 0.5188% increase in maximum shear stress $\tau_{\max}$ happens when E_a changes from 4GPa to 6GPa, and that of 12.31% in maximum peeling stress $\sigma_{\max}$. Therefore, it is obvious that $\sigma_{\max}$ are mostly affected by E_a while $\tau_{\max}$ does not be influenced too much.

Currently the in industry, most adhesive used in concrete-related areas are harden by mixing two or more component together by chemically reacting, such as polyester resin - polyurethane resin combination, polyols - polyurethane resin combination and acrylic polymers - polyurethane resins combination. Those types of combined adhesive have a elastic modulus mostly ranging from 5GPa to 6GPa.

3) Thickness of FRP

Known in Figure 34, thickness of FRP plate has a positively linear influence on the maximum shear stress $\tau_{\max}$ while a negatively linear influence on the maximum peeling stress $\sigma_{\max}$. In this calculation, when hp = 2, 6mm, $\tau_{\max} = 0.2MPa$ and $\tau_{\max} = 0.361MPa$ with a discrepancy of 79.6326%; $\sigma_{\max} = 0.26MPa$ and $\sigma_{\max} = 0.223MPa$ with a discrepancy of -14.655%. Currently, in reinforced design, hp is determined by the required axial force without the consideration of $\tau_{\max}$.

Sometimes, extra thickness of FRP plate is added to the calculated value as a safety reservation in pursuit of security.

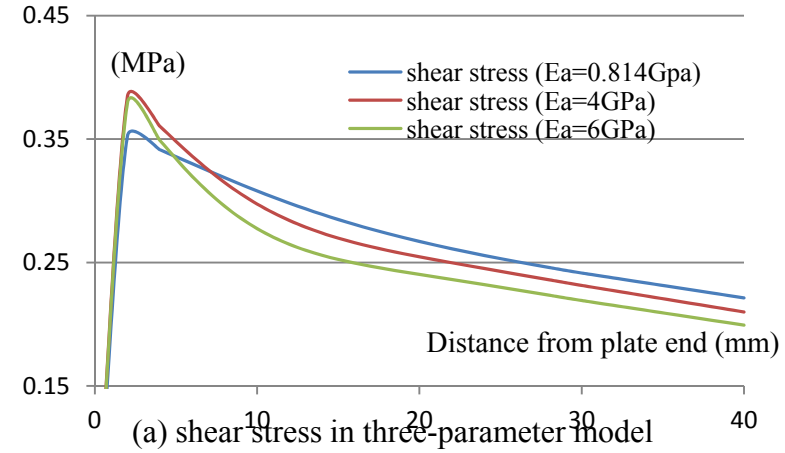

(a) shear stress in three-parameter model

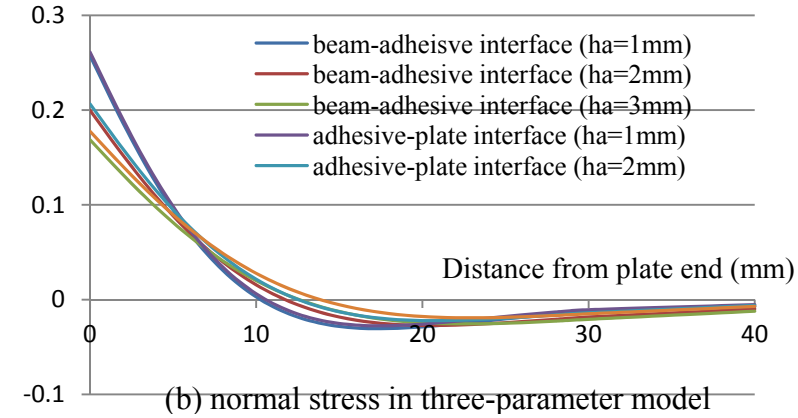

(b) normal stress in three-parameter model

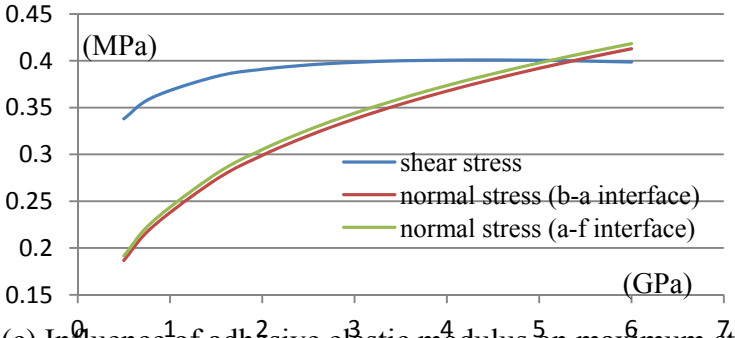

(c) Influence of adhesive elastic modulus on maximum stress

Figure 33. Effects of elastic modulus of adhesive on interfacial stress

Although this extra thickness improves the degree of safety in the view of overall damage (ie, Bending failure), it has great possibility to induce the local collapse of concrete beam due to

increase of τ_{max}. Therefore, in concrete design, it is rational to double check the maximum shear stress τ_{max} for the selected FRP thickness, or may be somehow dangerous.

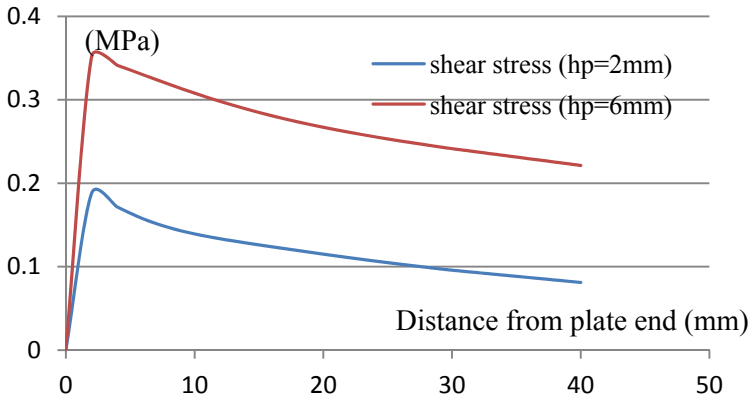

(a) shear stress in three-parameter model

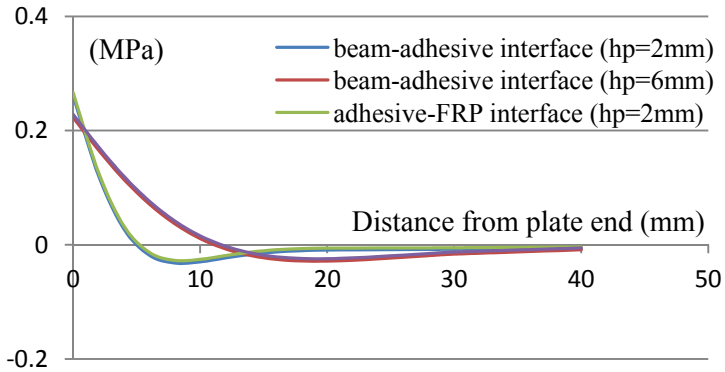

(b) normal stress in three-parameter model

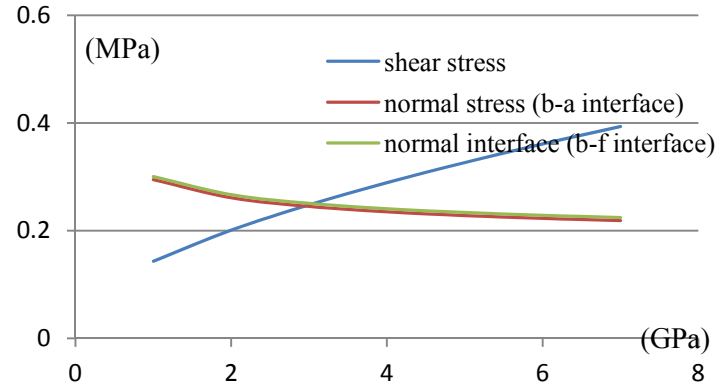

(c) Influence of FRP thickness on maximum stress

Figure 34. Influence of FRP thickness on interfacial stress

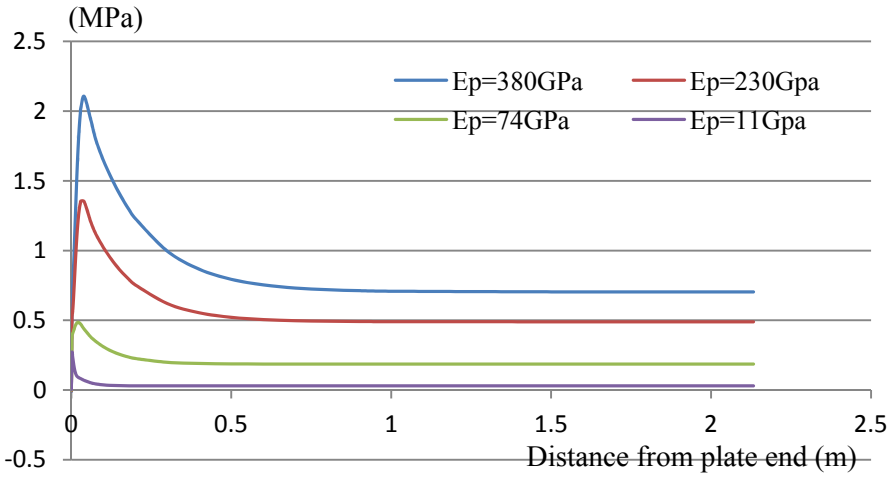

(a) shear stress in three-parameter model

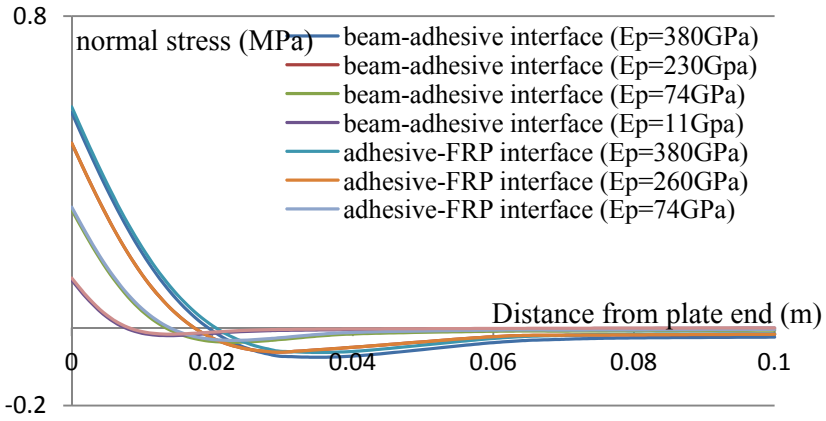

(b) normal stress in three-parameter model

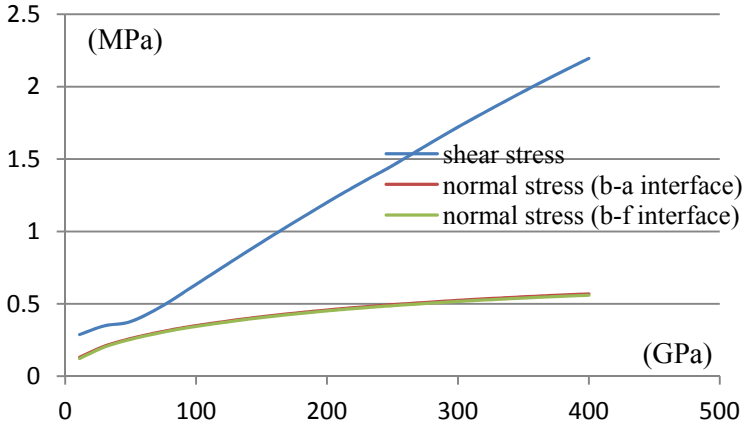

(c) Effects of elastic modulus of FRP on interfacial stress

Figure 35. Effects of elastic modulus of FRP plate on interfacial stress

4) Elastic modulus of FRP plate

In Figure 35, a linear relation can be built between the FRP elastic modulus and the maximum shear stress τ_{max}. τ_{max} increases with the grow of Ep and σ_{max} is almost not influenced. At present, the FRP plate used to strengthen the concrete mainly have: high elastic modulus carbon fiber CFRP plate (FTS-C5-30), Ep = 380GPa; high tensile strength carbon fiber CFRP plate (FTS-C1-30), Ep = 230GPa; Glass fiber GFRP plate, Ep = 74GPa.

Comparing the values of shear stress at Ep= 74, 230, 380 GPa, τ_{max} is 0.484MPa, 1.355MPa, and 2.105MPa. τ_{max} grows in 3.5 times from Ep = 74GPa to Ep = 380GPa. So, the firstly issue need to be consider to minimize the shear stress is choose the appropriate flexible materials with a low value of elastic modulus.

5) Distance from supporting point to FRP end

As known in Figure 36, distance from the supporting point to the FRP end L1 occupies a positively linear influence on the maximum shear stress τ_{max} while not much influence on the maximum peeling stress σ_{max}. Decrease of the distance is meaning increment of the bonding length, accordingly τ_{max} definitely runs low. When L1 = 0, 300mm, $\tau_{max} = 0.263MPa$, $0.283MPa$ with a discrepancy of 7.441%; This shows that FRP plate should pasted on the surface of concrete beam and reach the end of beam as much as possible to significantly reduce τ_{max}. But more costs are generated accordingly.

So, to meet the double requirements of safety and economy, the maximum shear stress should be double checked based on the selected L1.

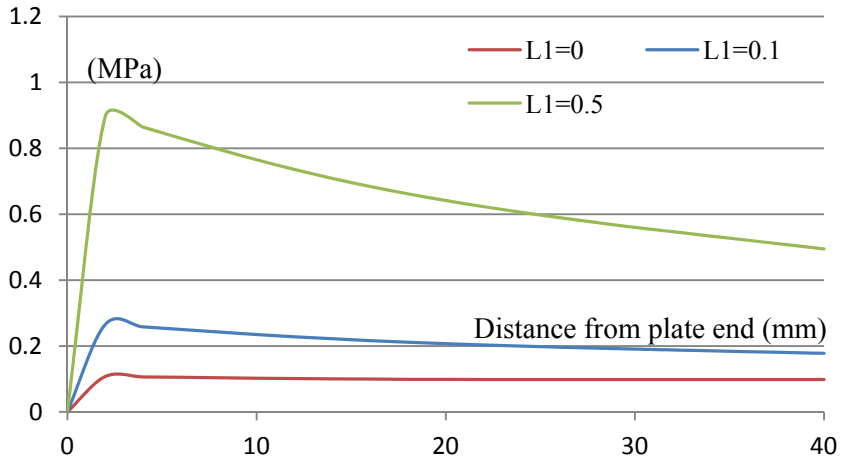

(a) shear stress in three-parameter model

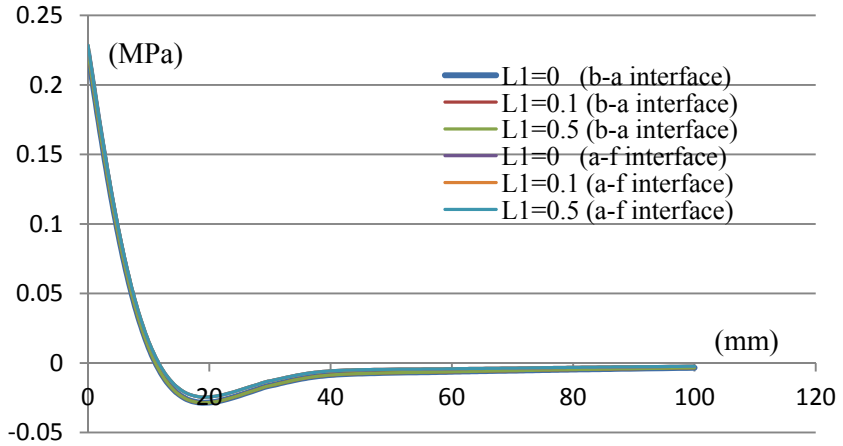

(b) normal stress in three-parameter model

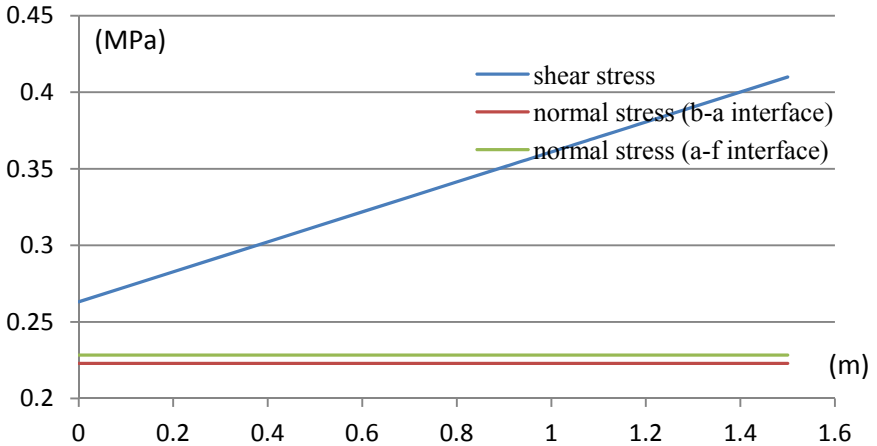

(c)Effects of distance from beam end to FRP end on interfacial stress

Figure 36. Effects of distance from support to FRP end on interfacial stress

6) Height of concrete beam

In Figure 37, it is easy to find that trends of σ_{max} and τ_{max} are mostly same, decreasing with the development of concrete beam height and following a non-linear relation. The reason of non-linearity is because under certain load, if hb increase, the axial force shared by the FRP drops, and according so does the maximum shear stress τ_{max}.

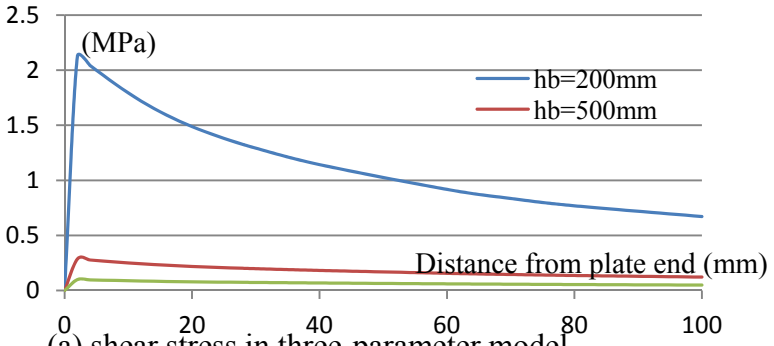

(a) shear stress in three-parameter model

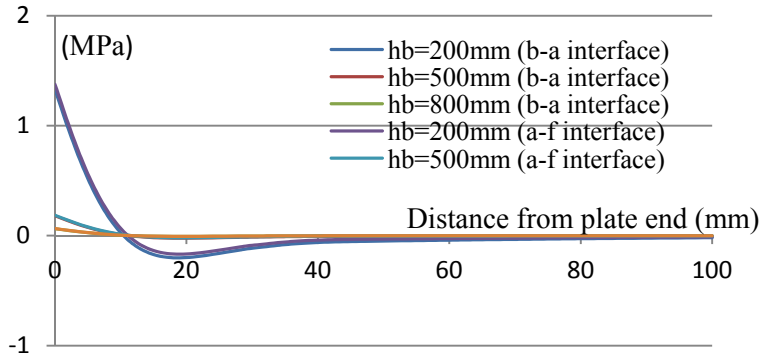

(b) normal stress in three-parameter model

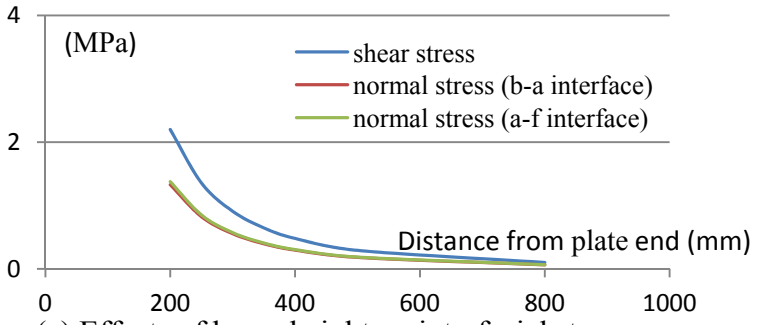

(c) Effects of beam height on interfacial stress

Figure 37. Effects of beam height on interfacial stress

CHAPTER 7. CONCLUSION

7.1. Summary

FRP debonding at the end is a commonly brittle failure type for pasted concrete beam. Based on the previous studies, following the development of interfacial stress theory, this study initially derived three-parameter model by analyzing the cross-section mechanics. Studies are on the light of on elasticity theory, and mainly focusing on constitutive relationship, bending performance and interfacial stress of FRP-reinforced concrete. The main achievement can be concluded as following six points:

1) Improving the bending strength of concrete beam with FRP can effectively improve the stiffness and ultimate bending capacity of the concrete beam, especially for the beam with a low reinforcement ratio.
2) The failure types of FRP-strengthened flexural beam have two catalogs: cross-section strength failure and debonding failure. The debonding failure occurs at FRP plate end. Local concrete is subjected to an integration of maximum bending and shear stress. Because debonding of the interface is belonging to brittle damage, so in practical engineering, this type of failure is not allowed.
3) The study comprehensively analyzed the development of elastic foundation models from one-parameter model to three-parameter model.
4) The study creatively built the governing differential equation from the segmental constitutive relation. Most of existing research are not satisfied with the free boundary

conditions, and the three-parameter model proposed in this thesis perfectly solved this problem.

5) It systematically considers the influences of the performance of concrete, FRP and adhesive on the bond properties, builds the elastic interfacial stress analysis model under the application of external forces, and quantitatively characterizes the effects of FRP elastic modulus, adhesive height, FRP height. General calculation formulas are worked out to suit all kinds of load: distributed load, concentrated load, and middle span load and so on. Comparing with the finite element method, the equations derived by the constitutive relations, considering the strain generated by moment, axial force and shear force, have a wide suitable range, high accuracy.
6) This study proposed a standard in identifying the failure type of FRP-faced flexural concrete beam, and provided logic methods to improve the bonding performance and peeling strength of the concrete-FRP interface from material selection, construction technologies, and so on. For example, appropriately choose the types and dimensions of adhesive and FRP, make sure enough bonding length or set U-stirrup.

7.2. Further Areas of Research

The interfacial failure of FRP-reinforced concrete is related to a complex mechanical problem about material nonlinearity, geometry nonlinearity, and the cracks development. During the study, the author feels the following problem need to be further studied:

1) Various ways to place the FRP plate and the reinforcing devices.

2) Destruction experiment and theoretical bond research at the end of FRP-faced concrete.
3) Theoretical studies of bending-strengthen beam and shear-strengthen beam under long-term external loads.
4) Mechanical performance for concrete columns with different types of cross-section: rectangular, square and round.
5) Mechanical performance of FRP-reinforced concrete beam under cyclic loading.
6) Theoretical studies of concrete beam in a variety of axial compression ratio, stirrup ratio, and so on.

REFERENCES

[1] Stephenson L. D., & Kumar A. (2009). *Corrosion prevention of rebar in concrete in highly corrosive environments*. DoD Corrosion Conference.

[2] Mehta P. K. (1990). *Concrete in the marine environment*. Spon Press.

[3] Abdulrahman A. et al. (2003). Migrating corrosion inhibitors for steel rebar in concrete. *Scientific Research and Essays,6,* 4152-4162.

[4] Manning D.G. (1996). Corrosion performance of epoxy-coated reinforcing steel: North American experience. *Construction and Building Materials,10,* 349-365.

[5] Hayfield P.C.S., & Warne M.A. (1989). Titanium based mesh anode in the catholic protection of reinforcing bars in concrete. *Construction and Building Materials,3,* 152-158.

[6] Amoushahi H., & Azhari M. (2009). Buckling of composite FRP structural plates using the complex finite strip method. *Composite Structures,90,* 92-99.

[7] Sayed-Ahmed E.Y. et al. (2009). Bond strength of FRP laminates to concrete: State-of-the-art review. *Electronic Journal of Structural Engineering,9,* 45-61

[8] Ferretti D., & Savoia M. Non-linear model for R/C tensile members strengthened by FRP-plates. *Engineering Fracture Mechanics,70,* 1069-1083.

[9] Teng J.G. et al. (2002). *FRP-strengthened RC structures*. UK: John Wiley & Sons.

[10] Teng J.G. et al. (2003). Behaviour and strength of FRP-strengthened RC structures: a state-of-the-art review. *ICE proceedings: Structures and Buildings,156,* 51–62.

[11] Lu X.Z. et al. (2005). Meso-scale finite element model for FRP sheets/plates bonded to concrete. *Engineering Structures,27,* 564-575.

[12] Chen J.F., & Teng J.G. (2001). Anchorage strength models for FRP and steel plates bonded to concrete. *Journal of Structural Engineering,127,* 784-79.

[13] Tripi J.M, et al. (2000). Deformation in concrete with external CFRP sheet reinforcement. *Journal of Composites for Construction,4,* 85-94.

[14] Ferracuti B. et al. (2007). Interface law for FRP–concrete delamination. *Composite Structures,80,*523-531.

[15] Chajes M.J. (2007). Bond and force transfer of composite material plates bonded to concrete. *ACI structural journal,93,* 208–217.

[16] Taljsten B.(1997). Defining anchor lengths of steel and CFRP plates bonded to concrete. *International Journal of Adhesion and Adhesives,17,* 319-327.

[17] Lee Y.J. (1999). Slip modulus of FRP sheets bonded to concrete. *Journal of Composites for Construction,3,* 161–167.

[18] Mazzotti C. et al. (2008). An experimental study on delamination of FRP plates bonded to concrete. *Construction and Building Materials,22,* 1409-1421.

[19] Yang J. et al. (2009). Interfacial stress analysis of plated beams under symmetric mechanical and thermal loading. *Construction and Building Materials,23,* 2973-2987.

[20] Guenaneche B. et al. (2010). Elastic analysis of interfacial stresses for the design of a strengthened FRP plate bonded to an RC beam. *International Journal of Adhesion and Adhesives,30,* 636-642.

[21] Wang J.L., & Zhang Ch. (2010). A three-parameter elastic foundation model for interface stresses in curved beams externally strengthened by a thin FRP plate. *International Journal of Solids and Structures,47,* 998-1006.

[22] Rao K.M., & Meyer-Piening H. R.(1991). Vibration analysis of FRP faced sandwich plates using hybrid-stress finite element method. *Computers & Structures,41,* 177-188.

[23] Brockmann W. et al. (2008). *Adhesive Bonding: Materials, Applications and Technology*. Wiley-VCH.

[24] Chen J. F., & Teng J. G. (2001). Anchorage strength models for FRP and steel plates bonded to concrete. *Journal of Structural Engineering,127,* 784-791.

[25] Neubauer U., & Rostasy F.S. (1999). Bond failure of concrete fiber reinforced polymer plates at inclined cracks-experiments and fracture mechanics model. *International Concrete Research & Information Portal,188,* 369-382.

[26] Nakaba K. Bond behavior between fiber-reinforced polymer laminates and concrete. *ACI Structural Journal,98,* 359-367.

[27] Dai J. G., & Ueda T. (2003). Local bond stress slip relations for FRP sheets-concrete interfaces. *Proc. 6th International Symposium on FRP Reinforcement for Concrete Structures,6,* 143-152.

[28] Yao J. , & Teng J.G. (2007). Plate end debonding in FRP-plated RC beams—I: Experiments. *Engineering Structures,29,* 2457-2471.

[29] Grande E. et al. (2008). Experimental study on the capacity of RC beam strengthened in shear by CFRP-sheets. Fourth International Conference on FRP Composites in Civil Engineering, Zurich, Switzerland.

[30] Brena S. F. et al. (2003). Increasing flexural capacity of reinforced concrete beams using carbon fiber-reinforced polymer composite. *ACI Structural,100,* 36-46.

[31] Arduini M. et al. (2004). Performance of one-way reinforced concrete slabs with externally

bonded fiber-reinforced polymer strengthening. *ACI Structural,101*, 193-201.

[32] Erhard G. (2006). *Designing with Plastics*. Hanser Publishers.

[33] Leone M., et al. (2009). Effect of elevated service temperature on bond between FRP EBR systems and concrete. *Composites Part B: Engineering,40*, 85-93.

[34] Tighiouart B. et al. (1998). Investigation of bond in concrete member with fibre reinforced polymer (FRP) bars. *Construction and Building Materials,12,* 453-462.

[35] Chajes M. J. et al. (1996). Bond and force transfer of composite material plates bonded to concrete. *ACI Structural Journal, 93,* 295-230.

[36] Baena M. et al. (2009). Experimental study of bond behaviour between concrete and FRP bars using a pull-out test. *Composites Part B: Engineering,40,* 784-797.

[37] Katz A., & Berman N. (2000). Modeling the effect of high temperature on the bond of FRP reinforcing bars to concrete. *Cement and Concrete Composites,22,* 433-443.

[38] Benachour A. et al. (2008). Interfacial stress analysis of steel beams reinforced with bonded prestressed FRP plate. *Engineering Structures,30,* 3305-3315.

[39] Yang J. et al. (2009). Interfacial stress analysis of plated beams under symmetric mechanical and thermal loading. *Construction and Building Materials,23,* 2973-2987.

[40] Guenaneche B. et al. (2010). Elastic analysis of interfacial stresses for the design of a strengthened FRP plate bonded to an RC beam. *International Journal of Adhesion and Adhesives,30,* 636-642.

[41] Rabinovitch O., & Frostig Y. (2000). Closed-form high-order analysis of RC beams strengthened with FRP strips. *Journal of Composites for Construction,4,* 65-74.

[42] Rabinovitch O. (2010). Impact of thermal loads on interfacial debonding

in FRP strengthened beams. *International Journal of Solids and Structures,47,* 3234-3244.

[43] Timoshenko S. (1953). *History of strength of materials.* New York: McGraw-Hill.

[44] Guenaneche B. et al. (2010). Elastic analysis of interfacial stresses for the design of a strengthened FRP plate bonded to an RC beam. *International Journal of Adhesion and Adhesives,30,* 636-642.

[45] Abdelouahed T. (2006). Improved theoretical solution for interfacial stresses in concrete beams strengthened with FRP plate. *International Journal of Solids and Structures,43,* 4154-4174.

[46] Malek A.M. et al. (1998). Prediction of failure load of R/C beams strengthened with FRP plate due to stress concentration at the plate end. *ACI Structural Journal,95,* 142-152.

[47] Goland M., & Reissner E. (1944). The stress in cemented joints. *Journal of Applied Mechanics,11,* 17–27.

[48] Witmer E.A. (1991). *Elementary Bernoulli-Euler Beam Theory.* MIT Unified Engineering Course Notes, 5–164.